Politecnico di Torino

Ingegneria Energetica e Nucleare
A.a. 2020/2021
Sessione di Laurea Dicembre 2021

Power to heat to power: Underwater energy storage solution BattMarines

Relatore:
    Prof. Eliodoro Chiavazzo
    Prof. Andreas Class

Candidato:
    Andrea Bellelli

ABSTRACT

A successful energy transition requires grid-scale electric energy storage and Carnot batteries represent a potential solution. BattMarines is a Carnot battery concept relying on storing large quantities of high-pressure steam ready to be expanded in a conventional steam power plant.

The key idea is to take advantage of high pressure ambient at large sea depths, so that a thin shell vessel can be utilized to store high quality steam at low cost. Power plant is built on a platform/ship with steam pipeline connection to the vessel on the sea floor.

The thesis considers the general concept including a rough description of plant configuration, thermodynamic efficiency, insulation requirements and potential materials. Several parameters' studies have been carried out to quantify performance.

In particular, granular glass and the mullite mineral foam have been identified as suitable insulation materials. Storing time strongly depends on the selection (days to weeks), while roundtrip efficiency is weakly influenced by the choice and lays between $41 - 44\,\%$.

The present conceptual study supports initial assumptions of an energetically feasible and economic competitive energy storage solution. Moreover, a suitable solution for the main challenge of sufficient thermal insulation in a high-pressure environment could be identified.

INDEX

1 INTRODUCTION

Electricity generation business is unique in commodity trading. Since their liberalization, electricity markets are characterized by a rather high volatility and one of the causes is the lack of large electrical energy storage systems: still today electrical power must be produced in the moment it is consumed. When some systemic power units unexpectedly become unavailable there have been occasions of blackouts or significant price spikes of electricity [1].

In typical conversion power plants, scaling to larger dimensions results in a decrease of the specific costs of the plant. This is usually not the case for electrochemical batteries [2], devices that store energy in chemical form and then turn it back into electricity. Different typologies exist on the market, with different characteristics. The most important of these is the difference between non-rechargeable batteries as alkaline batteries and rechargeable batteries as lithium ones that produce less waste thanks to the reversibility of the reaction.

Electrochemical batteries can be inefficient and comprise of materials that have high environmental and energy impacts. In addition, some materials, such as lithium, are scarce natural resources [3]. While it may help in storing renewable energy, it has environmental costs of its own. These energy storage devices will presumably never exist as large-scale energy storage systems. Anyway, the technology mix remains largely unchanged year-on-year and lithium-ion battery storage continued to be the most widely used, making up most of all new capacity installed [4].

The introduction of multiple renewable sources in the existing energy networks poses new challenges [5] (operational variability, real time network balancing and optimal demand management) and the development of large storage technologies has become more and more important for this reason. A low-carbon energy system requires adaptations to accommodate the changing patterns of energy production and consumption.

Energy storage will play a pivotal role in providing the required flexibility and offering balancing options to the integrated energy system. This holds true especially for thermal energy storage (TES) concepts, which have unique features and can be used to manage the variations in supply and demand at different scales, differently to electricity.

Currently, energy storage – which is a critical technology – is not on track to achieve the levels called for in the *Sustainable Development Scenario*, both in terms of its deployment and its performance [6]. At the moment, the main solution to large electricity storage problems is to accumulate energy in a different way than classical electrochemical batteries, namely in mechanical form. By means of well-known technologies, at a later time, when power is desired, the accumulated mechanical energy is easily transformed into electrical energy.

Mechanical energy can be stored in the form of:

- gravitational energy, by pumped-storage hydroelectricity (PHES, largest capacity and most mature energy storage technology currently available) and new research technologies like Vault towers [7];
- rotational kinetic energy (translational kinetic energy, hard at big scale), by a flywheel;
- pressure energy (compression energy), by compressed air energy storage [8] (CAES) in only two existing plants worldwide.

PHES is the only grid-scale Electric Energy Storage (EES) technology that has proven to be technically and economically viable up to the present day. Other megawatt-scale technologies are being developed and we are looking for alternative EES technologies [9]: an emerging one for the inexpensive and site-independent storage of electrical energy are the so-called Carnot Batteries. Also referred to as "Pumped Heat Electricity Storage" (PHES), a Carnot Battery transforms electricity into heat, stores the heat in inexpensive storage media such as water or molten salt and transforms the heat back to electricity when required.

The charging phase may be done with a traditional heat pump, electric heater, or other technologies. For the discharging phase any heat engine technology can be used, like Rankine or Bryton cycles [9]. When reaching the gigawatt-hours scale, these batteries have the potential to solve the global storage problem and enhance decarbonization, allowing a flexible coupling of power and heat sectors.

In this thesis, a proposal of a large dimension Carnot Battery system is made, described and simulated. Fundamental prerequisites for a feasible system are the need of a cheap and common storage media, a reasonable high energy density and a possible scaling to very large dimensions.

The idea consists in running a state-of-the-art steam turbine power plant in batch operation and store the high-quality steam in large quantities as a Carnot Battery system. Unfortunately, in common applications hot water at ambient pressure or quite low pressure is stored, since the wall thickness of the pressure vessel rapidly grows when increasing pressure difference between inside and outside.

In order to have available steam ready to be expanded at turbine inlet thermodynamic conditions of $T > 500\,°C$ and $p > 100\,bar$, or better in supercritical conditions of $T > 550\,°C$ and $p > 250\,bar$, an appropriate and unique pressure vessel is required. Seeking for special applications that could enclose large quantity of hot steam at high pressure, only the nuclear power containment system has appropriate scale and can withstand several bars of overpressure [10].

Underwater storage BattMarines could be a solution: submerge a vessel of dimensions similar to nuclear containment deep into the sea to store large quantity of high-quality steams for long periods (order of days) and connect it to common steam turbine power plant components placed above it on a platform on the sea level. In this way, overpressure problem is deleted since inner steam and outer seawater would have almost the same pressure and thin shell vessel will reduce the cost of the vessel itself, while common steam power plant components allow to reduce the cost of the attached power plant.

In this work the system configuration and the different system components are analyzed and the behaviour of the system simulated with the TIL Suite offered by the company TLK-Thermo GmbH, suitable for the stationary and transient simulation of freely configurable thermodynamic systems. The individual models in TIL are described using the modelling language Modelica.

2 NOMENCLATURE

A	$[m^2]$	Superficial area of solids
V	$[m^3]$	Volume
m	$[Kg]$	Mass
ρ	$[Kg/m^3]$	Density
$\dot{m}$	$[Kg/s]$	Mass flow rate
w	$[m/s]$	Velocity
g	$[m/s^2]$	Gravitational acceleration
T	$[K]$	Temperature
p	$[bar]$	Pressure
t	$[s]$	Time
h	$[J/Kg]$	Specific enthalpy
L	$[m]$	Length
d	$[m]$	Diameter
r	$[m]$	Radius
δ	$[m]$	Thickness
H	$[m]$	Height difference, depth
c	$[J/Kg\ K]$	Specific heat capacity
α	$[W/m^2\ K]$	Convective heat transfer coefficient
β	$[1/K]$	Thermal expansion coefficient
λ	$[W/m^2\ K]$	Thermal conductivity
U	$[W/m^2\ K]$	Overall heat transfer coefficient between the inside and the outside of a tank or pipeline
μ	$[Pa\ s]$	Dynamic viscosity
v	$[m^2/\ s]$	Cinematic viscosity
Nu	$[-]$	Dimensionless Nusselt number
Pr	$[-]$	Dimensionless Prandtl number
Re	$[-]$	Dimensionless Reynolds number
Ra	$[-]$	Dimensionless Rayleigh number
Gr	$[-]$	Dimensionless Grashof number
f	$[-]$	Dimensionless friction factor

ε	$[m]$	Surface roughness
η	$[-]$	Energy efficiency
Q	$[J]$	Thermal energy
$\dot{Q}$	$[W]$	Thermal power
W	$[J]$	Electrical energy
$\dot{W}$	$[W]$	Electrical power
σ	$[MPa]$	Mechanical stress (normal)
E	$[MPa]$	Longitudinal elastic modulus (Young modulus)
γ	$[-]$	Transversal contraction coefficient (Poisson ratio)
R	$[N]$	Resultant of external load

SUBSCRIPTS

amb	relating to ambient
avg	average value
ch	relating to charging phase
dis	relating to discharging phase
cp	charging pipeline
dp	discharging pipeline
max	maximal value
min	minimal value
tot	total value
T	turbine
P	pump
l	relating to fluid phase
v	relating to vapour phase
w	relating to the wall
i	relating to internal surface of the wall
e	relating to external surface of the wall
s	relating to steel
c	relating to concrete
fg	relating to foam glass

t	relating to turbine
th	thermal
m	mechanical
st	static
f	friction
is	isoentropic
lat	lateral surface
bot	bottom surface
top	top surface
hs	Relating to hot storage
cs	Relating to cold storage
θ	Circumferential
r	Radial
z	Axial
in	Input
out	Output

ABBREVIATIONS

HP	High pressure
IP	Intermediate pressure
LP	Low pressure
TES	Thermal energy storage
EES	Electrical energy storage
PHES	Pumped-hydro energy storage
CAES	Compressed air energy storage
SC	Supercritical
USC	Ultrasupercritical
LCOS	Levelized cost of storage

3 SYSTEM DESCRIPTION

In this chapter, the general concept of the storage system is described.

The goal of this large system would be to store at least an amount of energy, i.e., quantity of steam, such to allow the shutdown of a big conventional power plant, meaning to be able to run a big power plant in discontinuous operation, only when desired. A medium-term storage system is required in order to do this, able to lose very low percentages of total stored energy in many days. Longer storage periods can´t be obtained with sensible thermal energy storage.

As visible in figure 1 [11], showing the net electricity generation in Germany, even doubling the generation from renewable sources (especially solar and wind) while shutting down brown coal power plants wouldn't allow the country to produce the demanded energy in every moment of the day without the presence of suitable number of massive EES systems.
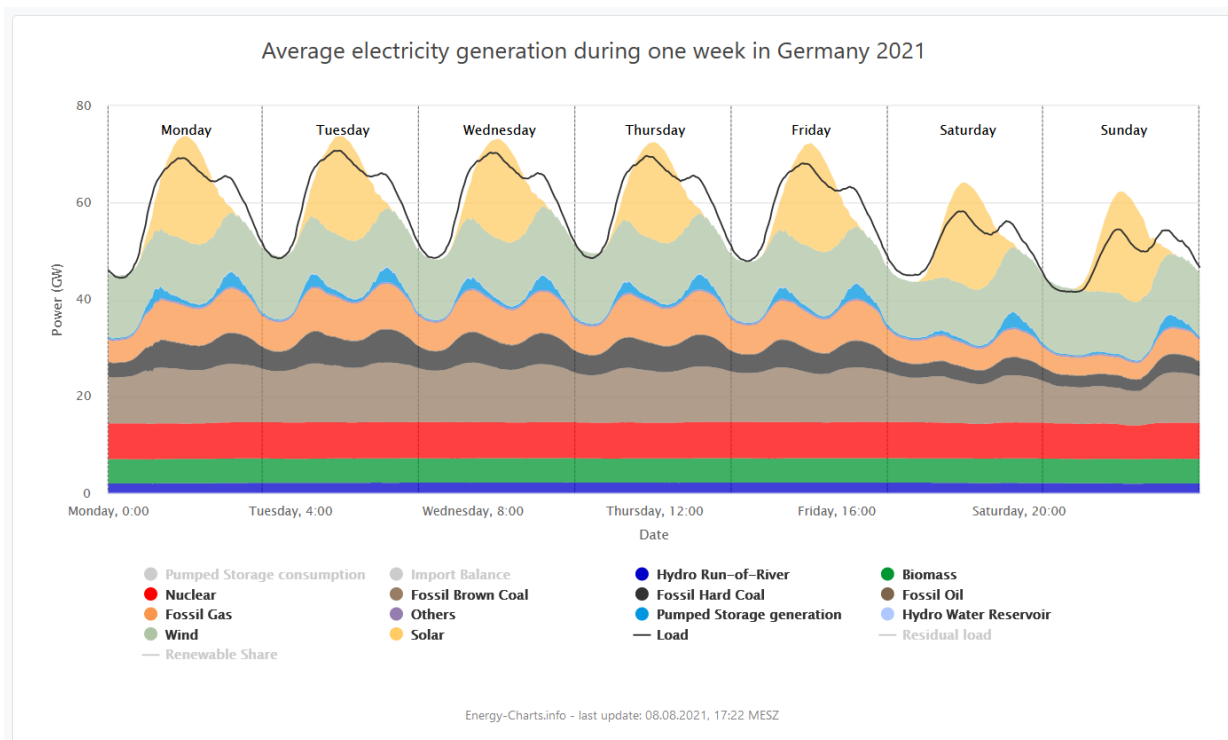
Figure 1 – Average electricity generation and load during one week in Germany 2021

In 2016, PHES with a worldwide capacity of about 130 GW constituted 99% of the total grid-scale EES storage [12]. During charging, surplus electrical energy is converted into potential energy by pumping water from a lower reservoir to a higher reservoir, while in the discharging phase water flows back towards the lower reservoir driving a turbine.

Carnot batteries can be used as well as grid energy storage to store excess power from variable renewable energy sources and to produce electricity when it is needed.

3.1 The Rankine cycle

A brief review of the Rankine cycle technology has to be done before the description of the storage system. This cycle is a thermodynamic cycle used in conventional electricity generation power plants and still today major part of electricity worldwide is generated by steam turbines driving rotary
generators.

The steam energy in form of pressure is transformed in mechanical energy, thanks to the steam turbine. Connecting an electrical generator to the rotating turbine shaft, the mechanical energy is then transformed in electrical one with high efficiencies. Electricity is sold to the electrical grid and it represents the source of incomes.

This technology is applied in many different installations: nuclear power plants, coal-fired thermoelectric power stations, biomass-fired power stations, concentrated solar power plants and geothermic plants. The heat is generated in different ways using various fuels, but the conversion from thermal energy to mechanical energy almost always happen in a steam turbine.

In its simplest configuration, the cycle is obtained with four components only:

Pump: compression of the fluid to the highest pressure;
Boiler: the compressed fluid is heated to the final temperature, undergoing phase change from liquid to vapor;
Turbine: expansion of the steam, fluid power transformed into mechanical power;
Condenser: vapour condensation, rejection of unavailable heat.

Additional necessary components that do not appear are the electric generator connected to the turbine and the electric motor that drives the pump, but their efficiencies are close to the unit, therefore they can be momentarily neglected.

The thermal efficiency, representing the fraction of heat that is converted into work, is the following:

$$\eta_{th} = \frac{W_T - W_P}{Q_{in}} \tag{3.1}$$
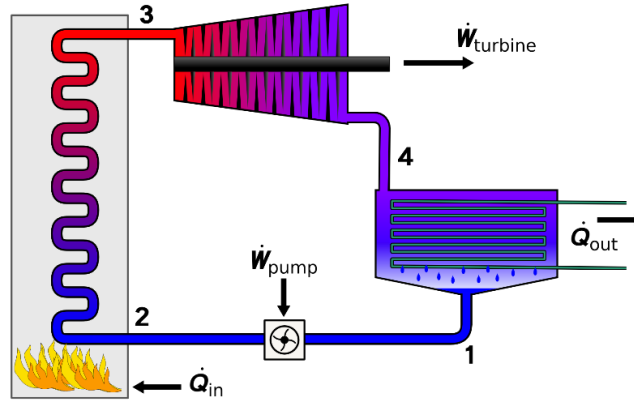
Figure 2 - Simplified schematic of a Rankine cycle [13].

In the ideal cycle, four ideal transformations take place in these components: two isobaric transformations in the boiler and in the condenser, two adiabatic transformations in the turbine and in the pump. It is shown in the figure 3 and compared with a more realistic cycle that is represented with a dashed line.
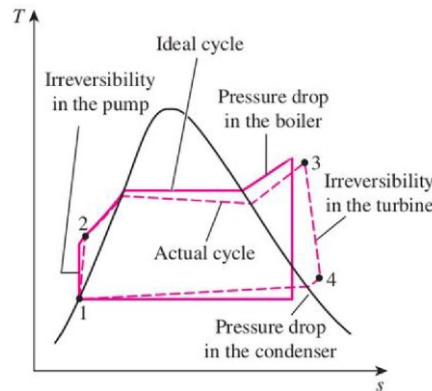
Figure 3 – Real Rankine cycle in T-s diagram [14]

Inefficiencies can be attributed to three causes [15]:

- Irreversibility of processes. Every heat engine is subject to the efficiency limitations imposed by the second law of thermodynamics. The maximum achievable efficiency is the ideal Carnot efficiency calculated as:

$$\eta_{carnot} = 1 - \frac{T_{cold}}{T_{hot}} \approx 56\ \% \tag{3.2}$$

- where $T_{hot} = 673\ \text{K} \ (400°C)$ and $T_{cold} = 293\ \text{K} \ (20\ °C)$. All real thermodynamic processes are somehow irreversible. They are not done infinitely slowly. Therefore, heat engines must have lower efficiencies than limits on their efficiency due to the inherent irreversibility of the heat engine cycle they use.

- Friction and heat losses. A part of the overall cycle inefficiency is due to the losses by the individual components. In real devices (such as turbines, pumps, and compressors)

a mechanical friction, heat losses and losses in the combustion process cause further efficiency losses.

- Design efficiency. Last and also important source of inefficiencies is from the compromises made by engineers when designing a heat engine (e.g. power plant). Cost and other factors must be considered in the design and operation of the cycle. As an example, ideally the steam exhausted into the condenser would have no subcooling, but real condensers are designed to subcool the liquid by a few degrees in order to avoid the suction cavitation in the condensate pumps. This subcooling increases the inefficiency of the cycle, because more energy is then needed to reheat the water.

There are several methods to improve the thermal efficiency of the Rankine cycle [16]. The first is to increase the maximum temperature reached in the cycle. In figure 3, the outer boiler conditions are of superheated vapour, meaning it represents already an improvement of the basic cycle, in which saturated vapour exits the boiler. Assuming that the maximum temperature reached is limited by the pressure inside the reactor pressure vessel, the remaining methods are reported in the following.

First, the thermal efficiency tends to increase as the average temperature at which energy is rejected decreases. The condenser provides a vacuum that maximizes the energy extracted from the steam, resulting in a significant increase in net work and thermal efficiency. Disadvantage of decreasing the turbine exhaust pressure is to significantly increase the specific volume of exhausted steam, which requires huge blades in last rows of low-pressure stage of the steam turbine.

Second, not only one turbine stage is present, but many of them. After expanding in the HP-turbine, the steam undergoes reheating to reach again high temperature, then remaining expansion takes place in the next steps. The reheating helps to reach a higher steam quality at the final stages of the expansion, reducing the risk for turbine blades to be damaged by water droplets.

The third fundamental improvement that allows the cycle efficiency to increase consists in the feeding water pre-heating and the connected reduction of amount of fuel needed in the boiler. Instead of losing part of the energy in the condenser, the temperature of the water entering the boiler is increased using steam extracted from different turbine stages. This process is known as heat regeneration. Vapour extraction reduces the variance between this cycle and the ideal Carnot cycle. Also, it permits to reduce the steam flow rate in last turbine stages and consequently decrease low pressure turbine blades dimensions, avoiding constructive challenges.

As discussed above, the efficiency of thermal power plants could be improved by increasing the initial steam parameters. Sub-critical fossil fuel power plants can achieve $36 - 40\%$ efficiency. Supercritical and ultra-supercritical thermal power plants have proven stable and effective for large-scale commercial power generation. Supercritical power plants ($p_{max} > p_{cr} = 22.1\ MPa$) can attain an efficiency $2\% - 3\%$ higher than sub-critical power plants while ultra-supercritical ($30MPa, 600^0C/600^0C$) thermal power plants boast an efficiency even $2\% - 3\%$ higher.

For many years this technology has been blocked to the limit of 538 °C for the superheated and reheated steam due to material limitations. Nowadays some kinds of stainless steels can operate up to temperatures above 600 °C and Nickel-based superalloys can approach 700 °C. Anyway, increasing the cycle maximum temperature has a huge consequence on materials costs.

In figure 4, the power generation cycle of a nuclear high-performance light water reactor is illustrated [17]. This thermodynamic cycle will be used as reference for the BattMarines system analysis, being a super-critical thermal power plant with quite high efficiency, but with a contained maximum cycle temperature. This will allow not to have excessively expensive materials and lower thermal losses.

Steam entering the HP-turbine is in super-critical conditions: it has a temperature of $494 \, °C$ and pressure of $226 \, bar$. Expansion happens in three stages, high pressure, intermediate and low turbines. A single reheat up to $441 \, °C$ is present. Three low pressure water preheaters and four high pressure water preheaters heat up the condensed water.

They are separated by a feedwater tank, a mixing chamber called deaerator in which all the mass flow rate of the cycle is collected. It also ejects gas and incondensable. With this component the feeding water line has been divided into the low-pressure region and the high-pressure region, enabling the pumping system to give the needed pressure in two stages, since the outer condenser pressure is well below the atmospheric pressure, around $0.0475 \, bar$, while the maximum cycle pressure is $250 \, bar$. Following the condenser is the condensate pump and following the deaerator is the boiler feed pump.

As represented in the figure, the thermal power input is $\dot{Q}_{in} = 2300 \, MW_{th}$ and the gross power output $W_{gross} = 1046 \, MW_{el}$. To get the net power output, the power autoconsumed by the cycle is calculated as the sum of the power consumed by the three pumps present, resulting in $W_{elcons} = 46 \, MW_{el}$.

Global efficiency:

$$\eta = \frac{\dot{W}_{gross} - \dot{W}_{cons}}{\dot{Q}_{in}} = \frac{1000 \, MW_{el}}{2300 \, MW_{th}} \cong 43,5 \, \%$$

(3.3)
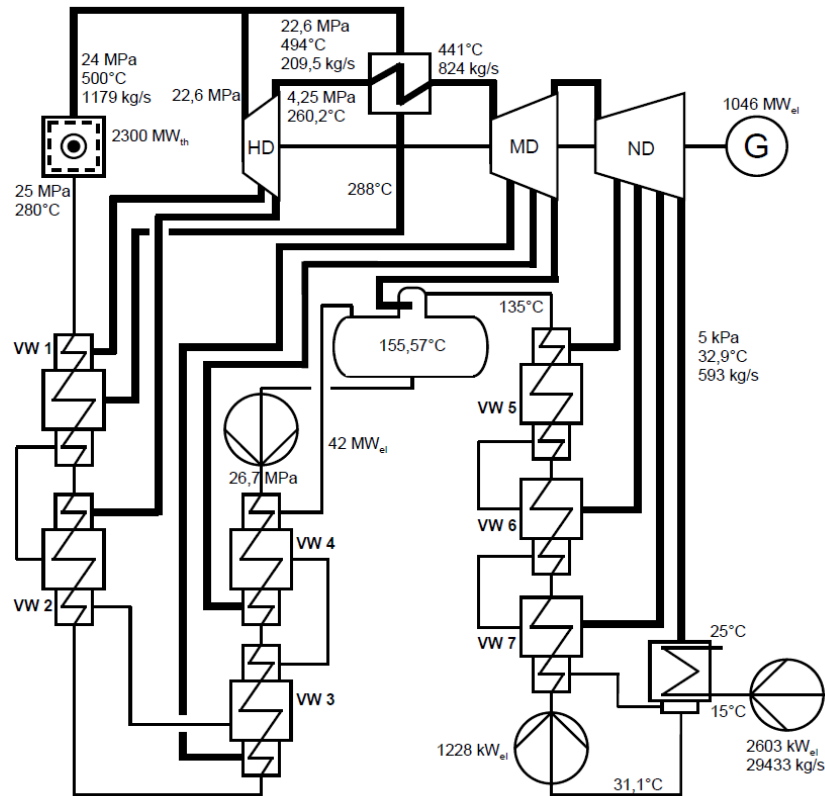
Figure 4 – Reference Rankine cycle.

3.2 BattMarines

Run "state of the art" steam turbine power plant in batch operation and store the high-quality steam in large quantity as a Carnot battery system.
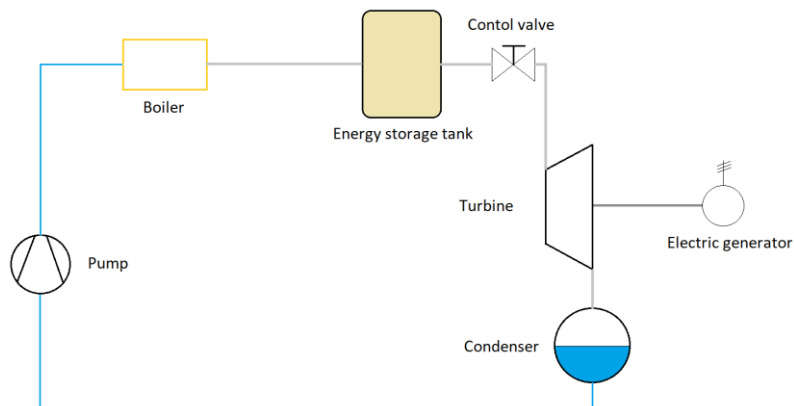
Figure 5 – Batch operation of Rankine cycle

Practically, an energy storage tank is added between the heat source of the system, e.g. a boiler, and the turbine inlet. A mid-term storage is desired, i.e. minimum storing time must exceed several hours (days), and during discharging a power output of $\sim 1\ GW$ is wanted,

therefore an energy of $\sim 1\ GWd$ should be stored in fully charged conditions to have a discharging phase durable up to one day.

At reference cycle inlet turbine thermodynamic conditions, specific volume of steam can be considered $v_v \sim 0,01\ kg/m^3$ and the specific steam consumption of the cycle, which represents the steam consumed per unit output of energy, is the following:

$$\frac{\dot{m}}{\dot{W}_{net}} \cong 4,24 \frac{kg}{kWh} \tag{3.4}$$

A huge high pressure-high temperature reservoir is needed, in fact the mass that needs to be stored is $\sim 10^8\ kg$ of steam, corresponding to a volume of $\sim 10^6\ m^3$ that can be accomplished by a cylinder with inner diameter and height of at least $100\ m$.

In existing common TES systems hot water at ambient pressure or at moderate overpressure is stored, since the wall thickness of the pressure vessel itself rapidly grows when the pressure difference between inside and outside increases. Not only pressure plays a role, but dimensions also: at a certain fixed wall thickness, the larger the diameter, the greater the pressure induced stresses.

For these reasons, the huge vessel needs to be installed in a high pressurized ambient. The only thinkable with pressures in the order of the desired ones is the deep sea, in fact water density is such that every $10\ m$ a gain in static pressure of $\sim 1\ bar$ takes place.

A thin shell of the reservoir would allow to reduce the total cost of the installation, but it is possible to have it only in case the pressure difference across the wall is relatively small. This means, depending on the desired turbine inlet steam pressure, different sea depths are required to store the steam at that pressure. In the estimation problem chapter, the required thickness of the reservoir will be discussed.

3.2.1 First representation

In the simplest representation, the platform on the see level and the underwater steam tank are shown. The platform has an electrical connection to the grid onshore, while platform and tank are connected through the alimentation or charging line and the discharging line.

The storage tank is illustrated as a stratified vessel, with cold liquid water at the bottom and hot steam at the top. The great dimensions allow this stratification to exist and the system must be able to keep separate volumes at different temperatures, maybe with the help of a moving separator of the two zones.

Energy content of the vessel is inversely proportional to the height of the liquid water contained in it, namely directly proportional to the steam filling level.
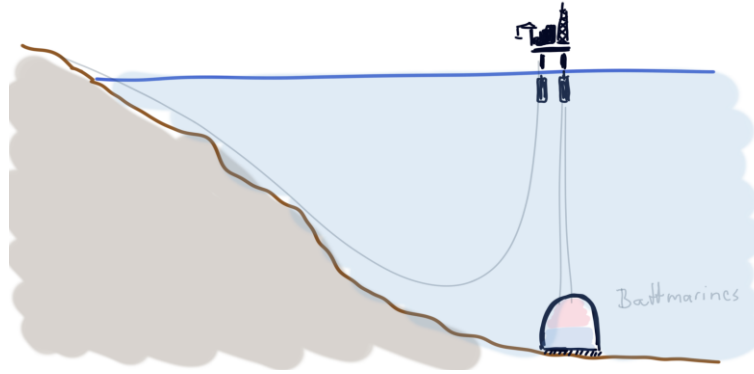
Figure 6 – BattMarines first proposal

There are a couple of physical obstacles to the realization of this plant configuration. The first one considered is the following: due to the great size of the submersed tank, the buoyancy force acting on it will be extremely high. The buoyancy force exerted on an object partially or fully submerged in a fluid is equal to the weight of the displaced fluid:

$$F_{bouyancy} = \rho \, g \, V \tag{3.5}$$

(3.5) shows the density of the liquid (seawater), the gravity constant and the volume of the part of the body immersed in the fluid, i.e. the displaced liquid volume. Two scenarios are possible: sinking or rising. The first is a downward vertical movement that occurs when the gravitational force on an object is greater than the buoyant force supporting it, while rising is the upward vertical movement that occurs when the gravitational force is lower than the buoyant force.

To sink the vessel, its mass must increase while keeping constant the volume. A reasonable solution is to fill it up with dense and heavy material: sand seems to be the most relevant solution due to its low price, high availability and quite low thermal conductivity. At constant volume, the necessary amount of filling material depends only on the specific weight of construction materials used.

Once the reservoir has reached the seafloor level, it needs to be stable on it. Since buoyancy forces are always acting on a submerged volume, a containment structure like a rack is probably necessary to let it maintain a fixed position. Installation challenges are huge, since suitable infrastructure does not exist.

3.2.2 Pressure control

Second physical challenge is related to the management of pressure instabilities and variations in the tank. As in common Rankine power plants, constant steam pressure is wanted at the turbine inlet, meaning the pressure in the tank is desired to be unchanged in time.

It isn´t possible to achieve this without always having the same amount of mass in the vessel: in figure 3, during charging the steam enters the tank, the total mass increases and the storing pressure increases accordingly, while during discharging the steam leaves the vessel and pressure reduces.

For the following reason, an opening at the base of the vessel is needed. The mass balance of the tank can in this way be equal to zero. Unfortunately, the working fluid and the ambient fluid aren´t interchangeable, being normal water the first and salt seawater the second. It means, a hydraulic connection is necessary at the bottom of the tank, letting freshwater flow in during the discharging phase and out during the charging phase. This is challenging, since the densities of supercritical steam and fresh water differ by an order of magnitude: $\rho_v \approx 100 \frac{Kg}{m^3}$, $\rho_l \approx 1000 \frac{Kg}{m^3}$.

A connection to a pressure holder through an expansion line as represented in figure 4 is a fundamental addition in the system configuration. A pressure holder is a pool or lake characterized by enormous surface area, that is hydraulically connected with the underwater pressurized tank in order to keep its pressure at an almost constant level, with very low oscillations. If the pressure holder area is sufficiently big, the height of the water level remains nearly unchanged during charging and discharging phases, allowing the static pressure of the corresponding water column to be constant.
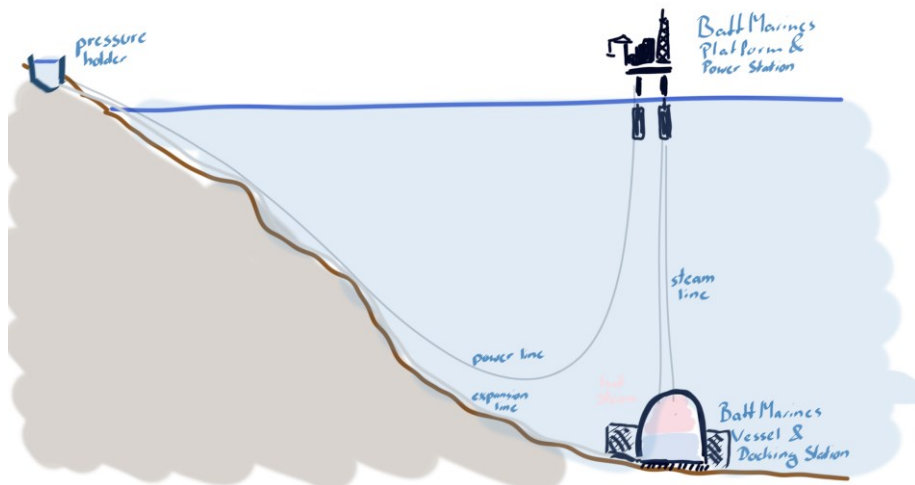
Figure 7 – BattMarines with pressure control

While the pressure of the seawater outside the tank at each depth is always the same, the pressure of every layer in the vessel varies according to the steam filling level. Considering the steam pressure is fixed at $250 \ bar$ and the tank height at $100 \ m$; two extreme situations can occur: storage system fully charged, when only steam is present, and storage system fully discharged, when only water fills the tank. In the first case the static pressure corresponding to a $100 \ m$ steam column is $\sim 1 \ bar$, whereas in the second case the static pressure related to a $100 \ m$ water column is $\sim 10 \ bar$.

It is therefore impossible to have exactly the same pressure at every height of the tank between the inside and the outside, reason for which it has to be decide if it is better to have slight overpressure in the inside or in the outside. This is only a matter of materials used in the vessel: steels are better to be used with inner overpressure, concrete prefers overpressure on the outside.

Seawater has slightly higher density than fresh water, therefore if the free surface of fresh water in the pressure holder was at sea level, the pressure at the bottom of the expansion line would be lower than the pressure of the sea at the same depth. Therefore, pressure holder free surface must be at an altitude on the sea level of around $60 - 80 \ m$, depending on the specific location.

The necessity of installing a pressure holder brings out the main disadvantage of this Carnot Battery system: as for the pumped-storage hydroelectricity, a geographical constraint exists. In fact, for desired pressures, there is the need of a sea depth of at least $2500 \ m \ (250 \ bar)$, that is at the same time located at a reasonable distance from the coast, being the hydraulic connection essential for the plant realization. Not all coasts are suitable for the installation of this system.

The hydraulic connection is a pipe made of concrete. It has no meaning using other materials, in fact the inner water is in thermal equilibrium with the outer seawater, therefore no thermal insulation is necessary. Also, pressure between inside and outside is almost the same all along the pipe. Concrete is much cheaper than stainless steel, that is the usual material adopted for underwater pipelines.

Only property required is a sufficiently high compressive strength, since at great depths the fluids reach $25 \ MPa$ pressure. Every kind of high-strength concrete is characterized by a higher compressive strength [18]. This expansion line will be therefore the less challenging, despite being the longest one of the system.

Geographical constraint isn´t too strong because this concrete expansion line will be one of the least critical components and for sure the cheapest one, meaning it could be even very long and its price negligible compared to the total plant cost. Only certain constraint is the sea death, for example North Sea has a maximum depth of $\sim 700 \ m$ and it couldn´t accommodate such system.

3.2.3 The Carnot battery operation

These above described system configurations have a thermodynamic complication, due to the behaviour of a Carnot battery.

The Rankine power cycle has consistently higher efficiency in the case water is preheated with steam extractions after being condensed with respect to the normal simple cycle, as already discussed. In addition, a Carnot battery system works properly between two temperature reservoirs, a low temperature and a high temperature one [9]. For these two reasons it is necessary to also have a preheated water storage system working as a low temperature heat reservoir.

The Carnot battery in the discharging phase is represented by the Rankine cycle, with the turbine sucking the steam from the hot reservoir, expanding it, condensing it and finally

heating it up with steam turbine extractions to fill the low temperature water reservoir at 280 ℃. Electrical power generated represents the source of income.
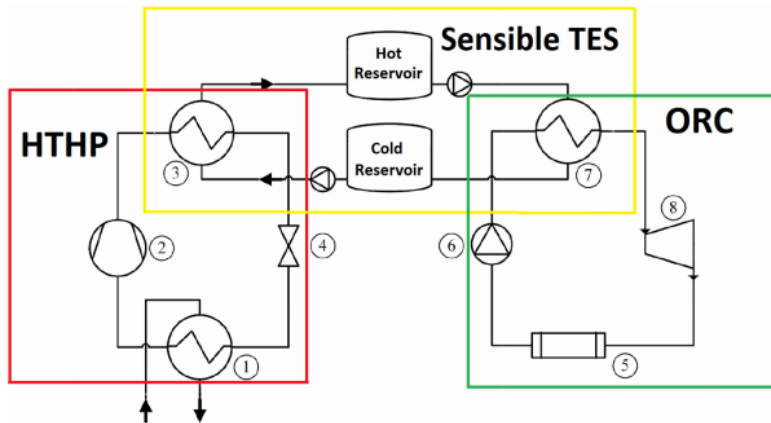
Figure 8 - PHES system with sensible thermal energy storage [9]

The Carnot battery in the charging phase is represented by an electric heater or a heat pump (figure 8), through which steam is generated from the stored cold water and the high temperature reservoir is filled up.
Two main possible configurations of the system are discussed. The first one could be seen as the simple configuration, where steam flows both in the charging pipeline and in the discharging one, meaning the low temperature reservoir is not existing and water doesn´t get preheated from steam turbine extractions. Basically, it is the same represented in figure 4 as second proposal, in which only the hot reservoir is located on the seafloor.
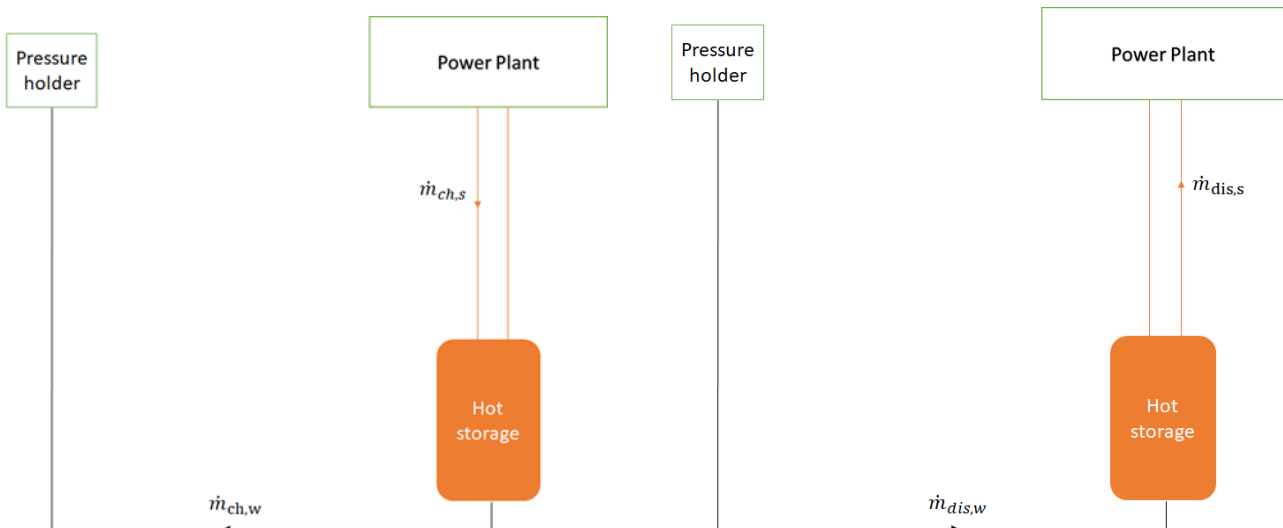
Figure 9 – Simple system configuration, discharging process to the left and charging process to the right

During discharging, the steam vessel is emptied and the steam flows naturally in ascending direction from the hot storage tank towards the platform and runs the Rankine cycle: it expands in turbines and condenses. Without condensed water preheating the discharging process efficiency is lowered. Steam extractions from turbines are useless if steam is not generated in the same time or if preheated water isn´t somehow stored.

During charging, water is heated by an electric heater on the platform, steam is generated and is pumped in descending direction towards the submerged hot tank filling it up.

This system design has many improvements possibilities. Firstly, introducing a cold storage tank for the preheated water would mean to increase the discharging process efficiency by applying regeneration in the Rankine cycle and also to reduce the required input power of the charging process.

In fact, the heat pump or electrical heater would have to heat up to the hot storage temperature starting from the preheated water temperature instead of the condenser temperature. Since they differ by more than 200 ℃, being the condenser temperature around 30 ℃ and the preheated water around 280 ℃, having a cold storage tank translates in having a much lower input power.

Secondly, the flow temperature is together with the pipe`s wall thermal resistance the most important parameter to characterize heat losses in the pipe itself. Keeping the same insulation design of the pipe, namely if the thermal resistance is fixed, when 280 ℃ water instead of the 500 ℃ steam flows in the descending submerged pipeline, there would be, very approximately, only half of heat losses to the sea, since the heat flux is proportional to the temperature difference between two exchanging fluids and the temperature difference would drop from 495 ℃ to 275 ℃, if the seawater temperature is fixed at 5 ℃.

This means to have, next to the steam storage system, also the low temperature reservoir on the seafloor, allowing also to have thin water tank wall.
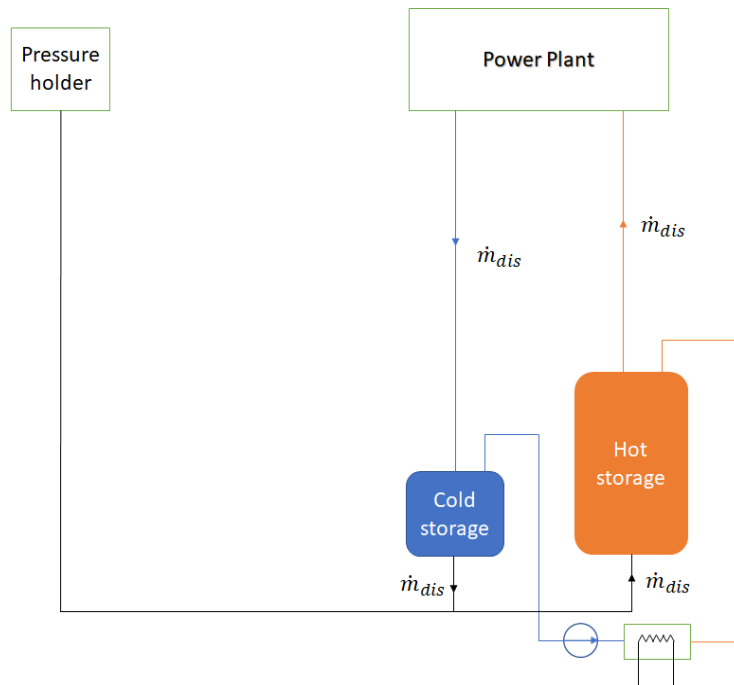
Figure 10 – Second system configuration, discharging process

The third benefit of this system configuration is to take advantage of the much higher density of water compared to the one of steam. In fact, being the pipelines vertical end extremely long, the static pressure due to gravity can´t be neglected even if steam is flowing. A column

of steam of $H = 2500\ m$ at $T = 500\ °C$ and $p = 250\ bar$ ($\rho = 89,75\ kg/m^3$) corresponds to a static pressure of:

$$p_{st} = \rho\, g\, H \approx 22\ bar \qquad (3.7)$$

This value of static pressure must be subtracted to the formula of pressure losses calculation in descending steam line and it must be added in case of ascending pipeline. If water flows in the pipeline at inlet temperature of $T = 280\ °C$ and $p = 250\ bar$, the density of the medium is one order of magnitude higher that the steam case: $\rho = 777\ kg/m^3$. The resulting static pressure is:

$$p_{st} = \rho\, g\, H \approx 190\ bar \qquad (3.8)$$

This value subtracted from the total pressure losses in the water pipe with inlet pressure of 250 bar would give rise to a negative value of pressure losses, namely there is an important gain in pressure head. For this reason, if descending pipeline was water filled, there wouldn´t be the need of having high pressure at pipeline inlet, meaning the pumping system of the Rankine cycle would require less input energy.

To conclude, the roundtrip efficient of energy storage system decreases drastically without the presence of a preheated water reservoir. Discharging process is shown in figure 10, during which hot storage tank is emptied and cold storage tank is filled up; charging process is shown in the next figure. It happens completely on the seafloor if an electric heater is considered.
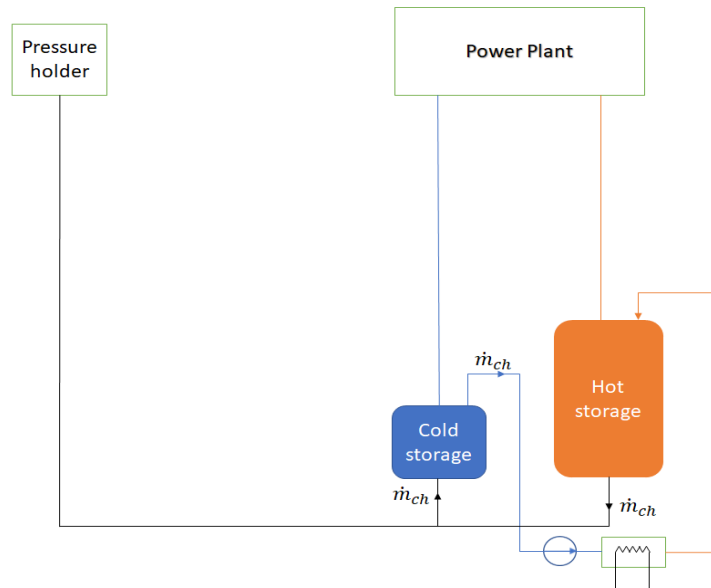
Figure 11 – Second system configuration, charging process with electric heater

The charging pipeline in this second configuration would be much shorter and less challenging than the discharging ones. It lies on the seafloor together with the electric heater, since it connects the cold to the hot storage and they both are installed underwater. The pressure at the top of both tanks is the same, therefore a pump is required only to compensate for the pressure losses in the charging pipeline.

Both the long vertical pipelines are theoretically discharging pipelines because the mass flow rates in both pipelines flow simultaneously and have the same value. In fact, after being expanded and condensed, the working fluid is preheated to the cold storage temperature and flows continuously towards the seafloor.

The charging mass flow rate is different or can be different from the discharging one in both configurations. The estimation problem is performed considering the second system configuration, but also the vertical descending steam pipeline of the first configuration will be analysed.

3.2.4 Suitable locations

The reference power cycle has inlet turbine pressure of $226\ bar$ and the static pressure loss in the ascending steam pipeline are approximately known: underwater tanks should contain pressurized fluid at least at a pressure of $\sim 250\ bar$.

Using the free software project OpenSeaMap [19], few examples of suitable locations are shown. In Europe many possible locations are available in the Mediterranean Sea.

A suitable location can be Algiers on the north coast of Africa, where a depth of $2500\ m$ is located at around $12\ Km$ from the coast. North African BattMarines installations seems extremely attractive to be coupled with PV generated electricity, in fact the sun in these locations can shine during the day without any interruption for long periods, up to weeks during summer season, and big EES systems would be perfect to never lose surplus of renewable generated electricity.
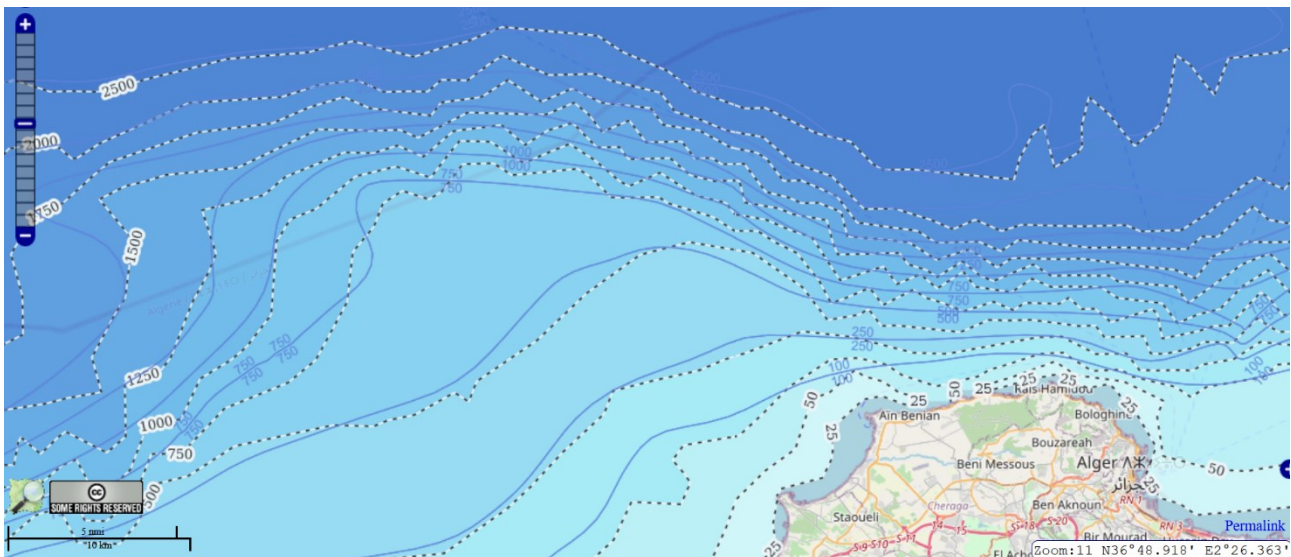
Figure 12 – Depth profile of the sea in front of Algiers coast

Available locations have been found also in Italy. In the Tyrrhenian Sea, off the coast of the city of Imperia, the sea reaches a depth of $2000\ m$ at around $20\ Km$ and a depth of $2500\ m$ at around $30\ Km$. Similar profile for south France coast (Nice, Marseille).
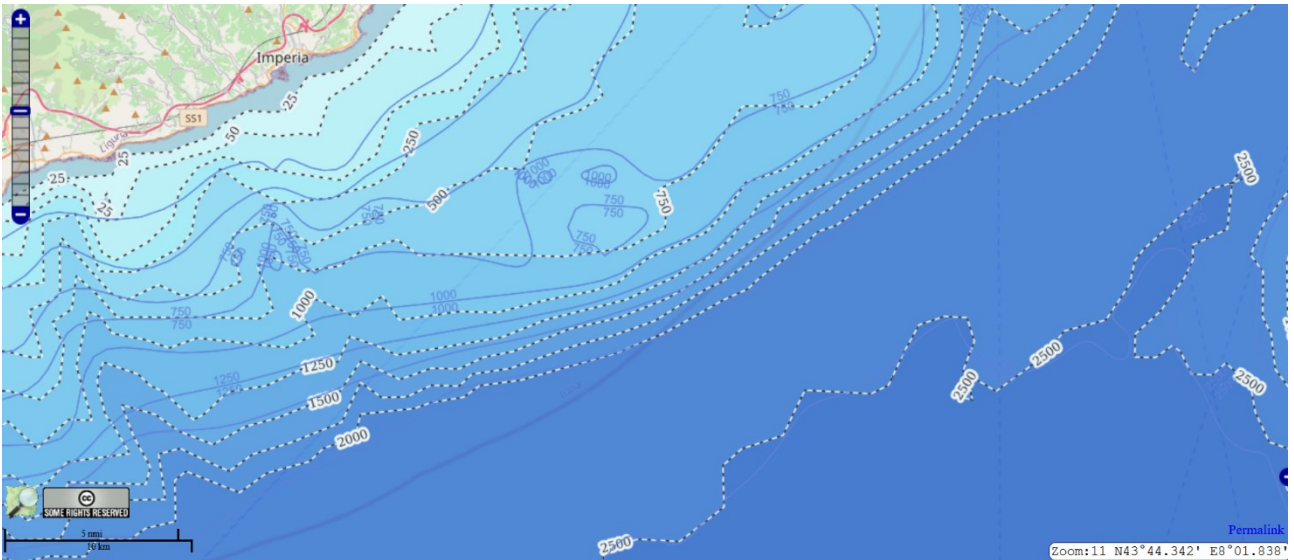
Figure 13 - Depth profile of the sea in front of Ligurian coast

A suitable location in south Italy is in Sicily. Off the coast of the city of Siracusa, the same sea water depth is reached at less than $10 \, Km$.

For such short distances, a potential alternative solution could be to have the whole power plant installed on the coast instead of a floating platform. The investment cost would be reduced without the necessity of having a platform, but pipelines connecting the plant to the storage system would face higher thermal losses and pressure losses due to increase in length and change of inclination.
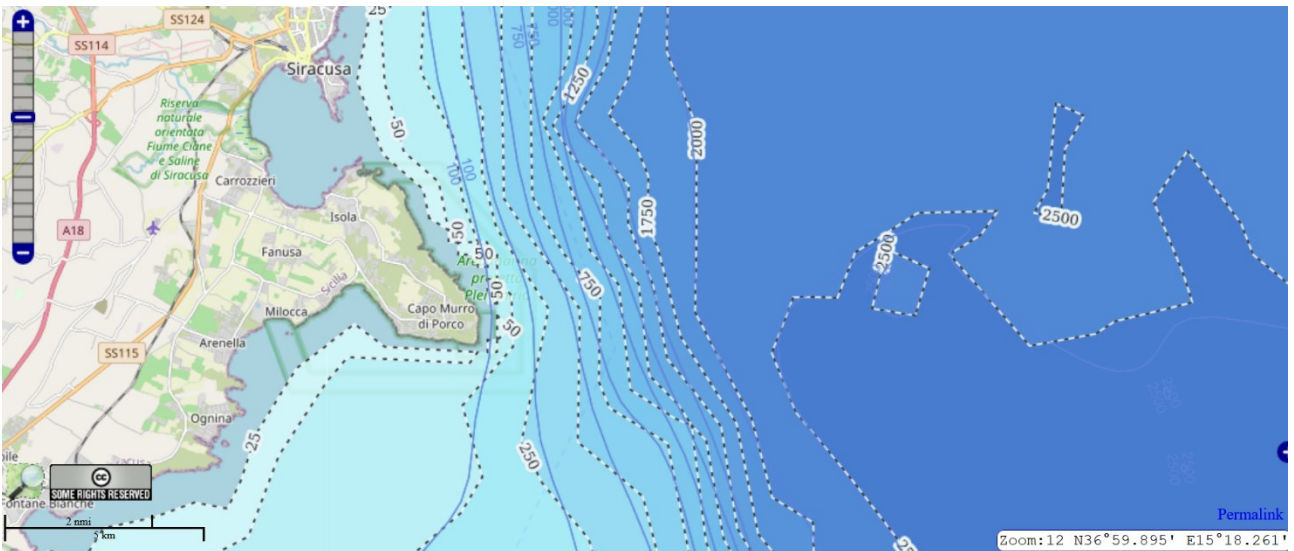
Figure 14 - Depth profile of the sea in front of Siracusa

The geographical constraint exists and will be really one of the decisive factors for the potential technology development, but it looks there are countries in which lot of locations would be available (Chile, Oceania, Japan). PHES has an as well strong constraint, but there are mountainous territories in which enough locations have been found as suitable and huge amount of energy is stored in some regions of the world.

It wouldn´t make any sense trying to develop another big-scale storage technology with the same geographical constraint of PHES. But these constraints are much different, therefore BattMarines could become a sort of alternative to PHES, for some of those locations where there are no mountains.

4 MATERIAL SELECTION

A material research is carried in this chapter, with the main goal of finding suitable thermal insulating materials able to work in such hostile environments.

The two most common construction materials nowadays are steel and concrete.

Austenitic stainless steel is used in common supercritical steam pipeline in power plants. Stainless steel is defined as iron-base alloy containing at least 10 % chromium, a composition that prevents the iron from rusting and also improves thermal properties. Austenitic is one of the five stainless steel classes, widely used in both conventional and nuclear power plants because of their excellent corrosion resistance and mechanical properties at elevated temperatures.

The main interest of the paper is to discuss the energetical feasibility of the storage system. Thermal behaviour of components, i.e., their thermal or energetic efficiency, is therefore the most significant to be studied. For thermal insulation purpose, two are the main material properties that have to be always considered: thermal conductivity and thermal capacity. Heat losses are proportional to the first, while the second influences the thermal inertia of the system.

Thermal conductivity of austenitic stainless steels lays in between $\lambda_s = 15 - 20 \, W/m \, K$ at ambient and high temperatures [20], while concerning the heat capacity, an average value can be set at $c_s = 500 \, J/Kg \, K$. It could be defined as a poor thermal conductor with a quite low capacity.

Concrete is a very common and cheap material also in marine application. It is a composite material composed of fine aggregate bonded together with a fluid cement that hardens over time. Its mechanical strength is more than one order of magnitude lower than the steel one, while its thermal conductivity at high temperatures has one order of magnitude less than steel, namely $\lambda_c = 1,5 \, W/m \, K$ [21]. Concrete is a poor thermal insulator.

Disadvantages of this material are the limited maximum service temperature around 500 ℃ and its high heat capacity of $c_c = 1000 \, J/Kg \, K$. A great amount of energy is required to heat up concrete to the operating temperature, approximately double the energy required for stainless steel. This will have to be carefully considered since a huge quantity of material is composing this system.

Both materials have great corrosion resistance and excellent durability in fresh water.

4.1 Insulator research

Commonly used thermal insulation materials, for example in buildings, do not have to withstand high temperatures and mechanical loads as in these underwater components. A good thermal insulator is considered to have a thermal conductivity lower than or in the order of $0,1\ W/m\ K$.

If the supercritical steam has to be stored for days without losing consistent amount of energy, probably a too thick concrete layer is required to properly insulate and later it will be estimated to prove it, therefore a suitable good insulator is desired.

Ansys Granta EduPack is used for this purpose of insulator research. It is a unique set of teaching resources that support materials education providing a comprehensive database of materials and process information that is always kept up to date with the latest resources and data [22].
Three are the properties of interest:

- the material has to be a good heat insulator; therefore, it should be characterized by an enough low thermal conductivity value;

- supercritical steam temperatures have to be withstood, so the maximum operating temperature should have a lower limit of $550\ ℃ - 500\ ℃$, depending on the specific hot storage steam conditions;

- the wall faces pressurized steam on one side and high-pressure seawater on the other, therefore it is under compression. Its compressive strength should be higher than the pressure of those fluids, for example higher than $25\ MPa$, plus a safety operation margin.

It is possible to create charts to visualize material properties as an integral step to material selection. Bubble charts can be created using properties that have a numerical range or a continuous value and this is the case of the three properties of interest. More databases are available in the software, namely introductory and advanced levels.
The three following graphs have been plotted in the advanced database, in which almost all known materials are reported: thermal conductivity vs maximum service temperature, compressive strength vs maximum service temperature, compressive strength vs thermal conductivity.

In these kind of plots not only single materials can be compared each other, but also materials of the same type or family can be gathered together to offer a better visualization of the possible working region of groups of material.
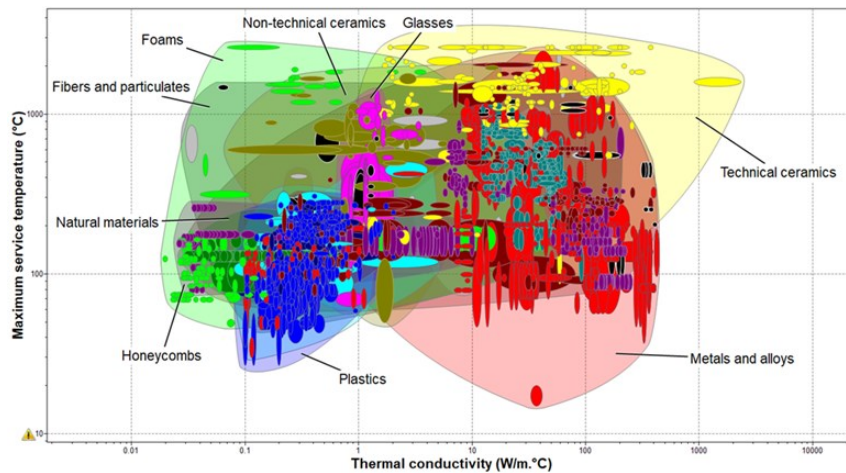
Figure 15 – Thermal conductivity vs Maximum service temperature

Thermal properties are illustrated in figure 15. It suggests that it isn't hard to find materials suitable to work up to temperatures higher than 500 °C. There are some kinds of foams, ceramics, glasses, metals and alloys that can withstand such high temperatures.

Concerning thermal conductivity, it has been said common thermal insulators are characterized by values lower than $0,1\ W/m\,K$. Some natural materials, foams, honeycombs, fibers and particulates belongs to this region. Materials with one order on magnitude higher thermal conductivity can be seen as poor thermal insulator, as for example concrete.
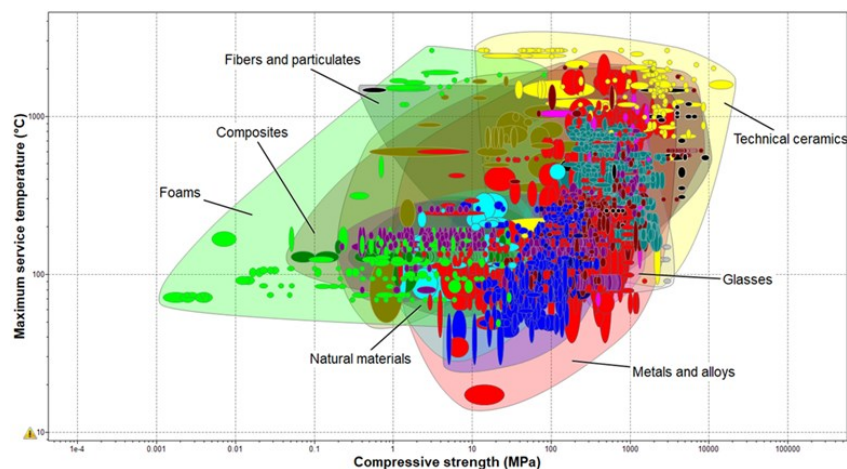
Figure 16 – Compressive strength vs Maximum service temperature

Concerning the compressive strength, classes of materials available in the desired range are many: polymers, ceramics, composites, glasses, metals and some natural materials. Even combining the request of maximum service temperature and compressive strength, a remarkable amount of material families would be capable of satisfying it.
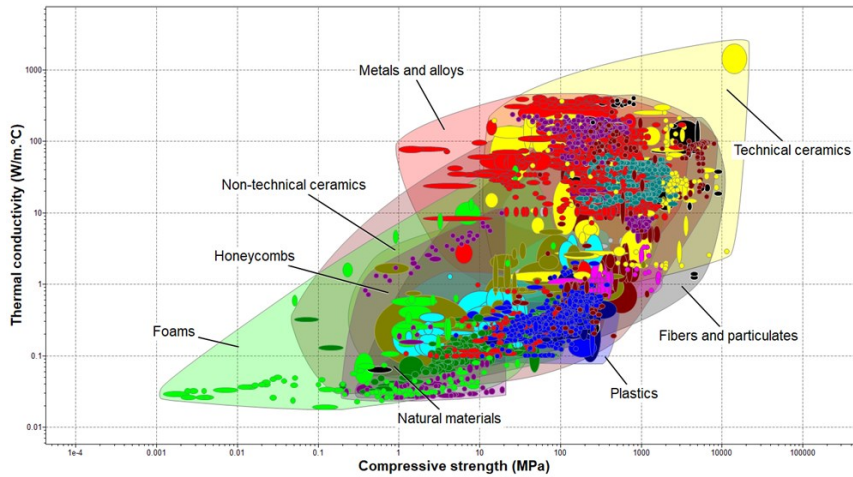
Figure 17 – Compressive strength vs Thermal conductivity

Figure 17 shows that all good heat insulators haven´t enough compressive strength. Only one material looks suitable from the third graph viewpoint: cardboard. Unfortunately, it can´t even reach a temperature of 100 ℃.

Observing the three graphs together, problems occur when we try to find a material that accommodates all requirements. In fact, the foams region does not reach the minimum needed compressive strength and the natural materials region can't reach the maximum service temperature threshold.

With the help of this advanced database, it is possible to search more in detail between a lot of existing materials. The first graph is represented again but only the region we are interested in is highlighted.
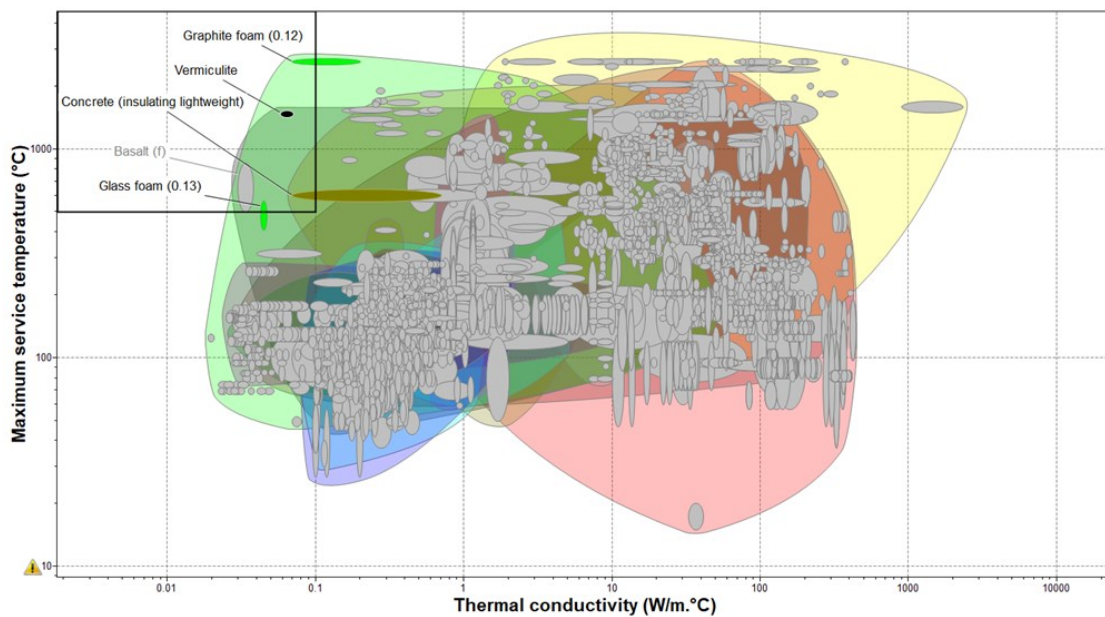
Figure 18 – Region of interest

The working region of the wanted material is marked with a black rectangle in the graph. Only few materials satisfy thermal requirements. In particular they are five: graphite foam, glass foam, basalt fibre, vermiculite and a type of lightweight concrete. This last one (long horizontal brown ellipse) can be rejected since it can reach a maximum compressive strength of $8\ MPa$ only and also the thermal conductivity would be lower than the wanted limit at temperature higher than the room temperature (the displayed thermal conductivities are valid at room temperature, around 23 ℃).

Vermiculite is a mineral composed of hydrated laminar magnesium-aluminium-iron silicate [23]. It has many applications as acoustic insulator but also as thermal insulator. Unfortunately, its compressive strength is even lower than $1\ MPa$.

Basalt is an extrusive rock formed from rapid cooling of lava rich in magnesium and iron. Basalt fibre can be obtained from it and then it is used in textile applications for fire protection, as a reinforcing material in concrete or as high temperature insulation [24]. Its compressive strength is much higher than the needed one and the thermal conductivity lower than $0,05\ W/mK$. This material would be perfect, but it is a fiber and an excessive amount of it would be required to build the wall of a $100\ m$ diameter tank. Moreover, this means enormous costs.

Basalt rock could be used in the form of particulate material, but thermal conductivity of solid basalt rock lays between $2-3\ W/m\ K$ [25], therefore only slightly lower value could be reached with particulates basalt insulation layer. It can be seen as a very poor thermal insulator; therefore, a remarkably thick insulation layer would be desired.
Graphite foam seems to be a really interesting solution, however reported thermal properties, in particular the thermal conductivity range, are wrong [26].

At this point, exclusively glass foam remains. Its thermal conductivity at room temperature is low enough to be considered an excellent heat insulator, but it can´t withstand temperatures slightly higher than the hot storage one and, certainly, these foams do not have the needed compressive strength.

However, some porous material able to work at high temperatures, can be an interesting solution when they are characterized by an open-cell structure, meaning when all pores are connected to each other. In fact, it is theoretically feasible to inject pressurized gas in the porous material to have high pressure in the pores themselves, basically creating a pressurized ambient in the solid foam.

Imagine the tank wall to be composed by two stainless steel layers facing both fluids with an insulation open-cell porous material layer in the middle. All three layers undergo compression because on both external and internal side they face a fluid under pressure that squashes them. However, if an inner pressure force exists in the middle layer, equivalent to the pressure of the two fluids, the compression force seen by the foam layer is null and exclusively the foam solid matrix has to withstand such compression force, being immersed in a pressurized ambient.
Basically, it is the same concept of having an air layer in between the steel. If the air is at the same pressure of both fluids, only two steel layers are under compression. The problem of

having only air as insulator is related to natural convection heat exchange: very thin air layers are good thermal insulators, since the fluid is almost completely still, conduction is the main heat transfer mechanism occurring together with radiation and thermal conductivity of air is extremely low; however, increasing the thickness, increases the contribution of natural convection and heat is easily transferred due to air motion. Moreover, radiation effect increases when the temperature difference between two surfaces facing the air increases and this is the case if one single thick air layer exists instead of many thinner layers.

In conclusion, air or other low conductive gases can be used with small thicknesses, so a succession of gas layers and low conductive solid layers should be needed and could be a possible solution to the problem.

Having a porous material with high porosity, namely with great amount of air in it and with small pores dimension, would mean to create a huge number of solid barriers enclosed by steel surfaces with huge number of air layers in between: radiation effect would be drastically reduced. It is comparable to a configuration with massive amount of air and solid layers repeating each other.

Unfortunately, foam glass has a closed-cell structure in which all pores are isolated [27], hence it isn´t possible to create a pressurized ambient in the porous structure. Since common insulation materials aren´t usable in this application, the research region of the material has to be expanded: materials with room temperature thermal conductivity $< 1\ W/m\ K$ are investigated.
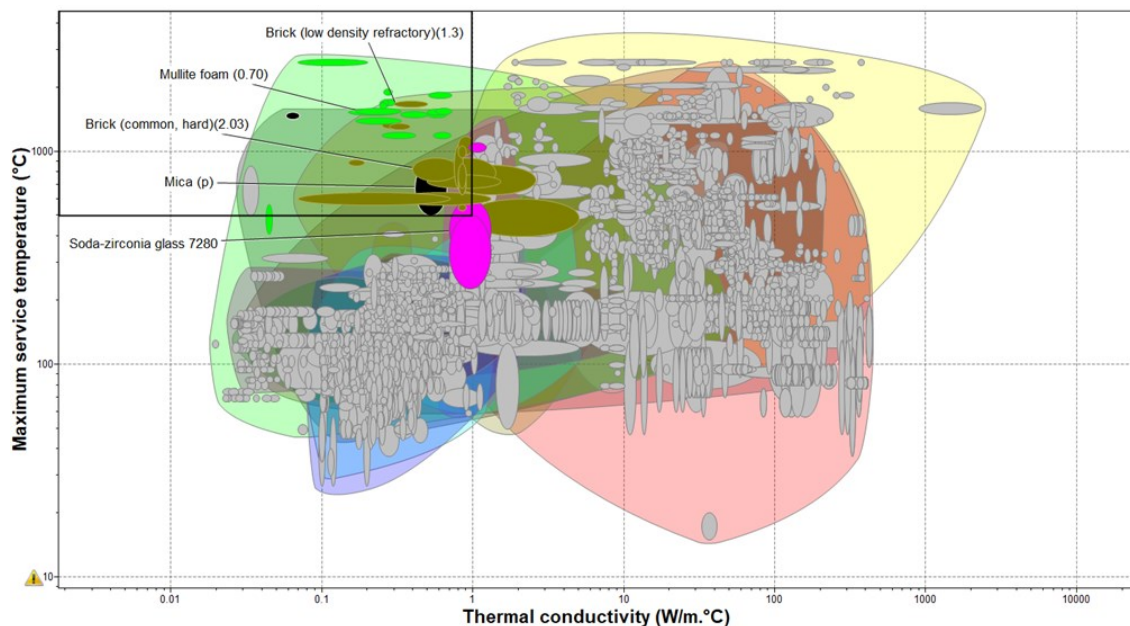
Figure 19 – Expanded region of interest

More materials are included in this new graph region: some foams including alumina foam, mullite foam and cordierite foam. Additionally, mica mineral and some kind of glasses belongs marginally to the region.

Glass has a thermal conductivity of a poor insulator around $\lambda_{glass} = 0{,}8 - 1\ W/m\ K$ at room temperature, that increases with the temperature. A reasonable solution is to use glass particulates instead of glass foam, or any other cheap and sufficiently resistant low conductive material. Having a thick layer of glass particulates would mean for the heat to have a more

difficult path towards the cold surface, due to the presence of air in the wall and the smallness of the contact area between glass fragments.

Among the extended region materials, the one characterized by the lowest value of λ is the open-cell structure mullite foam.

Mullite is a rare silicate material that can be found in two different forms: $3Al_2O_3 \cdot 2SiO_2$ or $2Al_2O_3 \cdot SiO_2$. Although it exists as a natural mineral, occurrences in nature are extremely rare [28]. Industry relies on synthetic mullites which are achieved by melting various alumina-silicates such as kaolin, clays or fine silica and alumina to high temperatures. It is widely used for refractory applications.

It has great mechanical properties, in particular a compressive strength in the order of $1\ GPa$ [29], its melting point is $> 1800\ ℃,$ that is higher than the one of steel, and the thermal conductivity belongs to the interval $2 - 6\ W/m\ K$.

Having a foam of this material would allow to reach the desired thermal conductivity order of magnitude. Moreover, the open-cell structure of the foam itself would permit to inject a pressurized gas in the all-connected pores. If the mullite foam is contained in between two solid material layers, a pressurized ambient in the intermediate foam layer can be created and the solid matrix of the foam, namely the mullite, can withstand up to huge compressive loads. The research is conducted both for the hot storage tank and the steam pipeline insulation, since the deeper parts of the pipeline face the same environmental condition of tanks. The involved temperatures are the same and therefore thermal properties need to be equal or similar. Only the part of pipelines that is closer to the see surface could be insulated with a material less resistant in compression, but it won´t be the case since no other materials have been found.

The descending water pipeline and the cold storage tank insulation could probably be designed with other materials, in fact the involved temperatures are much lower: materials have to support maximum temperatures in the order of $T_{cs} \cong 270\ ℃$. The potential insulation materials still have to withstand the same great compressive strength of before at low depths and have a very low heat conductivity value, but their maximum operating service temperature can be lower.

Four possible insulation layer materials for steam components are briefly studied and compared. Temperatures in the internal surface and the external one are considered to be $T_{in} = 525\ ℃$ and $T_{out} = 5\ ℃$ (corresponding to sea water and steam temperatures, that is like having isothermal steel layers).
Suitable materials for the steam pipeline are of course appropriate for the water pipeline too. However, also one material that can be interesting for the water pipeline only has been found and is described.

4.2 Air

Air is a gas with thermal conductivity of $\lambda_{air} = 0,026\ W/m\ K$ at ambient temperature and pressure with the great advantage of being basically free. In this specific application, if thermal conductivity is hypothesized to be constant in the thickness and it is evaluated [30] at average temperature in the layer, the value is almost double, but still in the order of a good insulator:

$$\lambda_{air}(260\ °\text{C}, 250\ bar) = 0,0485\ W/m\ K \qquad (4.1)$$

Heat is transferred across an air space by a combination of conduction, convection and radiation. Heat transfer by conduction is inversely proportional to depth of the air space. Convection is mainly dependent on the height of the air space and its depth. Heat transfer by radiation is relatively independent of both thickness and height, but is greatly dependent on the reflectivity of the internal surfaces.

This last heat transfer mechanism can´t be neglected if temperature difference between the two air facing surfaces is consistent, reason for which it is preferred to have multiple air layers to break up the total temperature difference.
Air gaps are widely used as building insulation technique, and they are absolutely effective when the layer has little thickness. Convection contribution becomes greater than the conduction one already at thickness of few centimetres. Figure 20 [31] shows that even for low temperature insulation with normal materials, radiation heat transfer dominates at small thicknesses and convection contribution becomes greater than the conduction one already at thickness $> 1\ cm$.
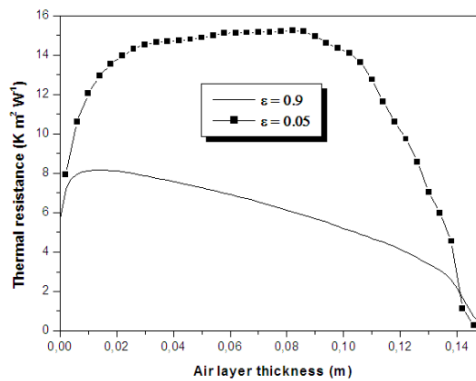
Figure 20 - Thermal resistance as a function of the air cavity thickness, case of a cinderblock

In case of internal surfaces of low reflective material, slightly bigger thicknesses can be achieved keeping the heat resistance value to a constant level. Increasing the air cavity thickness beyond these limits will not increase the thermal resistance of the cavity due to the development of natural convection.
Wall of the hot storage tank has a thickness in the order of meters; therefore convection would be surely too dominant. Its combination with radiation heat transfer between two surfaces of around $\Delta T = 500\ °\text{C}$ makes the effect of conduction negligible.

4.3 Concrete

Concrete is another potential usable cheap material. Advantage of concrete is the reduction of its thermal conductivity with increase of temperature. It remains anyway a poor insulator, but a thick wall would allow to obtain good insulation levels.
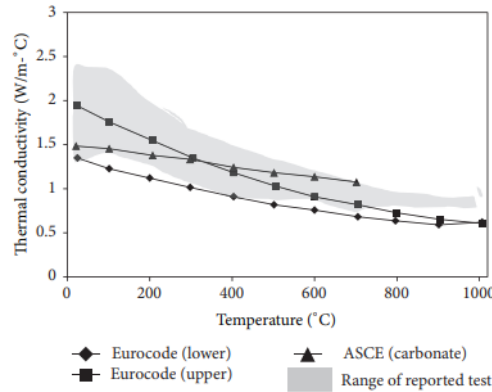
Figure 21 – Conductivity of concrete with temperature [21]

In order to be the most general possible, the grey area of all reported tests is considered. At room temperature an average value between report tests is $\lambda_c = 2\ W/m\,K$, while at maximum operating temperature of $\sim 500\ °C$ it lays around $\lambda_c = 1,2\ W/m\,K$. A logical average value valid from room temperature to hot storage temperature can be $\lambda_c = 1,5\ W/m\,K$.

Mechanical properties of concrete deteriorate with increasing temperature. Compressive strength isn´t an exception, but literature test data show that the compressive strength at $\sim 500\ °C$ can lay in a range varying from ambient temperature compressive strength to half of that value. A strong concrete is required to have adequate mechanical properties at high temperature.
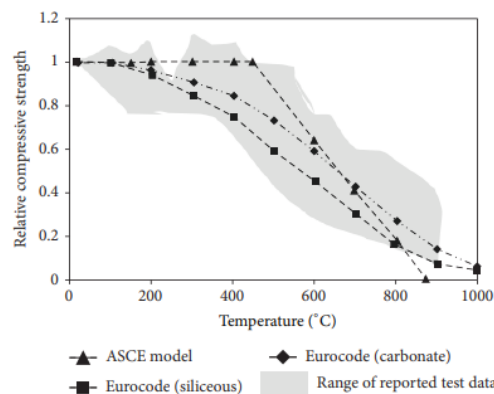
Figure 22 – Compressive strength of concrete with temperature [21]

Tensile strength of concrete is about 10 % of its compressive strength and steel is used to increase it to greater levels, to obtain the so-called prestressed concrete. Steel bars are bad for

thermal conductivity, but they can have small impact if every bar lays on an isothermal surface.

4.4 Glass particulate

Glass is a common and cheap material with room temperature thermal conductivity laying around $\lambda_{glass} = 0.8 - 1\,W/m\,K$, that is approximately half compared to concrete conductivity at room temperature, but at high temperature this value slightly increases. The below chart displays a thermal conductivity of $\lambda_{glass} \cong 1.4\,W/m\,K$ at hot storage temperature. An average value in the operating temperature range of steam components can be set to $\lambda_{glass} \cong 1.2\,W/m\,K$.
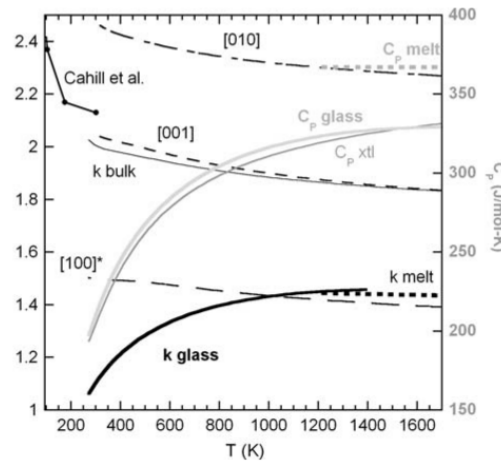
Figure 23 – glass conductivity vs temperature

The idea of using particulate material comes from the necessity of deleting radiation and convection heat transfer in an air insulation layer. It is possible to create a kind of mixture of low conductive gas and a low conductive solid material, simply by inserting glass fragments into the pressurized air layer. Glass fragments are considered to be of spherical shape and they can be found on the market of different sizes, from the μm scale to the mm scale. The smaller the spheres diameter, the smaller the pores dimension and therefore the lower the effect of radiation and convection heat transfer.

The porosity of porous or granular materials is defined as:

$$\varphi = V_{empty}/V_{tot} \tag{4.2}$$

Granular packing geometry has an impact on the effective thermal conductivity of the insulation layer. If all the spheres have exactly the same dimension, two limit configurations can occur: straight or close packing. The packing angle lays in the interval $\pi/3 < \theta < \pi/2$ and the porosity is a function of it [32]:

$$\varphi = 1 - \frac{\pi}{6\,(1 - cos\theta)\sqrt{1 + 2\,cos\theta}} \qquad (4.3)$$

$$25,95\,\% < \varphi < 47,64\,\%$$

In the most simplified model, thermal conductivity of particulate material follow a general rule of mixture. Radiation heat transfer can be neglected together with convection if empty spaces are narrow enough, approximate conductivity is therefore underestimated.

$$\lambda = \lambda_{air}\,\varphi + \lambda_{glass}(1 - \varphi) \qquad (4.4)$$

$$0,65\,W/m\,K < \lambda < 0,9\,W/m\,K$$

Conductivity of air is almost independent from pressure but increases with temperature. It has been evaluated at average wall temperature and it resulted in $\lambda_{air} = 0,042\,W/m\,K$.
With maximum porosity the value is almost halved, still not considerable a good insulator. Compressive strength of glass is on order of magnitude greater than concrete, glass spheres can easily withstand the pressure of the air in the particulate layer
Disadvantage of glass is its maximum operating temperature of $\sim 500\,°C$, therefore it couldn't be used to insulate at higher steam temperatures. It seems more appropiate for water components.

An average value of glass and air thermal conductivities in the temperature range of water components are $\lambda_{glass} \cong 1,15\,W/m\,K$ and $\lambda_{air} = 0,034\,W/m\,K$. Carrying out the same computation, slightly lower values are obtained:

$$0,62\,W/m\,K < \lambda < 0,86\,W/m\,K$$

4.5 Mullite foam

Glass foam would be the perfect material wanted if its porous structure was open-cell type instead of closed-cell. Mullite foam has been found to be the open-cell foam structure with the lowest thermal conductivity able to work at least at the desired temperature. Mullite solid material has extremely high compressive strength and for this reason, the mullite foam shouldn´t have mechanical problems being immersed in a fluid at underwater tank pressure, being its solid matrix extremely resistant.

Mullite insulation bricks with porosity levels up to 80 % are available on the market. They are usually used in the thermal preservation layers in various industrial furnaces and kilns in metallurgical industry, ceramic industry, chemical industry and can be used in direct contact with the flame [33].
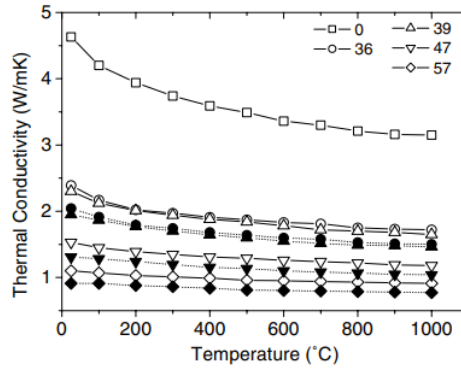
Figure 24 - Thermal conductivity vs. temperature for mullite samples of different porosity percentages [34]

Thermal conductivity of mullite decreases with temperature and the same is true for mullite foams with quite low porosity level. The more the porosity level, the less the decrease of conductivity with temperature increase: it is the effect of radiation heat transfer, which becomes more dominant the higher temperatures, but doesn´t play a big role at low porosity levels.

Many different typologies of insulation mullite foam bricks exists [33] and the JM23 model is considered. It is the lightest one, with the lowest classification temperature and thermal conductivity among all different products[35]. It can withstand $1260\ ℃$ and it could therefore be used at much higher temperatures. Conductivity seems to increase linearly with temperature at this high porosity; this table is reported from the product technical datasheet, temperature in $℃$ and conductivity in $W/m\ K$:

Temperature [℃]	Thermal conductivity [$W/m\ K$]
400	0,14
600	0,16
800	0,18
1000	0,20

From extrapolation, the value at $200\ ℃$ can be set at $0,12\ W/m\ K$. A constant value corresponding to hot storage tank wall average temperature has to be fixed. In order not to underestimate the thermal losses, Mullite foam brick insulation layer can be considered to have a constant thermal conductivity of $\lambda_{foam} = 0,14\ W/m\ K$.

Instead of a brick configuration, a little decrease in condictivity occurs if a gravel structure id used, basically a mullite foam particulate layer. Less material would be required.

Heat capacity of mullite foam bricks is in between the one of steel and the one of concrete, but being the material much lighter, lower amount of heat is required to warm up the brick layer to the operating temperatures.

A material with the desired conductivity order of magnitude has been found. Unfortunately, no applications of this kind exist for foamed materials. Tests have to be done to assure this material can operate in a $25\ MPa$ environment.

Figure 25 - Mullite lightweight insulation brick [35]

4.6 Reticulated vitreous carbon (RVC) foam

The region of interest from figure 18 can be expanded to lower temperature values when the research is conducted for water components. With a maximum operating temperature of $\sim 280\ ℃$, another kind of foam structure enters the working region: reticulated vitreous carbon foam. Its maximum operation temperature in air is about 350 ℃, while if installed in an inert ambient it can withstand much higher temperatures.
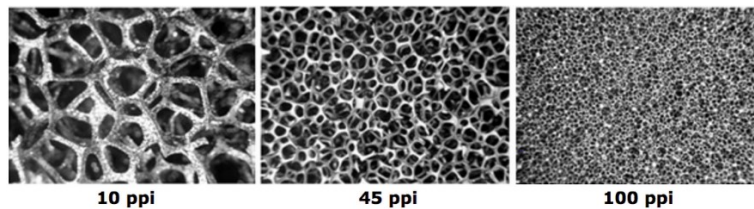
Figure 26 - RVC foam [36]

Solid structure of the foam isn´t as resistant as the mullite foam solid structure, but still quite strong. Thermal conductivity increases with temperature increase; it is reported a value of $0,085\ W/m\ K$ at 200 ℃ [36]. At room temperature its value is found to be 0,045 W/mK after extrapolation.

A value at average water componets wall temperature is fixed at:

$$\lambda \cong 0,08$$

Probably too high price per kilogram but lower quantity is required in weight due to very low density.

5 METHODS

This chapter defines those methods that are going to be used in the next estimation chapter.

In the feasibility study of submerged components, three are the most influencing aspects: pressure losses in the discharging steam pipeline, mechanical stresses and thermal losses characterizing every component.

5.1 Pressure losses analysis

When fluid flows through a pipe there will be a pressure drop that occurs as a result of resistance to flow. It is caused by internal friction of the fluid (viscosity) and friction between fluid and wall.
The pressure drop due to friction is calculated as:

$$\Delta p_f = \frac{1}{2} f \rho w^2 L/d \qquad (5.1)$$

The friction factor f is a dimensionless similarity parameter useful to describe the pressure loss in the straight pipe section. It is determined by empirical formulas available depending on flow regimes, laminar or turbulent. Flow regime is defined by the value of the dimensionless Reynolds number, function of fluid properties and system geometry, as:

$$Re = \rho w d \mu^{-1} \qquad (5.2)$$

Significant number of empirical correlations relate the friction factor to the Reynolds number. One of these is the Konakov correlation, valid for single phase flow in smooth pipes [37]. If Reynolds number lays in the interval $2300 < Re < 10e7$; the following Konakov correlation for the friction factor is valid:

$$f = (1,8log\ (Re) - 1,5)^{-2} \qquad (5.3)$$

This equation corresponds to the smooth pipe line in the Moody diagram, a graph in non-dimensional form that relates the friction factor, the Reynolds number and surface roughness for fully developed flow in a circular pipe. It can be used to predict pressure drop or flow rate down such a pipe.
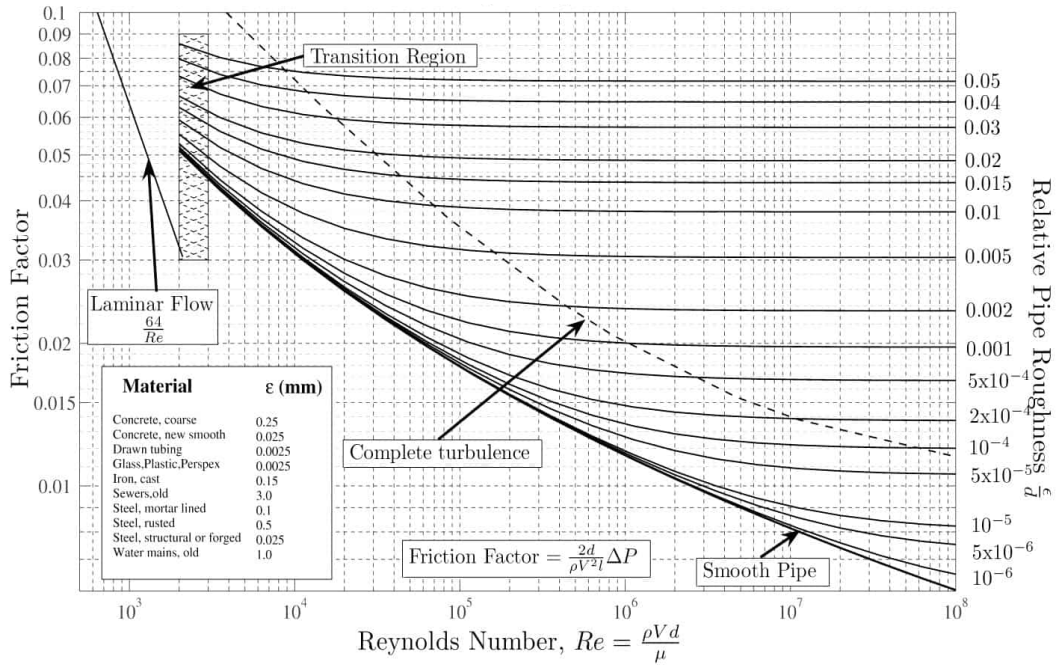
Figure 27 – Moody diagram

Pressure drop can also be significantly affected by a change in elevation in the piping system. If the starting elevation of a pipe is lower than its end elevation, there will be an additional pressure drop. Conversely, if the starting elevation of the pipe is higher than its end elevation, there will be an additional pressure gain.

Therefore, the pressure in vertical pipelines changes also due to the change in the static pressure. Static pressure in a fluid is determined by the height of the column of fluid situated above the considered point.

$$\Delta p_{st} = \rho \, H \, g \tag{5.4}$$

This contribution is expected to be dominant in the water pipeline, where density of the fluid is one order of magnitude higher than steam density.

$$\Delta p_{tot} = \Delta p_f + \Delta p_{st} \tag{5.5}$$

To conclude, a positive sign is given to the static pressure drop in case of descending flow direction and a negative sign is given for ascending flow direction.

5.2 Mechanical stresses analysis

In reservoirs for high pressure fluid, a dedicated theory describes the stress and strain distribution through the thickness of the shell for shell areas which do not include edges or any discontinuity [38]. Two possible cases are described in cylindrical walls, characterized by the following geometric constraints:

- Thin walls

$$\frac{\delta}{r_i} \leq \frac{1}{10} \tag{5.6}$$

- Thick walls

$$\frac{\delta}{r_i} > \frac{1}{10} \tag{5.7}$$

δ is the thickness of the wall and r_i the internal radius of the cylinder. A cylindrical reference system needs to be set, in which the three coordinates are the radial r, the circumferential θ and the axial z.

In thin walls theory [39], the circumferential stress σ_θ is supposed to be constant in the wall thickness and the radial equilibrium of a semi-cylinder is considered to evaluate it.
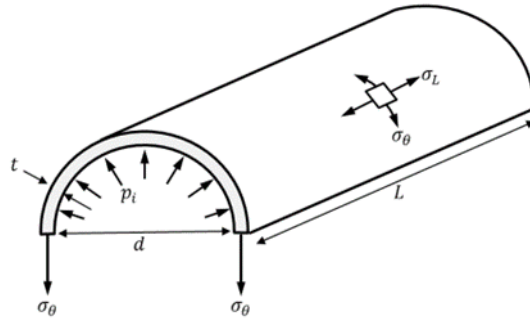
Figure 28 – Forces acting on a semi-cylinder, external pressure is also present

$$2 \, \sigma_\theta \, \delta \, L = p_i \, 2 \, r_i \, L - p_e \, 2 \, r_e \, L \tag{5.8}$$

It leads to the Mariotte formula:

$$\sigma_\theta = \frac{p_i \, r_i - p_e \, r_e}{\delta} \tag{5.9}$$

The radial stress is considered as well constant through the thickness:

$$\sigma_r = p_i - p_e \tag{5.10}$$

Last stress component remaining is the one along the axial direction, also constant. Boundary conditions are required, for example σ_z would be null in case of free unloaded ends, which is anyway not the case.
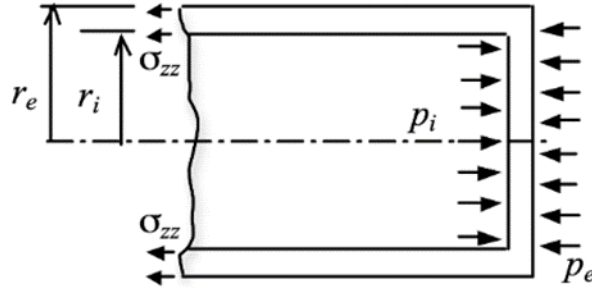
Figure 29 – Forces appearing in the axial equilibrium

$$p_i \, \pi \, r_i^2 - p_e \, \pi \, r_e^2 - \int_{r_i}^{r_e} \sigma_z \, 2 \, \pi \, r \, dr = 0 \qquad (5.11)$$

$$\sigma_z = \frac{p_i \, r_i^2 - p_e \, r_e^2}{r_e^2 - r_i^2} \qquad (5.12)$$

When the internal pressure equals exactly the external one, no stresses in any of the three principal directions act on the structure and therefore it can be seen as stress free. This is the main motivation of this storage technology concept: if this storage system was built on the ground in an atmospheric ambient pressure, there would be the necessity of a much greater wall thickness, in particular the one of the thermal insulating materials that hasn´t as good mechanical properties as steel.

Probably, the estimation of stresses in the tanks by means of the thin wall theory isn´t accurate enough, in fact the thickness will be in the order of meters and it is hard to think of constant stresses in such wall. Nevertheless, the theory is applicable and tell us the structure is stress free in case of zero pressure difference.

A different theory should be used to study stresses distribution in the top cover of the tank, namely the axisymmetric plates theory. A plate is a structural element in which one dimension is negligible with respect to the other two.

However, it won´t be discussed because the approach is the same and it isn´t challenging from the mechanical point of view, as it is instead the discharging steam pipeline.

Pipelines are characterized by considerably thick wall, being the thickness comparable to the inner radius. In thick wall theory, the following hypothesis are assumed: homogeneous isotropic material, only radial loads and complete axial symmetry of geometry, load and material. This means the stress status depends on one independent variable: the radial coordinate r. This model is more complex than the thin walls model, in fact there are seven unknown variables and seven equations are needed [38] to reach the following general differential equation:

$$\frac{d^2\sigma_r}{dr^2} + \frac{3}{r}\frac{d\sigma_r}{dr} + \frac{1}{r}\frac{E}{1-\gamma}\beta\frac{dT}{dr} = 0 \qquad (5.13)$$

When stresses are only caused by pressure while temperature is constant through the wall thickness, this general differential equation is homogeneous and the so called Lamè equations are obtained:

$$\sigma_{r,m} = A - \frac{B}{r^2} \tag{5.14}$$

$$\sigma_{\theta,m} = A + \frac{B}{r^2} \tag{5.15}$$

Radial and circumferential stresses through the thickness of the thick wall can be evaluated. The integration constants A and B can be found from boundary conditions, applying the correct pressure conditions at internal and external radius of the vessel.

$$\sigma_{r,m} = -p_i \frac{r_i^2/\chi^2 - \xi^2}{1 - \xi^2} - p_e \frac{1 - r_i^2/\chi^2}{1 - \xi^2} \tag{5.16}$$

$$\sigma_{\theta,m} = p_i \frac{r_i^2/\chi^2 + \xi^2}{1 - \xi^2} - p_e \frac{1 + r_i^2/\chi^2}{1 - \xi^2} \tag{5.17}$$

One dimensionless variable has been used in place of radius to have simple formulation, $\chi = r/r_e$.

$$\chi = r_i/r_e = \xi \text{ which corresponds to internal radius}$$

$$\chi = r_e/r_e = 1 \text{ which corresponds to external radius}$$

The axial stress is related to constraint conditions and end edges axially constrained condition is taken as reference, meaning:

$$\varepsilon_z = 0 = \frac{1}{E}[\sigma_z - \gamma(\sigma_r + \sigma_\theta)] \tag{5.18}$$

$$\sigma_{z,m} = \gamma(\sigma_{r,m} + \sigma_{\theta,m}) \tag{5.19}$$

If there is a strong variable temperature field across the thickness, i.e., a radial thermal gradient, the effect of temperature must be considered. In fact, thermal induced mechanical stresses can´t be neglected sometimes. In pipelines this is the case, especially in the steam one, where a difference of $\Delta T \approx 500$ °C exists in a quite small thickness. Given an internal and external temperature, the local temperature at the coordinate r is described by a logarithmic equation:

$$T = T_e - (T_e - T_i) \frac{\ln(r/r_e)}{\ln(r_i/r_e)} \tag{5.20}$$

Substituting (5.20) in (5.13) and solving, a complete solution is obtained: it is the sum of the Lamè homogeneous equation and the particular integral.

$$\sigma_{r,th} = A - \frac{B}{r^2} + K\, ln(r/r_e) \tag{5.21}$$

$$\sigma_{\theta,th} = A + \frac{B}{r^2} + K\,(1 + ln\,(r/r_e)) \tag{5.22}$$

$$K = \frac{E\,\beta\,(T_e - T_i)}{2\,(1 - \gamma)\,\ln(r_i/r_e)} \tag{5.23}$$

Boundary conditions consist in setting the radial stress equal to zero on both inner and outer radius, that means only temperature effect is considered and not the pressure. This allow to obtain integration constants, radial and circumferential stresses in a generic point of the vessel are then:

$$\sigma_{r,th} = K\,ln\xi\,(\frac{\xi^2}{1 - \xi^2}\left(1 - \frac{1}{\chi^2}\right) + \frac{ln\chi}{ln\xi}) \tag{5.24}$$

$$\sigma_{\theta,th} = K\,ln\xi\,(\frac{\xi^2}{1 - \xi^2}\left(1 + \frac{1}{\chi^2}\right) + \frac{1 + ln\chi}{ln\xi}) \tag{5.25}$$

Also the axial stress varies along the thickness and combining the elasticity equation with these two previous equations it is calculated in case of end edges axially constraint (axial strain is null):

$$\sigma_{z,th} = \gamma\,K\,ln\xi\,(\frac{2\xi^2}{1 - \xi^2} + \frac{1 + 2\,ln\chi}{ln\xi}) \tag{5.26}$$

Because both stresses, mechanical and thermal induced, simultaneously exist in the wall, superimposition of effect can be applied [40] in all three principal directions:

$$\sigma = \sigma_m + \sigma_{th} \tag{5.27}$$

One last formula must be introduced, that is a simple estimation of the minimum required pipe wall thickness as function of inner pressure. It will be required when considering foam material thermal insulation.

$$\delta_{min} = \frac{p_i\,D_{out}}{2\,(QF\,\sigma_{\theta,max} + p_i\,Y)} \tag{5.28}$$

will be used according to [41], where quality factor QF and a coefficient Y can be selected depending on the pipe configuration.

5.3 Thermal losses analysis

Heat losses in the tank can be modelled in two different ideal ways.

Perfect thermal stratification: due to great density differences, the colder subcritical water in the tank remains constantly in the lower zone, while the hot supercritical water remains in the upper zone. We can distinguish between two constantly separated volumes, both at constant temperature, the upper one at the highest temperature of $525\,°C$ and the bottom one at the lowest temperature of $5\,°C$. Heat exchange with the ambient through walls and heat conduction towards the bottom water layer don´t cause a change in temperature in the upper layer, but they enhance "condensation" of some of the steam, so that the liquid level increases and the steam one decreases. Steam filling level describes the energetic status of the tank.

Perfect mixing: constant temperature in the whole tank, "steam quality" describes the energetic status of the tank and heat losses towards the sea result in a reduction of the tank steam quality. With this method the steam quality must be good enough to enter the turbine and so it has to be continuously monitored. Unity steam quality means full charged system, null steam quality means fully discharged system.

Real tank behaviour will be somewhere between these two models, closer to the perfect stratification due to large dimensions.
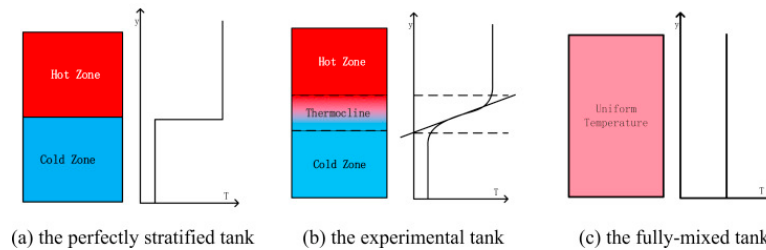
(a) the perfectly stratified tank   (b) the experimental tank   (c) the fully-mixed tank
Figure 30 – Possible configuration

In figure 30 (b) a more realistic configuration is represented: a thermocline exists in between the hot and the cold zone, that is the region in which all thermal gradient is exploited. During the storing time, the thickness of the thermocline increases. The thicker the thermocline, the lower the effectiveness of thermal stratification.

I adopt another different configuration for the estimation problem: hot zone at constant temperature and cold zone that exploits the whole temperature gradient; it is the same of having hot zone and a thermocline for the remaining height of the tank. Linear temperature profile in the thermocline is hypothesized.

Only supercritical water at the maximum temperature is allowed to leave the tank and reach the turbine. Therefore, the stored energy is entirely contained in the supercritical steam layer at constant temperature and directly proportional to the steam filling level H_v, that lays in the interval $0 - 100\,m$. It corresponds to $0 - 100\,\%$ charging level of the system and I refer to

its value in percentage with the variable $H_{v,\%} = H_v/100$. The mass of supercritical steam (at maximum temperature) and the stored energy are:

$$m_v = V_{tot}\, \rho_{hs}\, H_{v,\%} \tag{5.29}$$

$$Q_{stored} \cong m_v\, \frac{\dot{W}_{net,ref}}{\dot{m}_{tot,ref}} = m_v\, 0{,}236\, \frac{kWh}{kg} = m_v\, 849{,}6\, \frac{kJ}{kg} \tag{5.30}$$

The ratio between the net power output and mass flow rate of the reference cycle won't be exactly equal to the later simulated cycle, but differences should be limited and as approximation it seems fine.

Thermal behaviour of the tank is examined in terms of time required to lose 1% of the stored energy, considered as the maximum allowable losses. Supercritical steam in the hot storage tank loses some of its energy towards the ambient in three directions: towards the top, the bottom and the lateral surface. If the top cover is a flat element, its thermal resistance is easily evaluated for plane wall configuration. Instead, for the lateral surface the cylindrical wall configuration is adopted. Concerning the loss to the bottom, it has been already mentioned that 100 % filling level won't be reached and a minimum height of subcritical water is always there in order to allow good thermal stratification.

The bottom sand filling layer in the tank is considered to be at seawater temperature and in the fresh water layer above all the thermal gradient is exploited, with temperature varying from sea temperature to supercritical steam temperatures. Bottom thermal resistance is easily estimated treating the water layer as a wall with a proper thickness and thermal conductivity.

$$R_{top} = \sum_n \frac{\delta_n}{A_{top}\, \lambda_n} \tag{5.31}$$

$$R_{lat} = \sum_n \frac{\ln\left(r_{n,out}/r_{n,in}\right)}{2\,\pi\, H_v\, \lambda_n} \tag{5.32}$$

$$R_{bot} = \frac{\delta_l}{A_{bot}\, \lambda_l} \tag{5.33}$$

$$\dot{Q} = \frac{\Delta T}{R} \tag{5.34}$$

$$\dot{Q}_{tot} = \sum_i \dot{Q}_i = \dot{Q}_{top} + \dot{Q}_{lat} + \dot{Q}_{bot} \tag{5.35}$$

n stands for the number of different layers, λ_l is the conductivity of subcritical water evaluated at average temperature in the water height.

R_{top} is the exclusive constant heat resistance, because it does not depend on the steam filling level of the tank. Instead, the parameter H_v appearing in the lateral resistance formula and the parameter δ_l appearing in the bottom resistance formula (equal to the height of liquid inside the tank) change with time and are related:

$$H_{hs} = H_v + \delta_l \tag{5.36}$$

The time needed to lose 1% of the stored energy is the following:

$$t_{1\%} = \frac{0,01\ Q_{stored}}{\dot{Q}_{tot}} \tag{5.37}$$

Pipeline heat losses are simpler to be estimated. The thermal resistance of pipe wall can be found with the cylindrical geometry heat conduction theory:

$$R = \sum_n \frac{\ln (r_{n,out}/r_{n,in})}{2\ \pi\ L\ \lambda_n} \tag{5.38}$$

$$\dot{Q} = \frac{\Delta T}{R} \tag{5.34}$$

$$h_{out} = h_{in} - \frac{\dot{Q}}{\dot{m}} \tag{5.39}$$

Kind of thermal efficiencies of pipeline can be measured. In the steam pipeline the loss is defined as the ratio between the enthalpy variation in the pipeline and the reference cycle unit of energy generated per kilogram $\frac{\dot{W}_{net}}{\dot{m}} = 849,6 \frac{kJ}{Kg}$:

$$\eta_{th} = 1 - \frac{h_{hs} - h_{t,in}}{\frac{\dot{W}_{net}}{\dot{m}}} \tag{5.40}$$

The water pipeline loss is calculated as the ratio between enthalpy difference in the pipeline and enthalpy difference between hot storage tank condition and inlet pipeline condition:

$$\eta_{th} = 1 - \frac{(h_{hs} - h_{cs}) - (h_{hs} - h_{in})}{h_{hs} - h_{in}} = 1 - \frac{h_{in} - h_{cs}}{h_{hs} - h_{in}} \tag{5.41}$$

Enthalpy at the turbine inlet, namely at the pipeline outlet, is easily calculated as function of the heat losses and the thermal efficiency of the pipe can be estimated. It is defined as the ratio between the specific enthalpy loss in the pipe and the fixed maximum enthalpy difference exploitable by the turbines.

Estimation of total thermal heat resistances of tank and pipeline walls is carried out with the hypothesis of neglecting convection heat resistances, both the inner and the outer one. This means convection heat transfer coefficients approach an infinite value: inlet wall surface is at steam temperature and outer wall surface at seawater temperature.

Heat losses will be overestimated because of this hypothesis especially in the storage tank, even if the effect isn´t significant, being the conduction through the wall the most important and dominant heat transfer mechanism.

The pipeline is considered to be a $2,5\ Km$ long continuous tube without flanges, when in reality a seamless pipe segment of around $16 - 18\ m$ length is the longest currently on the market [], therefore more heat losses are present, and they are partly counterbalanced by the null convective resistances hypothesis.

Effect of flanges could be considered by increasing by a certain factor the heat losses evaluated for seamless pipe.

Cold storage tank is the last component to be analysed. The heat loss rate of fully charged cold storage will be computed considering top and lateral resistance in the same way of hot storage. Dimensions are still great, and stratification exists also in this tank, but density differences are much lower than the hot tank, therefore effectiveness of stratification is reduced. Bottom heat losses are estimated considering the whole temperature gradient existing across a sand layer of $10\ m$ thickness.

6 SYSTEM DESIGNING

6.1 Sea depth required

The higher the overpressure between the inside and the outside of a pressurized tank, the larger the tank wall thickness needed to withstand mechanical stresses in the material. For this reason, large storage vessels of pressurized fluid do not exist on the market and the proposed idea of this thesis can be a solution to this problem.

Even though surface water can be quite warm, the average temperature of the entire ocean is about 4 ℃. A typical temperature profile for open ocean, mid-latitude water is shown in figure 31 [42].
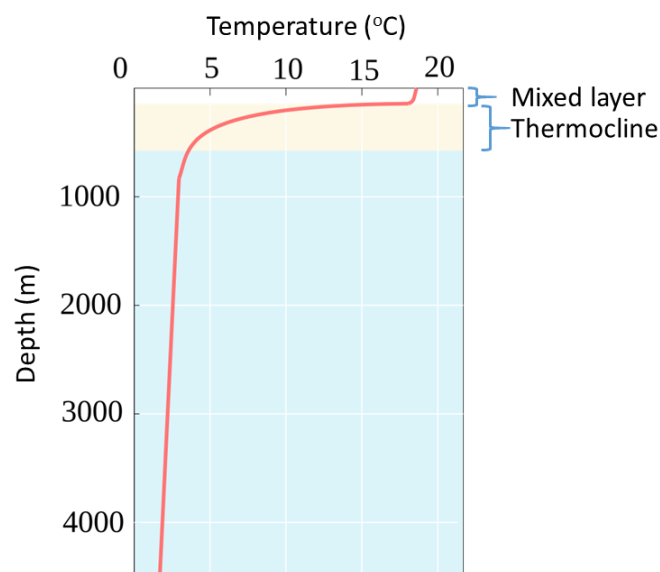
Figure 31 - Typical open ocean temperature profile, showing the mixed layer, steep thermocline, and relatively stable temperature at depth

Temperature is almost constant in the upper $100\ m$ in what is called the mixed layer, resulting from surface winds, waves, and currents. Below the mixed layer there is a rapid decline in temperature over a quite narrow increase in depth. This is called the thermocline. Below the thermocline

the ocean temperature is almost constant at about 4 ℃ down to 2 ℃ at the very bottom.

The density of fresh water is equal to $1\ g/cm^3$ at 4 ℃, but the addition of salt and other dissolved substances increases seawater surface density to between $1.02\ g/cm^3$ and $1.03\ g/cm^3$ [42]. The density of seawater can be increased by reducing its temperature, increasing its salinity, or increasing the pressure, but this last one has the least impact on density as water is nearly incompressible, so pressure effects are not very significant except at extreme depths.

Since temperature has the greatest effect on density, its profile is usually a mirror image of temperature profile (Figure 32). Density is lowest at the surface, where the water is the warmest. As depth increases, there is a region of rapidly increasing density with increasing depth, which is called the pycnocline and coincides with the thermocline, as it is the sudden

decrease in temperature that leads to the increase in density. Below the pycnocline, as for temperature, density is almost constant, or it continue to increase slightly towards the bottom.
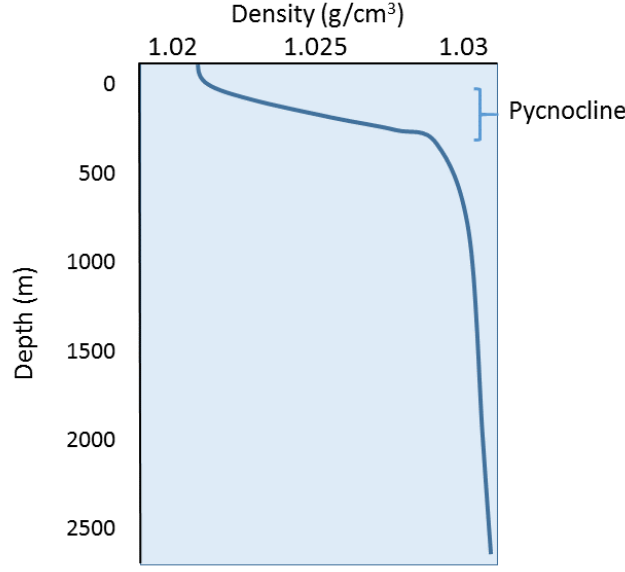
Figure 32 - density profile for the open ocean at mid-latitude

The sea depth required depends on the specific sea or ocean in which BattMarines is built. Approximately, if the inner pressure value is wanted to be around $p_{in} = 250 \, bar$ and the same value is wanted outside, the required depth is:
$$H = p \, / \rho \, g \, \approx 2480 \, m$$

Where the seawater density is considered to have an average value of $1028 \frac{kg}{m^3}$. At this depth the thickness would be a result of optimization between heat losses reduction and wall material costs, since a thickness in the orders of meters is necessary for energy losses while a lower one is required to withstand mechanical stresses.

6.2 Mass flow rates

6.2.1 Discharging mass flow rate

Without the underwater steam storage system, the steam would go directly in the turbine after being generated as in a normal power plant. The mass flow of the cycle is calculated with the hypothesis of having a $\dot{W}_t = 100 \, MW_{el}$ steam turbine exploiting an enthalpy difference of $1000 \, kJ/kg$ (realistic value of real steam turbine power plants, as in the HPLWR) and inlet thermodynamic conditions equivalent to the reference cycle.
$$h_{in,t} = h(494 \, °C, 226 \, bar) \, \simeq \, 3181{,}4 \, kJ/kg$$

$$h_{out,t} \, \simeq \, (3181{,}4 - 1000) \, kJ/kg = 2181{,}4 \, kJ/kg$$

$$\dot{m}_{dis} = \dot{W}_t / \, (h_{out,t} - h_{in,t}) = 100 \, kg/s$$

$\dot{m}_{dis}$ represents the mass flow in vertical pipelines. Being the steam pressure in the tank equal to 250 bar and the turbine inlet pressure fixed at 226 bar, it has been made the hypothesis that pressure losses in vertical steam pipeline can be around the difference between the two value and later this hypothesis will be verified or proved wrong.

In a potential future power plant, the mass flow rate should be an order of magnitude higher as in commercial Rankine power plants. To increase it, a ten times bigger turbine or more turbines of the same size can be installed on the platform, increasing consequently the output power of the cycle itself.

Basically, the system can be scale up just adding turbines on the platform and increasing the mass flow rate of the plant by enlarging the submerged pipelines size or number.

6.2.2 Charging mass flow rate

The charging mass flow rate is calculated hypothesizing to know the specific enthalpy difference (namely the temperature because pressure is known) between two storage tanks and fixing a value for the thermal power given by the electric heater. This value will define the charging time of the storage tank. Since the two tanks are meant to be kept at the same pressure, a pump is needed only to compensate for the pressure losses in the charging pipeline laying on the seafloor. Temperature of the cold tank is hypothetized to be $T_{cs} = 270\,°C$ and the hot tank temperature $T_{hs} = 525\,°C$.

$$h_{cs}\,(270\,°C\,,250\,bar)\ \simeq\ 1181\ kJ/kg$$

$$h_{cs}\,(525\,°C\,,250\,bar)\ \simeq\ 3255{,}8\ kJ/kg$$

With a thermal power input of $\dot{Q} = 100\ MW_{th}$ the mass flow rate would be:

$$\dot{m}_{ch} = \dot{Q}/\,(h_{hs}\ -\ h_{cs})\ \cong 48{,}2\ kg/s$$

Instead, with a thermal power input of $\dot{Q} = 200\ MW_{th}$:

$$\dot{m}_{ch} = \dot{Q}/\,(h_{hs}\ -\ h_{cs})\ \cong 96{,}4\ kg/s$$

One of the aims of the storage system is to provide accumulation capacity for renewable generated energy. When the renewable energy production is higher than the amount saleable to the grid, it is always more and more important to be able to store it and use it when profits can be done again by selling it.

The amount of renewable energy ready to be accumulated varies by large amount during time, for this reason the idea of the charging system is to have a variable power electric heater, in which value of thermal power transferred to the water is proportional to the electric current flowing in the resistor. Therefore, the charging mass flow rate isn´t constant, but it is proportional to the input power, which value can change.

An example can be to have a Carnot battery system of this kind close to an offshore wind park. The power generated by wind turbines is strongly not constant and it is characterized by intense variations in any time scale (from daily scale to hours/minutes scale).

In those moments where wind energy is in excess, i.e., during windy nighttime, the electricity is allowed to flow in the electric heater to charge the battery.

6.3 Steam pipeline

The charging pipeline situated on the seafloor is not a technological challenge as instead are the two discharging long vertical pipelines, hence it is not discussed. Superheated steam can flow at speeds up to $w_v = 40\ m/s$ [43], value already observed in existing steam plants.

$$A_{pipe\_v} = \dot{m}_{dis}/\rho_v\ w_v = 0,0299\ m^2$$

$$d_{pipe\_v} = (4\ A_{pipe\_v}/\ \pi)^{1/2} = 0,195\ m$$

Increasing the diameter, the pressure losses are reduced since velocity decreases, but the heat losses increase due to larger exchange area, so the calculation of the diameter value could be seen as an optimization problem. In reality, heat losses can be reduced drastically with insulation, therefore the diameter can be increased to reduce pressure drop and a thick insulation layer can be installed to manage heat dispersion in the ambient.

6.3.1 Pressure losses

The used correlation has been said to be valid foo single phase flow in smooth pipes. In real application, the steam pipeline should be able to operate near this condition and that means that for the steam pipeline not only the insulating material will be decisive but also the steel and its manufacturing, since it is needed as smooth as possible.

If an inner diameter of $d_{in} = 0,2\ m$ is used in calculations, corresponding to $w_v \cong 38\ m/s$ and properties are evaluated at hot storage tank thermodynamic conditions:

$$Re \approx 20e6$$

$$f = 0,00737$$

$$\Delta p_f \simeq 55,6\ bar$$

$$\Delta p_g \simeq 20,5\ bar$$

If the steam flows in descending direction, the total pressure change is obtained subtracting the static head to the pressure loss due to friction, in fact the static head is gained, and this results in $\Delta p_{tot} = 35,1\ bar$.

Oppositely, when the steam flows in ascending direction, the static head is added to the friction losses and the pressure difference becomes more significant, $\Delta p_{tot} = 76,1\ bar$.

With the considered diameter and mass flow, pressure losses are too high: steam would enter the turbine with a subcritical pressure of $p_{in,t} = (250 - 76,1)bar = 173,9\ bar$.

Since the vertical ascending steam pipe connects the tank to the power plant, the maximum value allowable for pressure losses can be calculated, such to have the wanted inlet turbine conditions.

The maximum losses to have supercritical water conditions at the turbine inlet at a pressure of at least $220,6\ bar$ and the maximum losses to have inlet turbine conditions equivalent to the reference cycle are calculated:

$$\Delta p_{max} = (250 - 220,6)\ bar = 29,4\ bar$$

$$\Delta p_{max} = (250 - 226)\ bar = 24\ bar$$

This pressure drop evaluation is implemented in an excel file in order to see the change of total pressure drop value changing the pipe dimensions, in fact friction pressure losses are function of pipe geometry, while this isn't true for static pressure that remains constant.

With software simulation more precise results will be carried out in the next chapter.
Results of the estimation are approximations since no discretization is considered and thermodynamic properties are considered constant along the whole tube length.
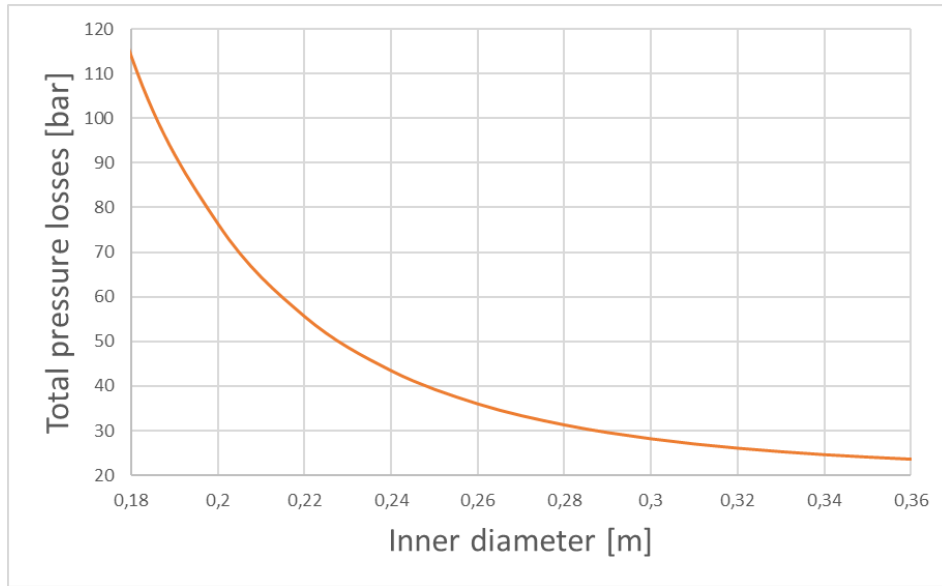
Figure 33 – Ascending steam pipeline total pressure losses as function of inner diameter

An inner diameter of at least $0,3\ m$ would be enough to remain in the supercritical region in the whole pipe. In fact, $d = 0,3\ m$ corresponds to $\Delta p_{tot} = 27,5\ bar < 29,4\ bar$.
Increasing the diameter to $d = 0,36\ m$ would mean to lose $\Delta p_{tot} = 23,7\ bar < 24\ bar$ and would allow the turbine inlet pressure to be around the desired $p_{in,t} = 226\ bar$. Large diameter steel pipe plays an important role in oil and gas transmission [44], in which diameters of half meter can be reached as maximum, therefore a $0,36\ cm$ inner diameter pipeline can be produced with the existing infrastructure.
However, the increase in diameter translates in an increment of heat exchange, therefore it could not be the best solution. The alternative, represented in the next figure, can be to increase the number of tubes, thus reduce the mass flow rate and the velocity in the single tube.
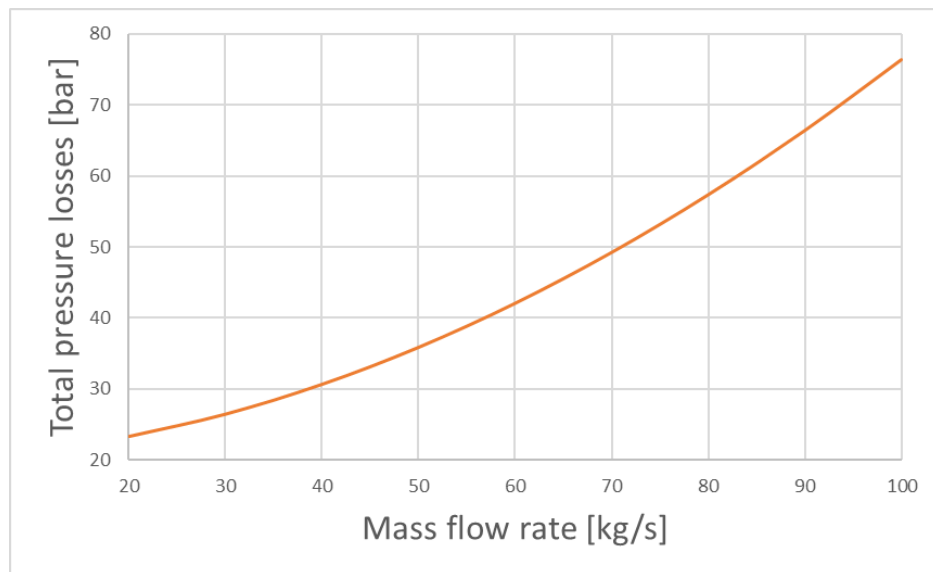

Figure 34 – Ascending steam pipeline total pressure losses as function of mass flow rate

With $100\ kg/s$ flowing in a single tube of $0,2\ m$ diameter, pressure losses are abundantly too great and the only solution is to reduce the velocity of the flow, i.e. the mass flow rate. This can only be done partitioning $100\ kg/s$ of steam in more pipes:

- using 2 pipelines would reduce to more than half the pressure losses, $\Delta p_{tot} = 35,8\ bar$
- using 3 pipelines is already enough to be in supercritical conditions at the turbine inlet, $\Delta p_{tot} = 27,7\ bar < 29,4\ bar$
- using 4 pipelines would result in $\Delta p_{tot} = 24,7\ bar$
- with 5 pipelines $\Delta p_{tot} = 23,3\ bar$

The curve of pressure losses has an asymptote at $20,5\ bar$, i.e., the static head of the steam, meaning that with 3 pipelines only around $7,2\ bar$ are lost in $2500\ m$ due to friction and with 4 pipelines only $4,2\ bar$.

The reduction of the steam velocity in the pipe is positive also from the thermal losses point of view, being the internal convective heat transfer coefficient reduced. This has anyway not huge effect, as major role is played by insulation material layer thickness.

Of course, multiplying by four the number of pipelines, also the cost increases by a factor of four. The configuration of single pipe with $d_{in} = 0,36\ m$ carrying the whole mass flow rate will be taken as reference in the next calculations.

6.3.2 Mechanical stresses

Since the external pressure varies in the depth from $1\ bar$ to $250\ bar$, mechanical stresses distribution in the wall changes consistently along the whole length. For this reason, the stress analysis will be carried out for the most critical position only: a pipe segment located near the seawater surface. The deeper the pipeline segment, the less challenging its mechanical behaviour, because the difference between inner and outer decreases with increasing depth. A wall of $\delta = 0,3\ m$ thickness is hypothesized. Pressure in the inlet is fixed at $p_i = 22,8\ MPa$ and $p_e = 0,1\ MPa$ at the outlet, while temperature difference is fixed at $T_i - T_e = 500\ °C$. Pressure induced stresses in the circumferential and radial direction are material independent and they are shown as function of radial distance from the pipe centre:
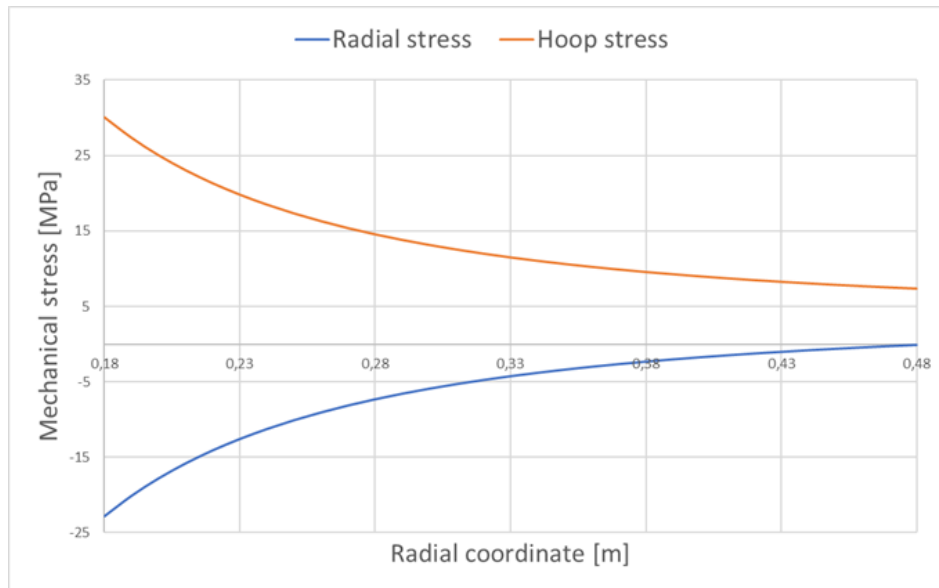
Figure 35 – Pressure induced stresses

Radial stress is equal to internal pressure on the internal surface and to external pressure on the external surface. Maximum stress in the whole thickness is the circumferential stress on the inner surface, with a value of approximately $\sigma_\theta \cong 30\ MPa$.

- **Stainless steel pipeline**

Without a temperature gradient existing in the thickness, any kind of steel can withstand the pressure induced stresses. Austenitic stainless steel properties [20] are needed to evaluate thermal induced stresses.

$$E_s = 200\ GPa\ ;\ \gamma_s = 0,3\ ;\ \beta = 1,4e - 5\ ^\circ C^{-1}$$

Figure 36 – Total stresses as function of radial coordinate in steel wall

When considering temperature gradient effect and applying the superimposition of effects, it is clearly visible a different scale on the y-axis, where stresses appear with almost two orders of magnitude difference. The hoop stress on the inner surface is sti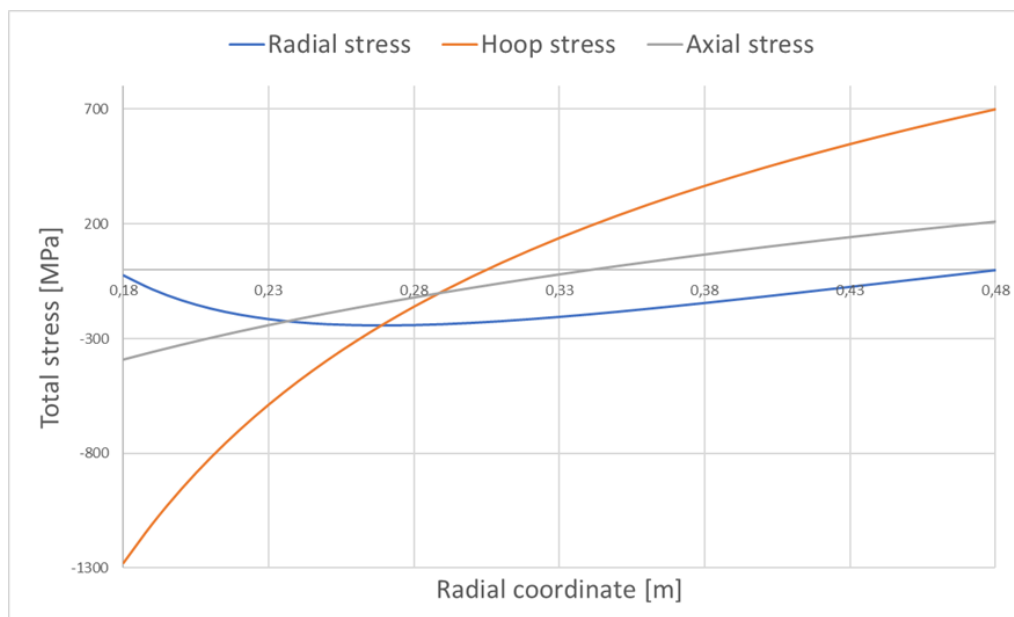ll the greatest value in the structure, but now there aren´t types of steel with such high yield strength, in particular this is true for austenitic stainless steels, the weakest among all stainless steels from this point of view.

A wall completely made of a single material isn´t able to withstand temperature gradient induced stresses.

- **Concrete**

The modulus of elasticity of concrete at room temperature varies over a wide range, $5 - 35\ GPa$ and decreases rapidly with the rise of temperature [21]. Let´s hypothesize a concrete of $15\ GPa$ elastic modulus which value is reduced by one third at average wall temperature.

$$E_C = 10\ GPa\ ;\ \gamma_c = 0,2\ ;\ \beta = 1e - 5\ °C^{-1}$$

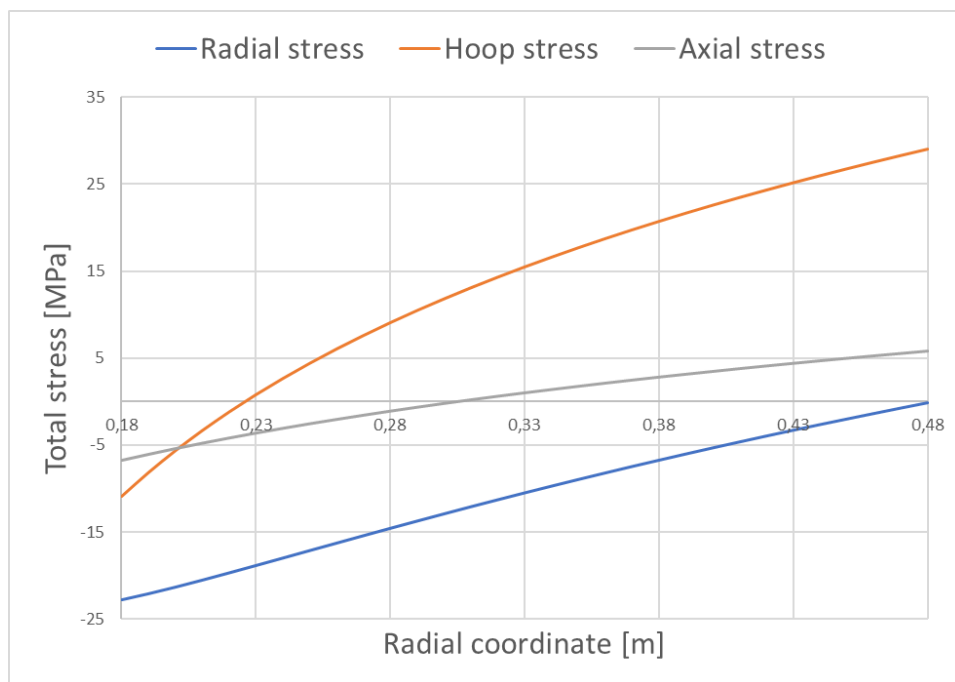Figure 37 – Total stresses as function of radial coordinate in concrete wall

Maximum stress existing is much higher than the elastic limit of usual concrete. Prestressed concrete would be required together with a multi-layer wall with different materials in which concrete shouldn´t be in the most stressed radial coordinate. With multi payer wall also the temperature gradient is divided between the layers.

- **Mullite**

This material is used in direct contact with the flame in ovens and other applications where refractory materials are needed. It is resistant at high temperatures and thermal gradient across it is not a complication.

Having an open-cell foam structure, the mullite foam insulation layer has to be contained between two stainless steel layers. The gas in the foam structure in deepest part of the pipeline, as well as in the hot storage tank, is at a pressure of $25\ MPa$. Pressure induced stresses shouldn´t be a problem in the foam structure if the pressure is constant in the thickness, in fact, only the solid matrix has to withstand everywhere a compressive strength equal to the gas pressure.

In the remaining length of the pipe, including the first part close to the sea surface, a solution has to be found: air in the foam insulation layer could be at the same pressure of the steam flowing in the pipe or at the pressure of seawater at that specific depth. In the first case, the whole pressure difference is taken over by the external steel layer, while in the second case by the internal steel layer. The lower the pressure of the air in the foam, the less stressed the reticular structure is; for this reason, the first configuration is considered.

Temperature gradient induced stresses in the steel aren´t considered since they are negligible, and it can be considered isothermal in the radial direction. in fact, with the mullite foam layer, almost all the gradient is taken by it, being the least conductive material.

If the air pressure in the insulation layer is wanted to be the same of the seawater at every depth, it has to increase linearly with depth as seawater does. In order to do so, every few meters in the vertical direction, a horizontal thin division layer cutting the mullite foam has to separate zones of different air pressure.

For example, in the first fifty meters below the sea surface, water pressure varies approximately from $1\ bar$ to $6\ bar$. A vertical annulus of the same height of mullite foam should have all pores connected each other with air at $3,5\ bar$ inside. In the next fifty meters, seawater pressure varies from $6\ bar$ to $11\ bar$ and a vertical annulus of the same height of mullite foam should have all pores connected each other with air at $8,5\ bar$ inside.

The horizontal separators between foam regions at different pressure can be easily made of a resistant material like steel, so that its thickness can be minuscule. Disadvantage is the increase of heat losses due to high steel conductivity, but the problem can be solved in many ways, for instance a zigzag shape instead of a simple linear one can be adopted to create a longer path for heat towards the outer surface. It can be well visualized in the vertical cross section of the annulus mullite foam layer.
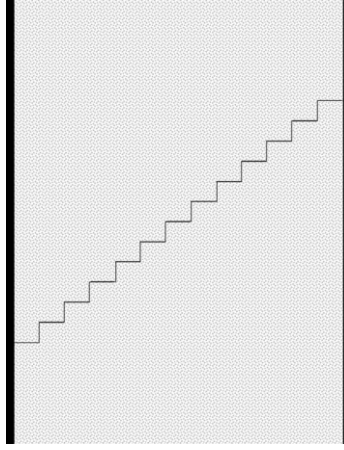
Figure 38 – Zigzag steel separator

In the most critical section of the pipeline, steam flows at around $22,8\ MPa$ and air in the mullite foam has a pressure of $0,2\ MPa$. The minimum thickness needed as function of the inlet pressure can be estimated with (5.28), considering for simplification inner pressure of $22,7\ MPa$ and null (atmospheric) outer pressure:

$$\delta_{min} = \frac{p_i\ D_{out}}{2\ (QF\ \sigma_{\theta,max} + p_i\ Y)} \cong 22\ mm = 2,2\ cm$$

Austenitic stainless steels are characterized by the lowest yield strength among all stainless steels, around $\sigma_{\theta,max} = 300\ MPa$ at room temperature. This value decreases with increase in temperature and at $500\ ℃$ it was considered to be $75\ \%$ of the room temperature one, namely $\sigma_{\theta,max} = 225\ MPa$. Quality factor $QF = 0,8$ for not seamless pipe is considered and coefficient $Y = 0,5$ required when $\delta < D/6$ [41].

A corrosion allowance of couples of millimetres is usually added to the minimum thickness, together with the erosion allowance. A thickness for the inner layer of steel is set at $\delta_s = 3\ cm$. Temperature has been said to be constant in the radial direction in the steel layer and mechanical induced stresses are the following:
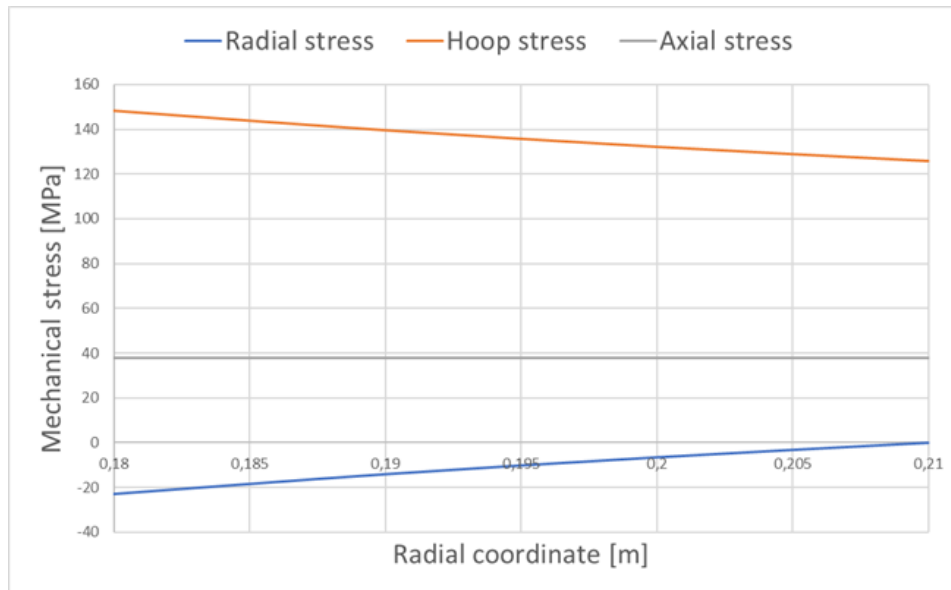
Figure 39 – Inner steel layer pressure induced stresses

Again, the most stressed point is on the inner surface and the highest stress is the circumferential, in this condition with a value of $\sigma_\theta = 148\ MPa$. This thickness seems to be enough, in fact a consistent margin exists between the maximum stress in the most stressed point of the entire pipeline and the elastic limit of the material.

The external stainless steel layer is also at constant temperature, but at the seawater temperature level, so mechanical properties are better. Additionally, pressure on the inside and pressure on the outside are the same or they differ by few bars: required thickness is lower than $1\ mm$. Considering corrosion and erosion allowance, its value can be conservatively fixed at $0,5\ cm$.

To have simple thermal resistances calculation I will consider it to be $1\ cm$.

- **Glass particulate**

Mullite foam bricks insulation has to be tested under these operating conditions; in fact such application of the material do not exist. The second-best solution in terms of insulation capability was found to be the particulate glass insulation.

Wall configuration would be the same of the mullite case, namely figure 38 and figure 39, with small glass spheres, contained between two steel layers, immersed in air at pressure equal to the fluid in the pipe at that specific depth. Glass compressive strength is great and temperature gradient in each sphere is low enough if spheres are tiny, also because most of temperature gradient happens in the air.

6.3.3 Thermal analysis

Heat losses are evaluated with a conservative approach: $\Delta T = 520\ °C$ is fixed, as if along the whole pipe length temperatures remains constant. In reality, only in the deepest segment this is the case, while it decreases slowly moving closer to the surface, meaning heat losses are going to be overestimated. In addition, convective heat resistances are neglected.

However, since flanges (and their insulation) are not included in the discussion, all these conservative hypotheses maybe do not lead to an overestimation of the losses.

- **Stainless steel pipeline**

Thermal conductivity value is fixed at average wall temperature at $\lambda_s = 17,5\ W/m\ K$. Thermal resistance, thermal losses and outlet pipe enthalpy are the following:

$$R = 3{,}56e - 6\frac{K}{W}$$
$$\dot{Q} = 146\ MW$$
$$h_{t,in} = 1795{,}86\ \frac{kJ}{Kg}$$

With a pipeline made exclusively of stainless steel, all the useful energy is lost towards the sea and it means thermal insulation efficiency is lower than zero. In fact, with the before given definition of efficiency, a negative value can be reached if more than $849{,}6\ kJ/Kg$ are lost.

- **Concrete pipeline**

Thermal conductivity value is fixed at average wall temperature at $\lambda_c = 1{,}5\ W/m\ K$. Thermal resistance, thermal losses and outlet pipe enthalpy are the following:

$$R = 4{,}16e - 5\frac{K}{W}$$
$$\dot{Q} = 12{,}5\ MW$$
$$h_{t,in} = h_{hs} - \frac{\dot{Q}}{\dot{m}} = 3130{,}86\ \frac{kJ}{Kg}$$

Heat losses are drastically reduced and pipeline outlet enthalpy has enough high value to enter the turbine in this case. Thermal efficiency of the pipeline can be calculated:

$$\eta = 1 - \frac{h_{hs} - h_{t,in}}{\dfrac{\dot{W}_{net}}{\dot{m}}} = 1 - 0,147 = 0,853 = 85,3\,\%$$

Insulation starts being quite effective, but still losses have to be reduced and a greater efficiency is required because it isn´t thinkable to have such percentage for a single system component.

- **Mullite foam insulated pipeline**

A multi-layer wall configuration is analysed: $3\,cm$ layer of stainless steel facing the steam with $\lambda_{s,i} = 20\,W/m\,K$; $1\,cm$ layer of the same stainless steel facing the seawater with $\lambda_{s,e} = 15\,W/m\,K$; $26\,cm$ layer of mullite foam bricks with $\lambda = 0,14\,W/m\,K$ in between those two layers.

$$R \cong 3,67e - 4\,\frac{K}{W}$$
$$\dot{Q} \cong 1,417\,MW$$
$$h_{t,in} = h_{hs} - \frac{\dot{Q}}{\dot{m}} = 3241,69\,\frac{kJ}{Kg}$$
$$\eta = 1 - \frac{h_{hs} - h_{t,in}}{\dfrac{\dot{W}_{net}}{\dot{m}}} = 1 - 0,0166 = 0,9834 = 98,34\,\%$$

1,66 % of turbine exploitable energy is lost in the concrete pipeline, therefore its thermal efficiency can be considered to be around $\eta = 98,34\,\%$. This value looks definitely satisfying, enthalpy at the pipeline outlet is greater than the required value of the reference Rankine cycle, meaning that with a such insulated pipeline a lower hot storage temperature is needed to have the desired inlet turbine conditions.

Further possible improvements can be studied creating the following graphs of heat losses and thermal resistances as function of insulation layer thickness:
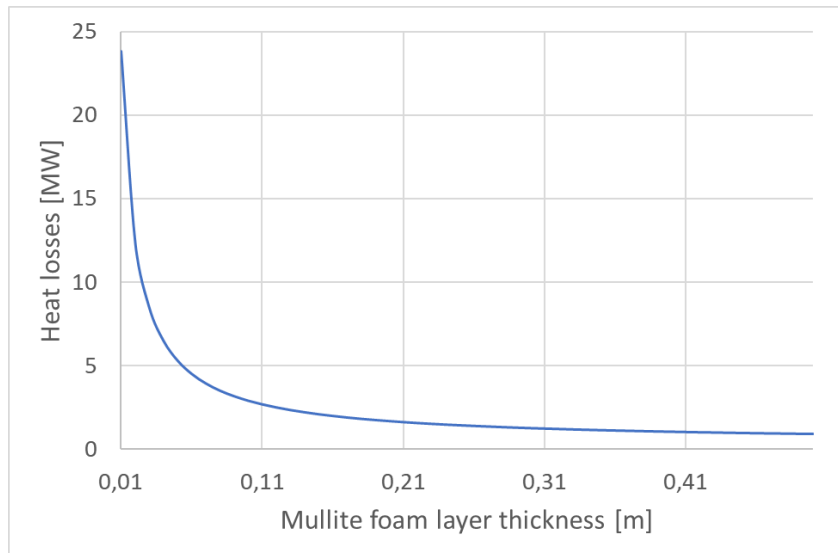
Figure 40 – Heat losses as function of insulation thickness

At low insulation layer thicknesses, huge decrease of heat losses occurs for a small increase of the insulation layer thickness. This effect is reducing more and more for higher thickness values, up to a point where infinitesimal decrease of heat losses takes place.

With a $7\ cm$ thickness the losses are about $4\ MW$; with $16\ cm$ thickness $2\ MW$ are the losses and up to $44\ cm$ would be required to reach $1\ MW$.

With the examined thickness of $26\ cm$ losses reach the low value of $1,417\ MW$. Thicker layers won´t reduce it significantly and this progressive drop of insulation thickness increase efficacy is explained by the fact that an infinite thickness layer would be needed to have null losses and unitary efficiency.

It can be seen in the heat resistance graph that every added centimetre has slower impact on the thermal resistance than the previous one.
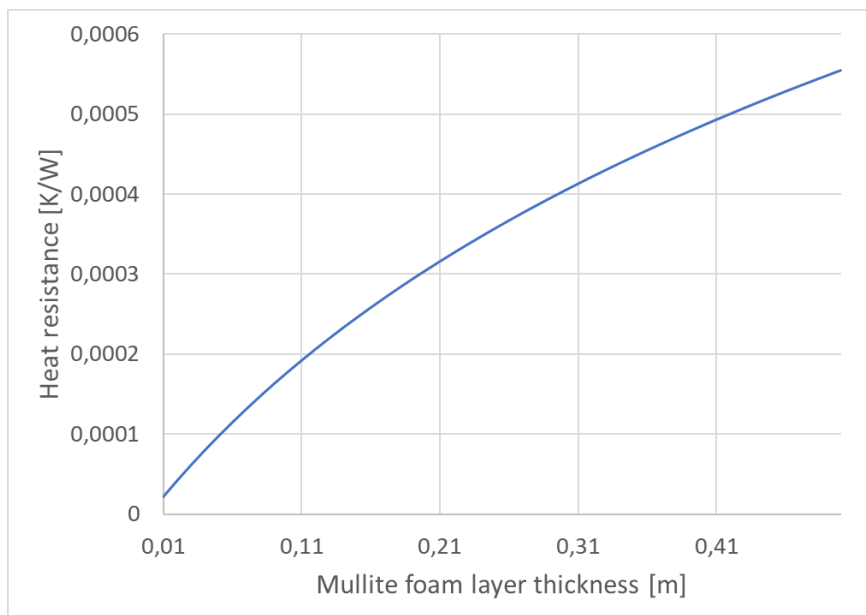

Figure 41 – Pipe wall heat resistance as function of insulation thickness

A combined energetical and economical optimization is required to determine the optimal value of mullite foam thickness. Intuitively, it can be said that $26\ cm$ is around the upper limit, in fact, already at about $20\ cm$ the heat losses curve starts being almost flat.

During storing time, the steam pipe has to be kept in hot condition to avoid long transient at the beginning of the discharging phase. It is probably better to have at least $26\ cm$ to avoid significant losses during storing.

- **Glass particulate insulated pipeline**

Glass is a much more common material, which disadvantage is the maximum working temperature at around 500 °C. Probably, in steam pipeline and tank, there´s the necessity of an additional layer between stainless steel and glass particulate to reduce temperature until the desired maximum one.

Thermal conductivity of particulate glass is fixed at $0,8\ W/m\ K$. Stainless steel and glass layers thicknesses are unchanged from mullite layer case.

$$R \cong 6,47e-5\frac{K}{W}$$
$$\dot{Q} \cong 8,04\ MW$$
$$h_{t,in} = h_{hs} - \frac{\dot{Q}}{\dot{m}} = 3175,4\frac{kJ}{Kg}$$
$$\eta = 1 - \frac{h_{hs} - h_{t,in}}{\dfrac{\dot{W}_{net}}{\dot{m}}} = 1 - 0,095 = 0,905 = 90,5\ \%$$

Significantly lower vale compared to mullite, but better insulation than concrete.
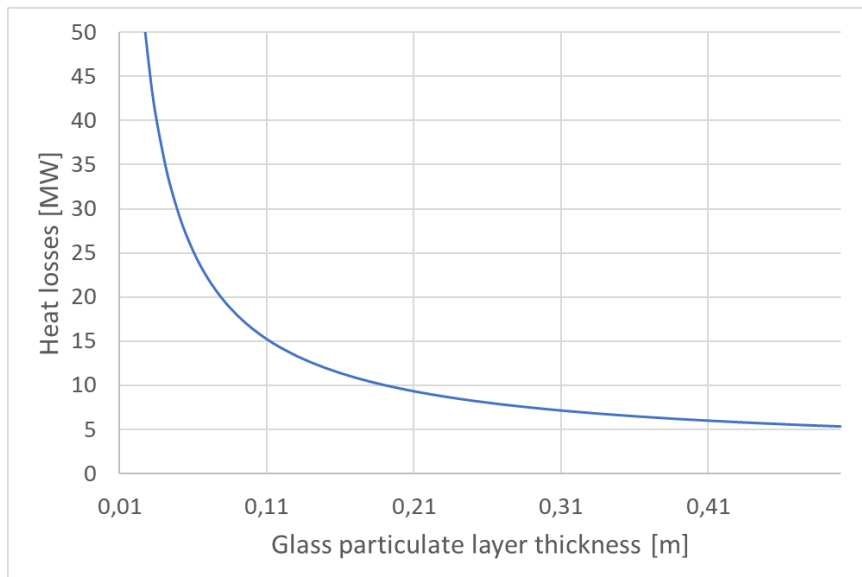

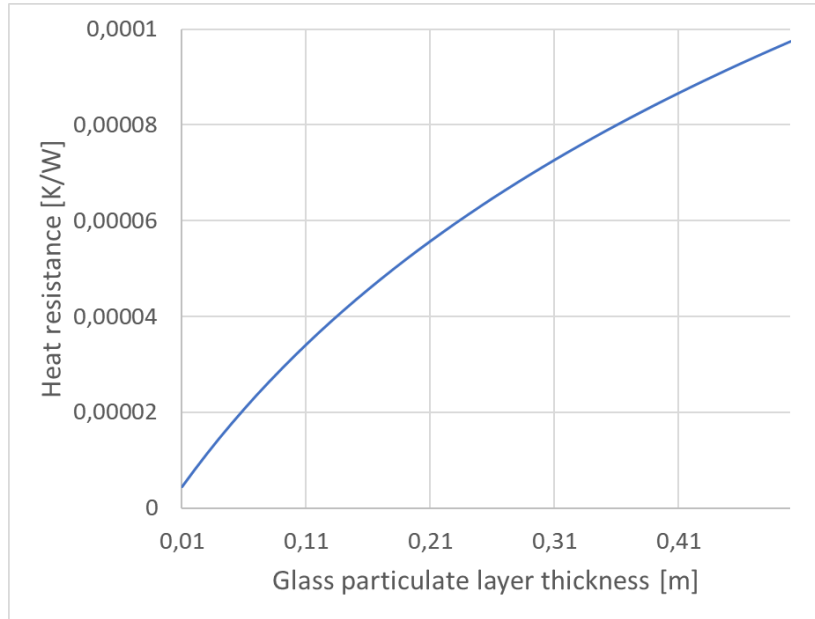Figure 42 – Heat losses as function of insulation thickness

Figure 43 – Pipe wall heat resistance as function of insulation thickness

6.4 Hot storage tank

6.4.1 Dimensioning

The goal of this battery is to store steam ready to be expanded from a conventional steam power plant that has normally electrical power output in the order of $1\ GW_{el}$. Because it wants to be used only in periods of peak demand, the amount of energy stpred is fixed at $1\ GWd$, meaning the disharging process can last up toone day starrting from fully charged system condition.

If both storage tanks are built of great dimensions, to increase the power output an increase of the discharging mass flow rate can occur just increasing the number of vertical pipelines.

From equation (3.4), the mass required to store $1\ GWd$ is computed, and a mass in the order of $m \approx 10^8\ Kg$ is obtained in fully charged conditions. This condition is only ideal, because the required stratification does not allow the tank to be completely full of steam.

The hot steam at $p_{hs} = 250\ bar$ and an average temperature in the whole tank of $T_{hs} = 525\ °C$ has a low density of $\rho_{hs} = 83,5\ Kg/m^3$, thus:

$$V_{hs} = m / \rho_s \approx 1.2 * 10^6 \, m^3$$

To have an idea of the dimensions, a possible solution in cylindrical shape could be:

$$d_{i,hs} \approx 115 \, m$$

$$H_{i,hs} \approx 115 \, m$$

One of the challenges of the whole system, probably the most important to overcome to make this big storage technology energetically feasible, will be the thermal insulation of this huge hot storage tank. Any kind of TES system has always the specification about its thermal losses rate and the more time the steam can be kept at a thermodynamic state suitable to enter the turbine, the higher will be the possibility of producing electricity in the desired moment and make it the most profitable possible. Its dispersion surface can be evaluated:

$$A_{base} = \pi \, d_{i,hs}^2/4 \approx 10387 \, m^2$$

$$A_{lateral} = \pi \, d_{i,hs} \, H_{i,hs} \approx 41547 \, m^2$$

$$A_{tot} = A_{lateral} + A_{base} \approx 51934 \, m^2$$

Even neglecting heat losses towards the bottom, this is a very large number, and the insulation has to be such that losses through this area are contained into certain values.

The whole mass of water in the cold storage needs a certain amount of time to be transformed into steam, inversely proportional to the entity of the thermal power delivered by the electric heater. The charging time of the storage system would be, in case of $200 \, MW_{th}$ as input power:

$$t_{ch} = m / \dot{m}_{ch} \cong 288 \, h = 12 \, days$$

This time is wanted to be high, but it is only depending on the entity of the heat input source. For example, making it of $1000 \, MW_{th}$ will result in a charging time of $t_{ch} = 57,6 \, h$. Moreover, the real storage will probably be used between certain limiting values of charging level, i.e., 20 % and 70 % (very approximate values) to maintain the upper part of the tank always at high temperature and allow always good stratification that is fundamental.

With the current existing infrastructure, it is hard to install such huge component on the seafloor at those depths. For many different reasons, a modular storage system will be preferred: instead of having a single hot tank, it is better to install multiple smaller tanks whose total volume is unchanged compared with the case of single tank.

A cylinder of height and diameter of $100 \, m$ can be replaced by 100 cylinders with same height and diameter of $10 \, m$ or by 25 cylinders with same height and $20 \, m$ diameter. These smaller tanks are easier to be installed and one advantage would be not to have global system failure in case of

damage of the single huge tank: if one of the multiple reservoirs fails and breaks it is sufficient to replace it with a new one.

In figure 44, the top view of the section of two hot storage tank designs are shown: the simple studied one on the left and a more realistic one on the right. Losses will be estimated only in the left configuration, the case of a huge $100\ m$ tank full of steam with a few meters' insulation wall, and they are going to be overestimated compared to the more complex realistic configuration.

In the simple configuration, the containment structure directly faces the supercritical steam and the whole thermal gradient is exploited across it.

In a realistic inner vessel design, a steel rack contains pressure vessels with diameters of $10-20\ m$ and everything is enclosed by the same huge cylindrical insulated containment structure. To store the same mass of steam as in the simple configuration, two of these containments are needed, that means great costs, but price per vessels should decrease if a great number of them is purchased.

All inner vessels have to be insulated properly but with a thin wall, in fact the main insulation remains the external big cylinder. All empty spaces inside of it are filled with sand, represented in the picture with black dots, in order to create a sort of solid material. Sand is perfect being a cheap and dense material ($\rho > 1500\ kg/m^3$), poor thermal insulator ($0,2 < \lambda < 2\ W/mK$) that can withstand high temperatures and it has quite high heat capacity ($c \sim 800\ kJ/kgK$) [45].

The real need of such configuration, that is the main advantage, is the pressure induced stresses reduction: the larger the diameter, the greater the stresses and the more expensive the required steel would be. Stresses in the inner tanks are low and the containment structure faces sand instead of the supercritical steam, that is like having a thicker solid wall to compensate for the pressure difference across the thickness.
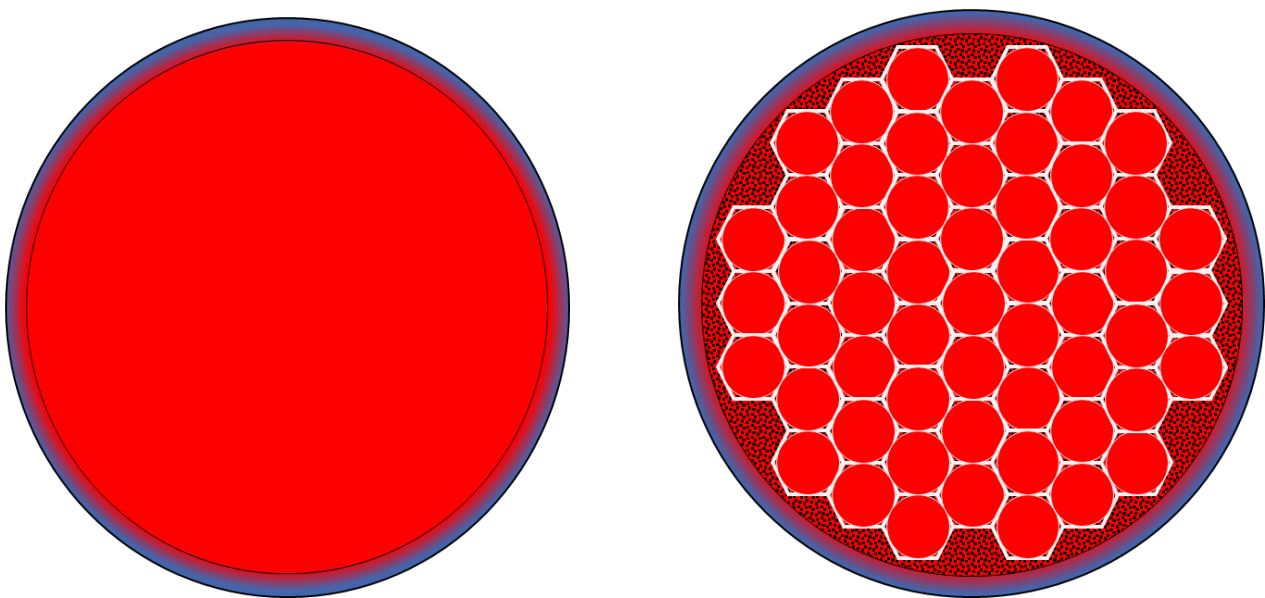

Figure 44 - Studied design (left) and realistic inner vessel design (right)

Quite great amount of energy would be required to heat up all cylinder's walls, sand, and external containment wall; but heat loss rate will be decreased consistently.

To quantify these stresses, a foam or particulate insulated wall is considered for both the containment cylinder and the inner cylinders. The maximum pressure difference is hypothesized considering a fully charged condition, so inner pressure constant at $250\ bar$, with air pressure in the foam varying accordingly to the outer pressure. Inner steel layer compensates for the pressure induced stresses.

A possible configuration could be the one represented in figure 45, in which the maximum pressure difference exists at the bottom and at the top, around $5\ bar$.

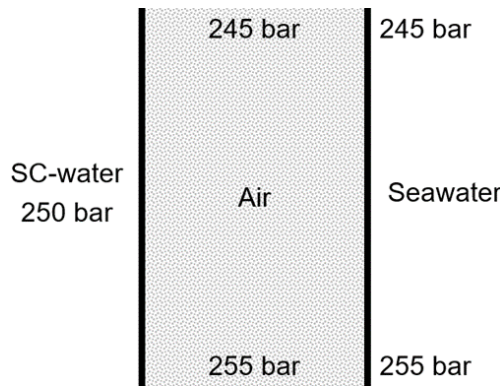Figure 45 – Section of 100 m height tank wall

6.4.2 Mechanical stresses

To justify the main motivation of the storage system, the maximum stress existing in the tank wall are evaluated as if the tank was built on the earth surface. Thick wall theory has to be applied in case the outer pressure is the atmospheric one, since walls are expected to be very thick. Temperature gradient effect is neglected, and thickness is fixed at $\delta = 10\ m$. In this theory, the hoop stress is always the highest among the three:

$$\sigma_{\theta,m}(r = r_i) \cong 138\ MPa$$

$$\sigma_{\theta,m}(r = r_e) \cong 113\ MPa$$

Even with ten meters thickness, only stainless steel would be able to withstand those high stresses. Yield strength of concrete is extremely low and not even comparable, the one of glass is one order of magnitude lower. Mullite foam yield strength is similar to concrete, it makes sense to consider it a potential insulation material only when immersed in a pressurized gas, namely when in a constant pressure ambient.

Hot storage tank with dimensions of $d_{i,hs} = H_{i,hs} = 100\ m$ and a wall thickness up to $\delta = 4\ m$ can be studied with the thin wall theory. The total volume is the following:

$$V_{i,hs} = \pi \frac{d_{i,hs}^2}{4}\ H_{hs} = 785398\ m^3$$

Inner and outer pressures are the exact same only in a first approximation. The structure isn´t stress free for real, but it will be characterized by small local variations of stresses during time due to filling level change of the tank, that causes locally internal pressure variations.

The largest pressure difference between inlet and outlet is set at $\sim 5\ bar,$ for the reason explained in figure 45. The stresses in a single material wall, that are material independent and constant in the whole thickness, would result in:

$$\sigma_r = -0{,}5\ MPa$$

$$\sigma_\theta = -31{,}75\ MPa$$

$$\sigma_z = -28{,}5\ MPa$$

Yield strength of any kind of stainless steel is at least one order of magnitude higher than the maximum stress characterizing the structure, therefore no problems at all can happen from mechanical point of view.

Prestressed concrete could be also adopted as potential material, but its thermal behaviour would be worsened by the prestressing steel.

Thin wall theory is probably wrongly adopted here, in fact pressure should be constant in the whole volume, which isn´t the case, and usually pressure containers dimensions are much smaller. It is hard to think at $4\ m$ thickness as a thin wall in which stresses are constant in the entire thickness, but the condition $\delta/r_i < 1/10$ is respected, therefore the analysis has a meaning.

With a particulate or foam material insulation layer, the two required stainless-steel layers facing both internal and external ambient are wanted to be quite thin. As discussed for the steam pipe, also this wall can have zigzag steel separators to create different pressure zones in the vertical direction of the insulation layer.

For example, with the same maximum pressure difference, considering an inner steel layer thickness of $\delta = 15\ cm$, maximum stress would be already quite high:

$$\sigma_\theta \cong 150\ MPa$$

No challenges occur for smaller size vessels. If $d_{in} = 15\ m$ and $\delta = 5\ cm$ only, the maximum stress is already low enough to use common marine steel with a great safety factor:

$$\sigma_\theta \cong 50\ MPa$$

6.4.3 Thermal analysis

A single specific system configuration is considered, namely at $50\ \%$ filling level, where $H_v \approx \delta_l \approx 50\ m$. The stored mass and the related energy would be:

$$m_v \cong 32,8e + 6\ Kg$$

$$Q_{stored} \cong 7740\ MWh$$

Thermal conductivity of subcritical water is for hypothesis evaluated at the average temperature along its thickness, $\lambda_l \approx 0,6\ W/m\ K$. Temperature difference between inlet supercritical fluid region and outside is a constant value of $\Delta T = 520\ °C$ and wall thickness also is constant, $\delta = 4\ m$.

Estimating losses in the realistic inner vessel design of figure 44 is complicated and it isn't done, but the temperature difference across the external confinement is quite a bit lower, therefore any reported result of heat loss is an overestimaetion of the relaistic design and any reported result of storing time is an underestimation.

- **Stainless steel tank**

$$R_{top} \approx 2,55e - 5\,\frac{K}{W}\ ;\ \dot{Q}_{top} \cong 20,4\ MW$$

$$R_{lat} \approx 1,22e - 5\,\frac{K}{W}\ ;\ \dot{Q}_{lat} \cong 42,6\ MW$$

$$R_{bot} \approx 0,01\,\frac{K}{W}\ ;\ \dot{Q}_{bot} \cong 0,052\ MW$$

$$\dot{Q}_{tot} = \dot{Q}_{top} + \dot{Q}_{lat} + \dot{Q}_{bot} \cong 63\ MW$$

$$t_{1\%} \cong 1,23\ h$$

In around one hour and fourteen minutes, $1\ \%$ of the useful energy get lost. In a bit more than $5\ days$ all the energy is dispersed towards the ambient.

- **Concrete tank**

$$R_{top} = 3,39e - 4\frac{K}{W} \; ; \; \dot{Q}_{top} \cong 1,53 \; MW$$

$$R_{lat} = 1,63e - 4\frac{K}{W} \; ; \; \dot{Q}_{lat} \cong 3,19 \; MW$$

$$R_{bot} \approx 0,01\frac{K}{W} \; ; \; \dot{Q}_{bot} \cong 0,052 \; MW$$

$$\dot{Q}_{tot} = \dot{Q}_{top} + \dot{Q}_{lat} + \dot{Q}_{bot} \cong 4,77 \; MW$$

$$t_{1\%} \cong 16,2 \; h$$

With a $4 \, m$ thick concrete wall, insulation seems to be quite effective. There is an improvement in storing time in comparison with stainless steel of a factor 13.

With an excel table, this calculation is carried out for every possible tank filling level. Total heat losses increase linearly with filling level, due to linear increase of lateral heat losses. In fact, losses towards the top are constant at $\dot{Q}_{top} = 1,53 \; MW$ and towards the bottom they have the smallest contribution, almost negligible up to a filling level of 80%.

Bottom heat losses grow slowly, then for high filling levels they have an exponential increase, passing from $\sim 0,13 \; MW$ to $\sim 2,6 \; MW$ in the range $80 - 99 \; \%$. This explains the shape of the curve at high filling levels.
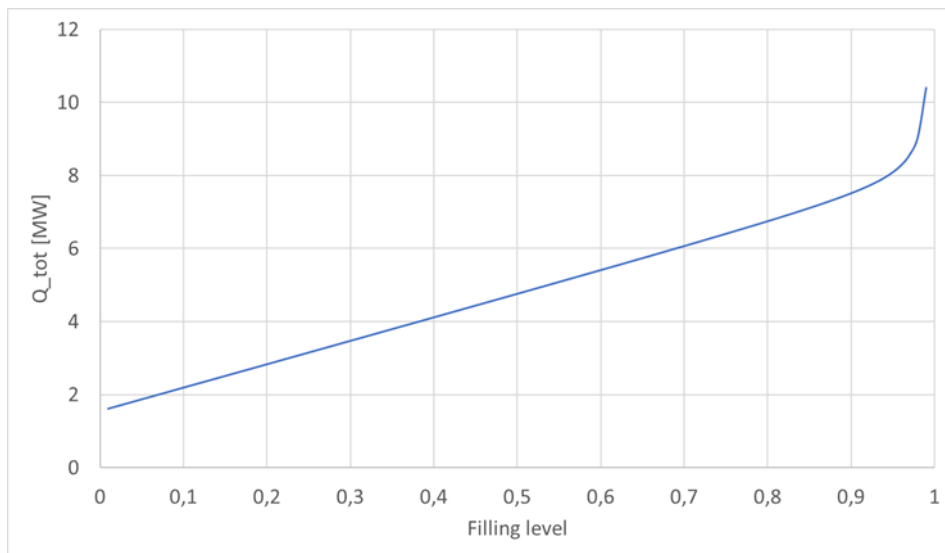

Figure 46 – Heat losses as function of filling level with $4 \, m$ of concrete

Bottom heat losses should somehow be reduced, especially for high filling levels; in any case the higher the filling level the greater the losses, therefore it is energetically favourable not to reach filling levels higher than a certain limit. Figure 47 suggests this limit could be around 0,9.
Top heat losses contribution on the total losses decreases with increasing filling level with a parabolic evolution; they account for 94 % of the total losses at minimum filling level and

for 14 % at maximum filling level. At half charged system they account for 32 % of the total losses.

However, this contribution is underestimated because of the perfect stratified storage assumption, according to which the hot layer is at constant temperature and every surface is facing supercritical fluid at the maximum temperature. In reality, only the top cover of the tank faces the maximum fluid temperature, and some thermal gradient exists in the supercritical fluid, therefore the temperature difference across the lateral surface isn´t as big as the one across the top cover. This is true especially for high filling levels. A thicker layer than the lateral one is recommended for the top cover thermal insulation.
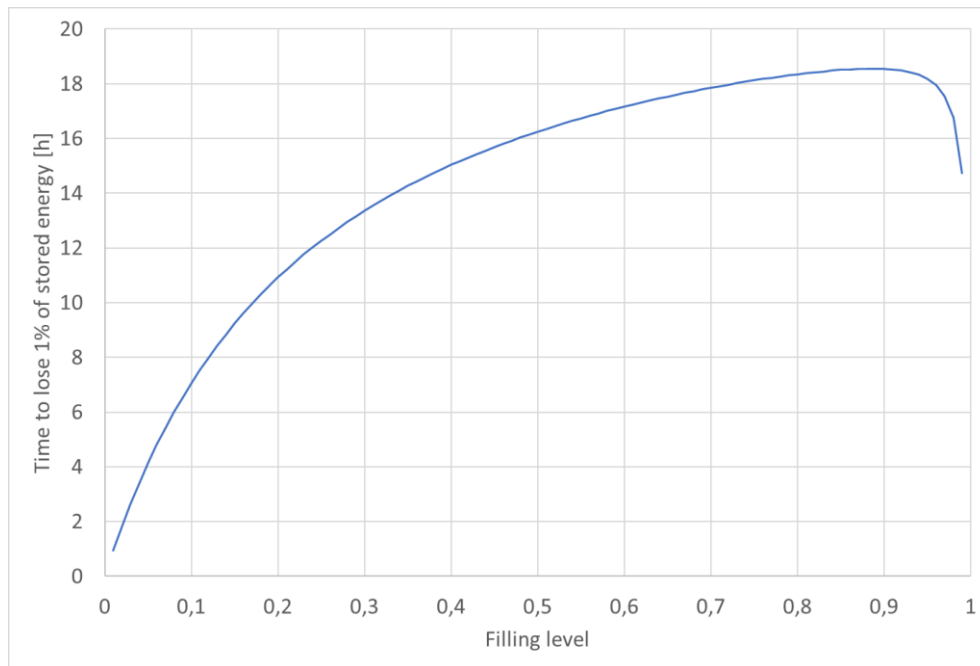

Figure 47 – Time to dissipate 1% of stored energy as function of filling level with 4 m of concrete

The simplified approach should make the time to lose 1 % of the stored energy underestimated. In fact, heat losses corresponding to a certain filling level are considered to be constant during the whole storing period, but in reality, they decrease with time, since the filling level itself reduces and, as a consequence, the lateral heat losses and the total. For high filling levels the time should be larger, that is, the curvature is in reality less pronounced, therefore this approach is conservative.

In order to have supercritical steam ready at inlet turbine temperature in the first moments after discharging process start, it is necessary to keep supercritical steam at hot storage conditions in the whole steam pipe $< 0,1$ %

Storage in the order of days is desired. If a storage time of 5 $days$ is considered, with this thick concrete wall the percentage of lost energy would be around 7,4 % at half charged system, which isn´t the desired low percentage.

- **Mullite foam insulated tank**

Mullite foam has been discussed as potential insulation material. In order to withstand the compressive strength, air at $25\ MPa$ has to be injected into the porous structure to create an ambient at the same pressure of the surroundings. This means the mullite foam can't be directly in contact neither with seawater nor with fresh water.

Two steel layers hypothesized both to be $\delta_s = 0{,}05\ m$ thick face the two fluids, mullite foam bricks of total thickness $\delta_{mf} = 1\ m$ are embedded in between in a pressurized ambient. Due to different temperature exposure, thermal conductivity of austenitic stainless steel has different values in the inlet layer and in the outer, respectively 20 and $15\ W/m\ K$.
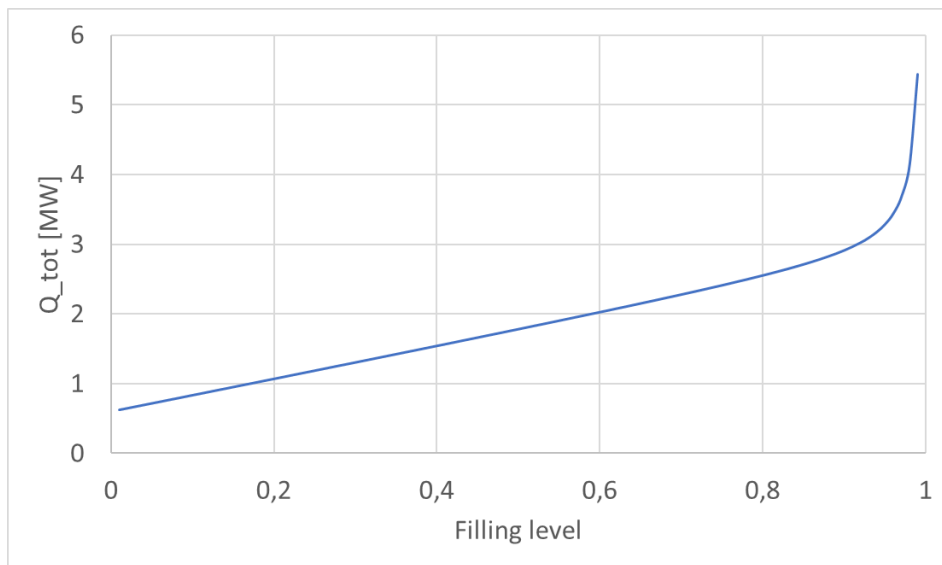

Figure 48 - Heat losses as function of filling level with $1\ m$ of mullite foam

At a filling level of 50 %, heat losses compared with the much thicker concrete layer are almost reduced by a factor of 3; time to lose one percentage point of the stored energy is $43{,}5\ h$. Bottom losses are always the same independently from the wall material; for this reason, the better the system is insulated, the greater the contribution of bottom losses on the total.

$\dot{Q}_{top} = 0{,}57\ MW$ are also reduced by almost three times and its contribution to the global heat losses is equivalent in percentages as the concrete wall case. Greater effect of bottom losses is visible in both charts; a filling level of more than 80 % shouldn't be reached, in fact the time needed to lose 1 % of the energy doesn't increase for higher filling levels.
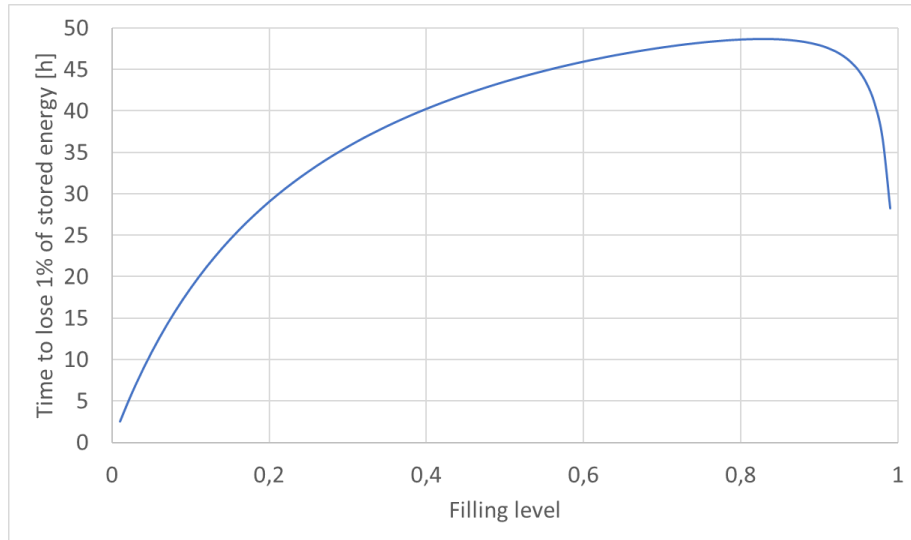
Figure 49 - Time to dissipate 1% of stored energy as function of filling level with $1\,m$ of mullite foam

When a short storing period in the order of hours is desired, one-meter thick insulation layer could be acceptable. Increasing the insulation thickness, losses can be further decreased, but efficacy of extra insulation thickness decreases with increasing thickness, as already mentioned.
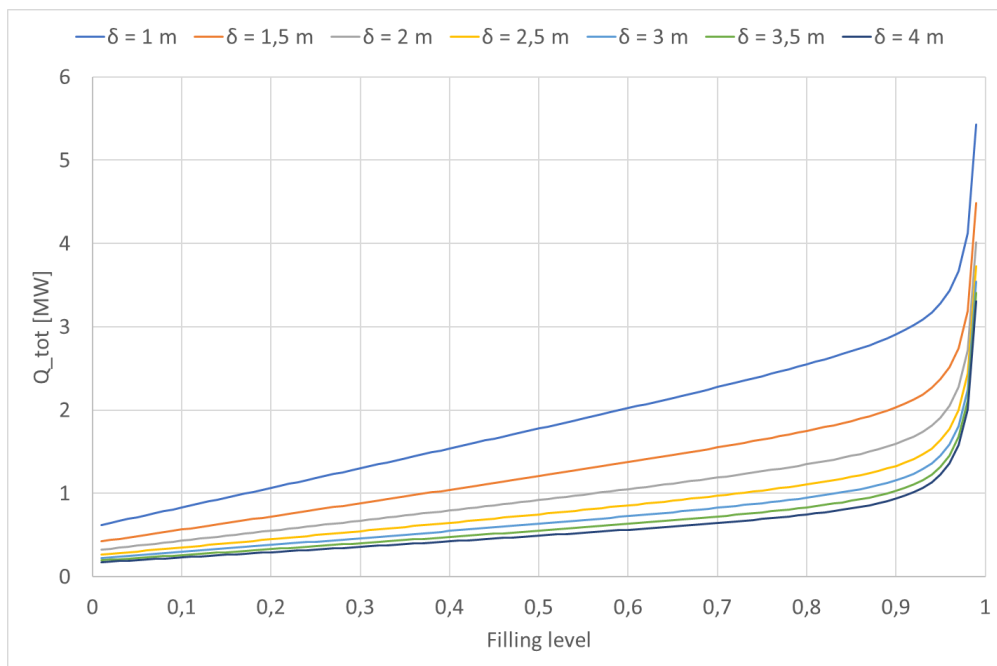

Figure 50 – Heat losses as function of filling levels for different mullite foam thicknesses

It seems to be unreasonable increasing excessively the thickness. Until $2 - 2,5\,m$ the reduction in heat losses is clearly pronounced, then it appears the effect is almost negligible. Figure 51 proves this wrong, in fact every add centimeter is useful to increase to storing time.
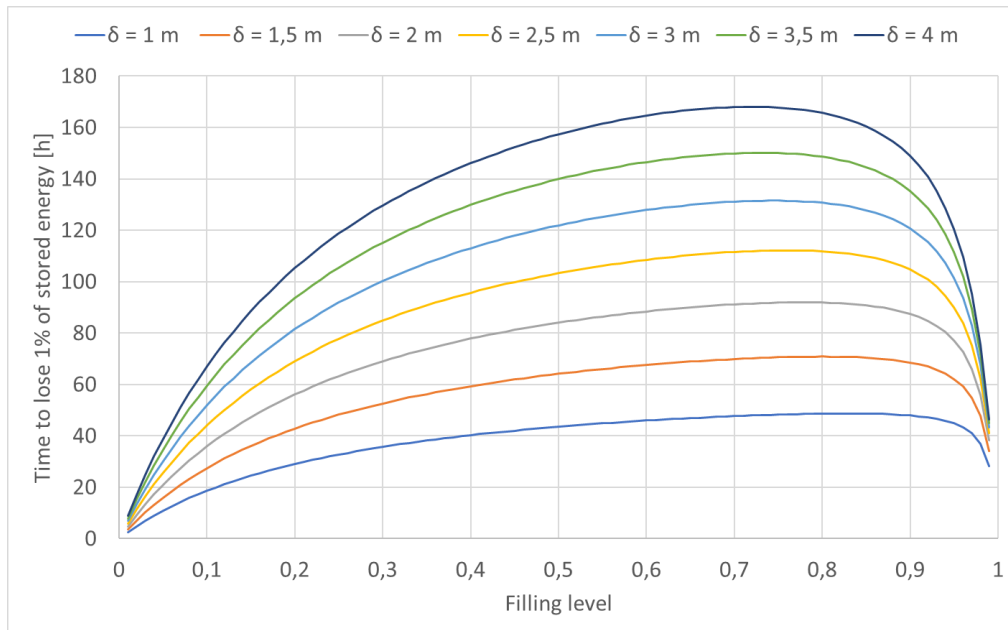
Figure 51 – Time to dissipate 1% of stored energy as function of filling level for different mullite foam thicknesses

Imagine a BattMarines installation in the Mediterranean Sea in front of the north African coast, in which input heat of the battery is obtained from electricity generated by large PV solar panels fields installed in the desert. It is usual to have periods in the order of weeks in which the sun shines continuously during the whole day and a redundant amount of renewable power could be available to charge this system. In such circumstances, it is desired to have a week-term storage system able to deliver back electrical power after great amount of time, unusual for common thermal energy storage tanks.

A mullite foam layer of $4\ m$ thickness would allow to keep the energy losses to extremely low value. Even with the very conservative hypothesis used, $6\ days$ and $13\ hours$ are required to lose only $1\ \%$ of the stored energy at half filling level.

In other possible installation locations, where the energy to charge the battery is also generated through renewable sources but production is more discontinuous, a shorter-term storage system could be accepted and with a thickness of mullite foam layer of $2\ m$ the same amount of energy is lost in $84\ hours$.

-   **Glass particulate insulated tank**

Second best solution has been found to be glass particulate insulation layer. This material should be adopted if mullite foam bricks can´t operate in an ambient at $25\ MPa$.
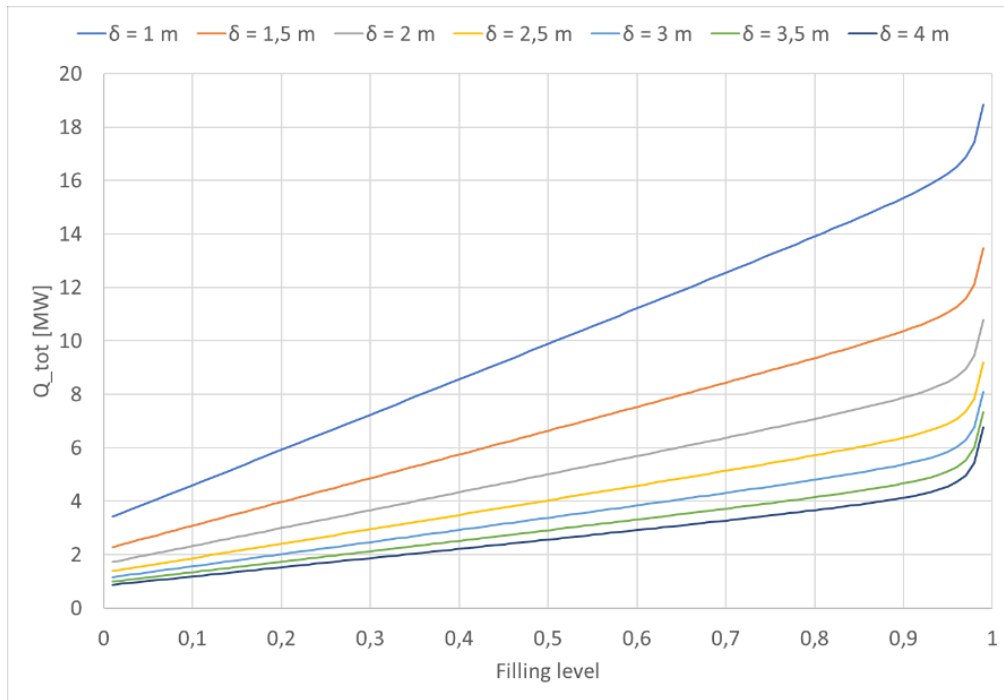
Figure 52 – Heat losses as function of filling levels for different glass particulate thicknesses
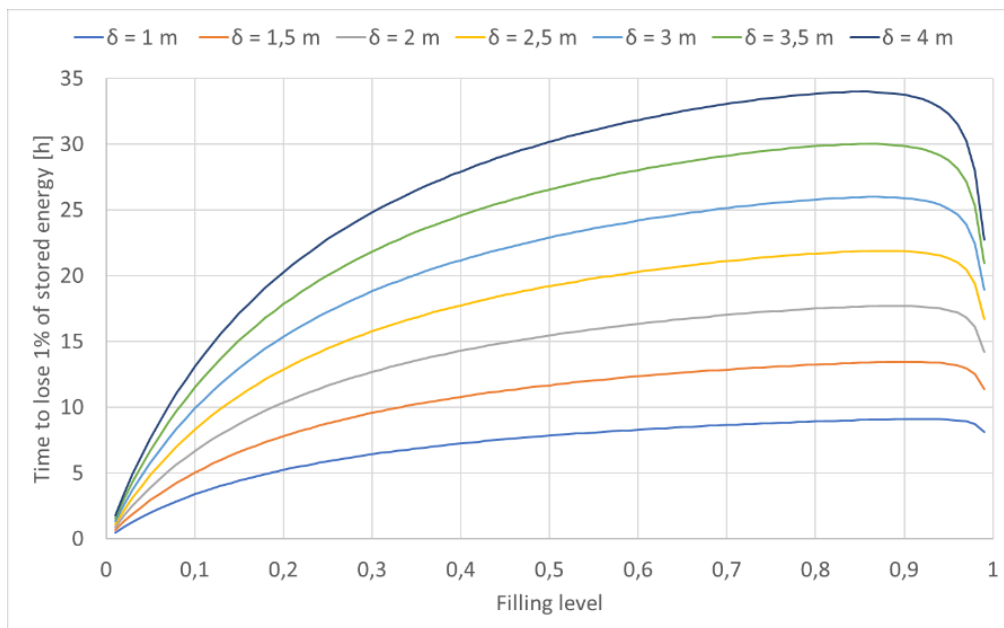

Figure 53 – Time to dissipate 1% of stored energy as function of filling level for different glass particulate thicknesses

Due to worse insulation efficiency compared to previous material, bottom losses effects are visible for higher filling levels. There is a factor bigger than 5 in the reduction of storing time compared to the mullite wall.

Storing times are in the order of many hours, up to more than $30\ h$ for high filling levels.

- **Bottom insulation**

For high insulation thicknesses, it is fundamental to reduce the losses toward the bottom. The idea is to take advantage of the great change in density of water with temperature shown in figure 54, that is the the reason why stratification really occurs and must be considered in these estimations.

Because the filling level never stays constant, it should be found a low conductive material that can operate in these supercritical steam temperatures and with a density such to be able to float exclusively in the subcritical water layer and not in the supercritical one.

With a movable separator between the subcritical and supercritical fluid, bottom losses can be reduced.
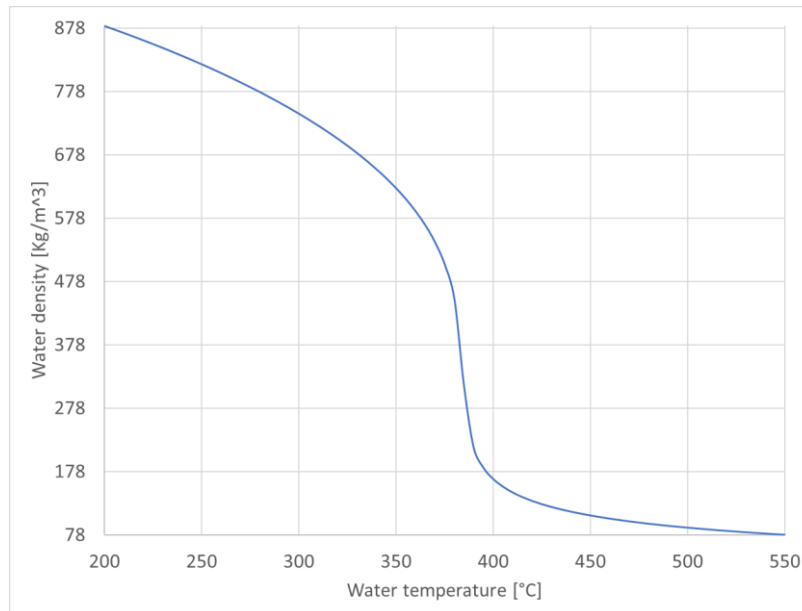

Figure 54 – water density vs temperature at a pressure of 250 bar

At storage tanks pressure, the fastest change in density as function of temperature happens in the $370 - 390\ °C$ interval, around critical water temperature, where density varies from $\sim 540\ Kg/m3$ to $\sim 215\ Kg/m3$.

At a temperature of $385\ °C$ the steepest point of the curve can be found, corresponding to a density of $\sim 312\ Kg/m^3$. A potential insulation material could have this density in order to be able to float on the underlying water and not on the supercritical fluid.

The hypothesis of having a fluid at constant temperature in the height corresponding to during storing time with the whole temperature gradient existing in the remaining height, a sort of half perfect stratification, is very approximate but reasonable for a simple estimation.

6.5 Water pipeline

For what concerns the water pipeline, since the mass flow rate must be the same of the steam pipeline and the density of the water is around ten times the density of the steam, the water velocity has to be ten times lower than the steam velocity, thus $w_w \approx 4 \ m/s$ with a diameter of $0,2 \ m$.

Design of this component is less challenging, being temperature gradients and mechanical stresses involved lower than the steam pipeline ones.

6.5.1 Pressure losses

In a first analysis, properties can be evaluated at reference cycle preheated water conditions, namely at 250 bar and 280 °C:

$$Re \ = \ \rho \, w \, d \, \mu^{-1} = 6419584$$

$$f = 0,00865$$

$$\Delta p_f \simeq \ 7 \ bar$$

$$\Delta p_g \simeq \ 190 \ bar$$

$$\Delta p_{tot} = \Delta p_f - \Delta p_g \ = \ -183 \ bar$$

A consistent gain of pressure occurs in the water pipeline. For this reason, when $250 \ bar$ are wanted at a depth of $2500 \ m$, inlet pipe pressure has to be much lower. Pumping system of the Rankine cycle will consume less energy than the reference cycle, because most of the pressure in gained in this pipeline.

Considering an inlet pressure of $70 \ bar$ at the same temperature, the pressure gain reduces to $\sim 180 \ bar$ and the goal is achieved. This pressure drop evaluation is implemented in an excel file in order to see the change of total pressure drop value changing the pipe dimensions.
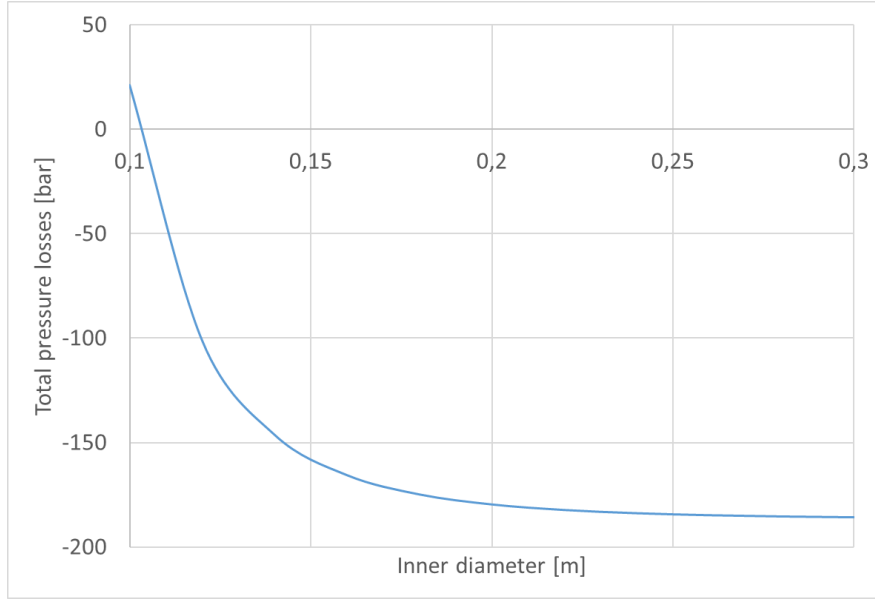
Figure 55 – Descending water pipeline pressure losses as function of diameter

This curve gives even better the idea that no big challenges occur in the water pipeline. Smaller diameters could be used for it and still have consistent pressure gain. It is senseless to have a smooth water pipeline if such gain of pressure takes place, in fact, it would only mean to install more expensive equipment to gain few more bars out of $\sim 180\ bar$. Rough pipe will be used and for rough pipes the curve has to be shifted slightly upwards, but again consistent values of pressure gains are obtained. In the simulation chapter smooth and rough water pipes behaviour will be compared.

To conclude on the water pipe, its design will be the result of an optimization between its cost (related to the inner diameter) and the energy required by the pumping system of the power plant, because decreasing the diameter results in decreasing of pressure gained.

6.5.2 Mechanical stresses

The closer to the sea surface, the more stressed the structure is. As for the steam pipe, insulation is probably going to be made with a porous material or a particulate structure that require to be contained in between stainless steel layers. If the inlet pressure is constant at $8\ MPa$ and the insulating layer contains air at ambient pressure, the minimum thickness of the inner steel layer would be:

$$\delta_{min} = \frac{p_i\ D_{out}}{2\ (QF\ \sigma_{\theta,max} + p_i\ Y)} \cong 4\ mm = 0{,}4\ cm$$

$\sigma_{\theta,max} = 250\ MPa$ has been fixed to a higher value than steam pipe case due to lower temperature, quality factor $QF = 0{,}8$ for not seamless pipe is considered and coefficient $Y = 0{,}5$ required when $\delta < D/6$.

Inner steel layer thickness can be set to $\delta_s = 1\ cm$ and the outer one as before to $0,5\ cm$, but it is fixed to $1\ cm$ for simplicity of thermal analysis. No challenges occur in the water pipeline.

Three materials are analysed as insulators. Mechanical properties of two of them have been already mentioned, only reticulated vitreous carbon foam hasn´t been yet considered. In water tank and in the deepest part of the water pipeline, the solid matrix of the foam material has to withstand the greatest compressive strength.

Also this material seems potentially applicable, but still it should be tested because of lack of experience in foam behaviour under these conditions.

6.5.3 Thermal analysis

Three insulation configurations performances are compared, with a total wall thickness of $15\ cm$, namely $13\ cm$ of insulator contained in two steel layers one centimetre thick each. Inner steel thermal conductivity will be set at $\lambda_s = 17,5\ W/m\ K$ corresponding to the new temperature.

$\Delta T = 270\ °C$ is fixed all along the tube with $d_i = 0,2\ m$. Inlet enthalpy is fixed at $h_{in}\ (275\ °C\ ,70\ bar) \cong 1210,3\ kJ/kg$.

- **Glass particulate**

$$R \cong 7,76e - 5\frac{K}{W}$$
$$\dot{Q} \cong 3,478\ MW$$
$$h_{cs} = h_{in} - \frac{\dot{Q}}{\dot{m}} = 1175,5\frac{kJ}{Kg}$$
$$\eta_{th} = 1 - \frac{h_{in} - h_{cs}}{h_{hs} - h_{in}} \cong 98,3\ \%$$

Insulation is effective but thermal flux is quite important.

- **Mullite foam**

$$R \cong 3,555e - 4\frac{K}{W}$$
$$\dot{Q} \cong 0,759\ MW$$
$$h_{cs} = h_{in} - \frac{\dot{Q}}{\dot{m}} = 1202,7\frac{kJ}{Kg}$$
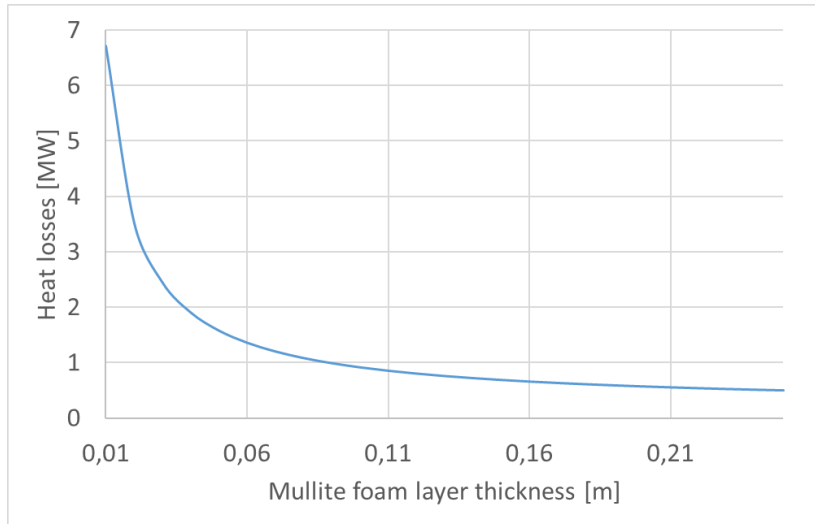$$\eta_{th} = 1 - \frac{h_{in} - h_{cs}}{h_{hs} - h_{in}} \cong 99,6\ \%$$

Figure 56 – Heat losses function of mullite foam thickness

Less than 1 % of the energy content is lost and temperature difference between inlet and outlet is almost negligible, in fact the reduction of temperature due to heat transfer is counterbalanced by its increase caused by pressurization.

- Vitreous carbon foam

$$R \cong 6,205e - 4\frac{K}{W}$$
$$\dot{Q} \cong 0,435 \ MW$$
$$h_{cs} = h_{in} - \frac{\dot{Q}}{\dot{m}} = 1206 \ kJ/kg$$
$$\eta_{th} = 1 - \frac{h_{in} - h_{cs}}{h_{hs} - h_{in}} \cong 99,8 \ \%$$
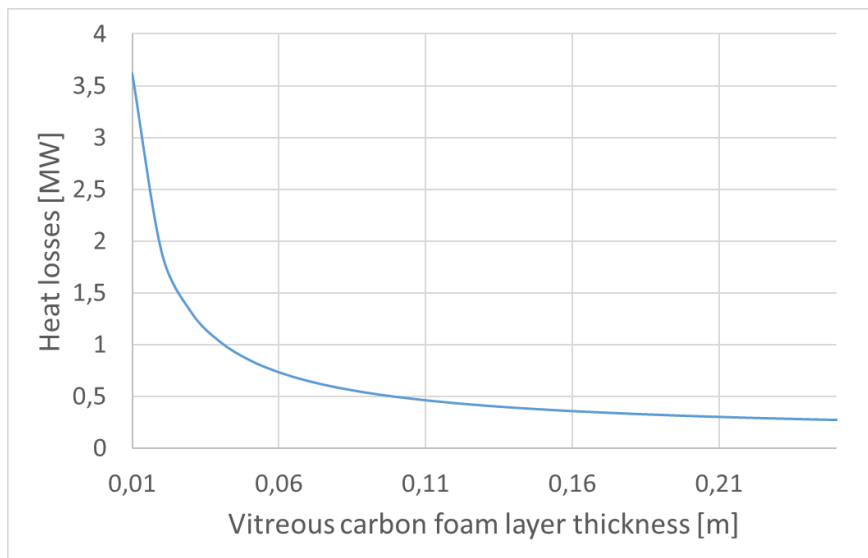

Figure 57 – Heat losses function of RVC foam thickness

With this material as insulator, heat losses can actually be neglected in the water pipeline.

6.6 Cold storage tank

The preheated water is pumped underwater at a pressure of $250\ bar$ and temperature $T_w \cong 275\ ℃$, with a density of $\rho_w = 785\ \frac{Kg}{m^3}$:

$$V_{cs} = m\ /\ \rho_w\ \approx 1.27 * 10^5\ m^3$$

Due to a factor 10 in density increase, required volume is one tenth of the steam tank volume. Cylindrical shape of the tank, a solution could be:

$$d_{cs} \approx 55\ m$$

$$h_{cs} \approx 55\ m$$

Mechanical stresses aren't a challenge to be managed, in fact, the cold storage tank will face almost null pressure difference at any height because the density of the stored liquid is similar to the seawater density.

As mentioned for the steam components, to have water entering the cold tank at appropriate thermodynamic conditions just after the start of discharging process, the water pipeline has to be kept at cold storage temperature during the whole storing period.

The cold storage is filled up during discharging phase. At the end of it, charging process could start at any time, depending on the availability of redundant renewable generated electricity, and could last from hours to days, depending on the amount of this electrical energy. For these two reasons, cold storage requires proper insulation as well.

The cold storage temperature is around $\sim270\ ℃$, corresponding to $\Delta T = 265\ ℃$ between inner and outer wall surface. Thermal losses are expected to be much smaller than the hot storage tank, both because of lower temperature and lower exchanging surface. Materials previously discussed, in particular mullite foam, should allow to insulate properly with a thin wall.

7 SYSTEM SIMULATION

7.1 Introduction to TIL

The company TLK-Thermo GmbH offers platform independent software products [46]. It has a broad range of software related to physical modeling and simulation, interoperability between different programs, software for the model-based design and analysis of systems as well as visualization software for both measurement and simulation data.

TIL Suite is suitable for the stationary and transient simulation of freely configurable thermodynamic systems [47]. Thanks to the substance property library, TILMedia – a component of the TIL Suite – system simulations can be performed extremely quickly and accurately. The individual models in TIL are described using the modeling language Modelica.

The Modelica Language [48] is a non-proprietary, object-oriented, equation based language to conveniently model complex physical systems containing, e.g., mechanical, electrical, electronic, hydraulic, thermal, control, electric power or process-oriented subcomponents. Modelica Simulation Environments are available commercially and free of charge, such as Dymola, which is used.

DaVE [46] is a visualization and simulation environment that is suitable for both the post-processing and the online display of dynamic data sets. It is used to show some of the simulation results.
Figure 58 shows fluid types existing in TILMedia. All figures in this introduction subchapter are taken from the TIL documentation.

Name	Description	Symbol
Gas	ideal gases / gas mixtures	G
VLEFluid	Compressible two-phase fluids, vapor/liquid, pure substances / mixtures	VLE
Liquids	Incompressible single-phase fluids	L
Solid	Temperatur dependend properties	S
SLEMedium	Two-phase fluids: **s**olid/**l**iquid **e**quilibrium	SLE

Figure 58 – Fluid types in TILMedia

The VLEFluid type will be adopted to simulate steam components and supercritical water components, the Liquids type is used for the feed-water cycle. Other fluid types aren't needed.

The library is structured in different types of packages, which are indicated by different icons. Each package has ready-to-use component models, which are also indicated by different icons. Those models that will be used are briefly introduced.

- **SIM – System Information Manager**

The System Information Manager is necessary in all system models of this library. It defines the substances which are used in the component models of the system. The substances are selected by replaceable records in the SIM model. In every simulation, water is selected as working fluid in the SIM. No other substances are selected.
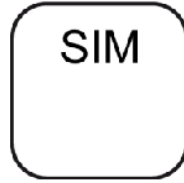

Figure 59 – SIM icon

- **VLEFluid cell**

The VLEFluid cell maps a flow of a compressible two-phase, vapor or liquid fluid flow. This cell model covers substances and mixtures. Figure 60 represents the structure and equations of the model.

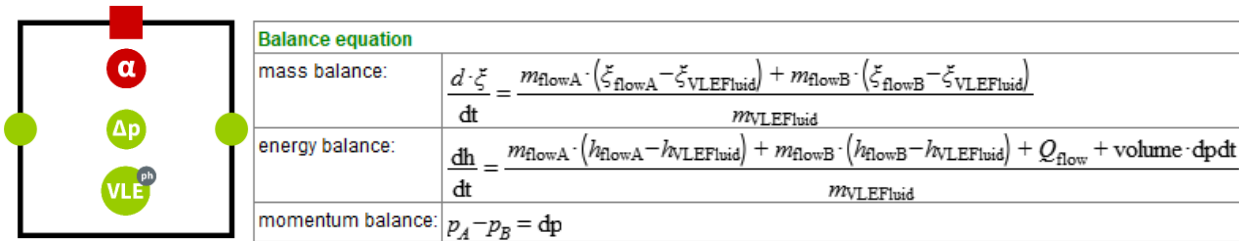| Balance equation	
mass balance:	$\dfrac{d \cdot \xi}{dt} = \dfrac{m_{\text{flowA}} \cdot \left(\xi_{\text{flowA}} - \xi_{\text{VLEFluid}}\right) + m_{\text{flowB}} \cdot \left(\xi_{\text{flowB}} - \xi_{\text{VLEFluid}}\right)}{m_{\text{VLEFluid}}}$
energy balance:	$\dfrac{dh}{dt} = \dfrac{m_{\text{flowA}} \cdot \left(h_{\text{flowA}} - h_{\text{VLEFluid}}\right) + m_{\text{flowB}} \cdot \left(h_{\text{flowB}} - h_{\text{VLEFluid}}\right) + Q_{\text{flow}} + \text{volume} \cdot \text{dpdt}}{m_{\text{VLEFluid}}}$
momentum balance:	$p_A - p_B = \text{dp}$

Figure 60 – VLEFluid cell icon and constitutive equations

The VLEFluid cell contains a replaceable pressure drop model. The model provides different correlations for the calculation of the pressure drop, regarding the geometry information and the substance properties. Predefined universal approaches, as well as correlations derived from the literature are provided in the library.

The convective heat transfer of the VLEFluid flow is calculated, using a replaceable heat transfer model, considering the geometry information and the substance properties.
The model provides a heat transfer coefficient (lpha). As for the pressure drop model, predefined correlations are provided in this library.

The heat port enables the consideration of a heat flow rate from the outside. The heat flow rate is calculated using the equation:

$$Q_{\text{flow}} = \text{alphaA} \cdot \left(T_{\text{heatPort}} - T_{\text{Liquid}}\right)$$

The VLEFluid cells are based on a finite volume approach, using ideally mixed volumes. Unfortunately, it hasn´t been possible to simulate the hot storage tank because of the VLEFluid cell behaviour: having ideally mixed volumes doesn´t allow to simulate properly

thermal stratification, which is definitely required to have supercritical steam. Moreover, there isn´t a tank component available.

- **Liquid cell**

The liquid cell maps the flow of an incompressible single-phase fluid. Compared with the VLEFluid cell, pressure drop and convective heat transfer coefficient computational procedures are equivalent, while mass and energy balance equations are different.
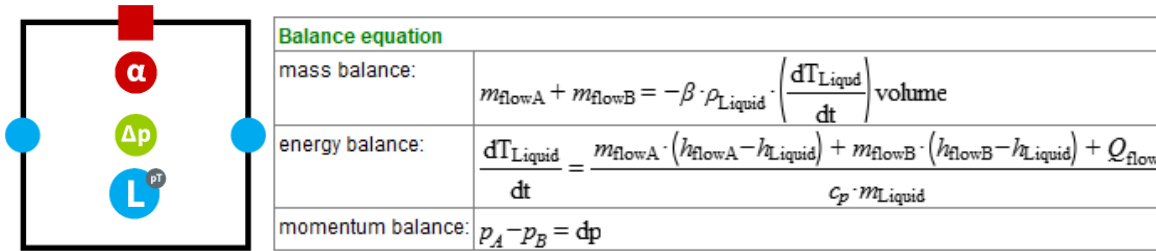
Balance equation	
mass balance:	$m_{flowA} + m_{flowB} = -\beta \cdot \rho_{Liquid} \cdot \left(\dfrac{dT_{Liqud}}{dt}\right) \text{volume}$
energy balance:	$\dfrac{dT_{Liquid}}{dt} = \dfrac{m_{flowA} \cdot \left(h_{flowA} - h_{Liquid}\right) + m_{flowB} \cdot \left(h_{flowB} - h_{Liquid}\right) + Q_{flow}}{c_P \cdot m_{Liquid}}$
momentum balance:	$p_A - p_B = dp$

Figure 61 – Liquid cell icon and constitutive equations

- **Wall cell**

The wall cell contains four heat ports: portN, portS, portW, portE. The model uses a transient energy balance, considering the heat capacity of the material. A heat conductance to the ports is calculated using either a fixed heat resistance or a geometry and material-based heat resistance.
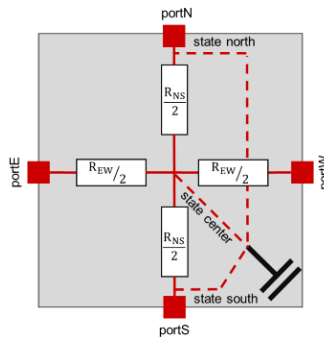

Figure 62 – Wall cell icon

- **Boundary elements**

Boundary models determine the conditions at the boundary of the system.
In the VLEFluid boundaries the user can determine enthalpy or temperature, mass fraction, pressure / mass or volume flow rate.

In liquid boundaries the user can determine enthalpy or temperature, pressure / mass or volume flow rate.

With overdetermine boundary the thermodynamic state is completely known, therefore the system needs also an underdetermined boundary. The other possible configuration is to have two normal boundaries in the system.

Thermal boundary in red can be single or multi-port depending on number of cells at which the boundary is connected; temperature or heat flow rate can be given as input. With the normal mechanical boundary (grey color) rotational speed can be given as input.
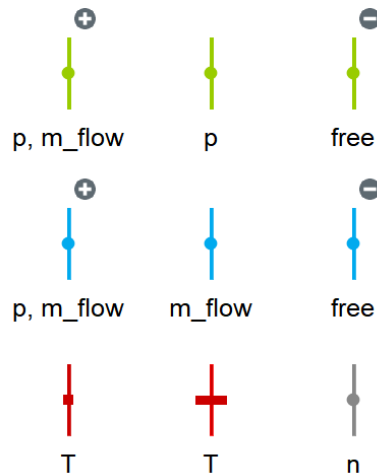

Figure 63 – Boundaries' icons

- **Pressure state model**

The pressure state model is needed whenever a VLEFluid model with a volume is used. This model defines a pressure level by implementing a pressureStateID, to which the corresponding VLEFluid components had to be assigned. The pressureStateID will be displayed with a number inside the component's icon.

It is required because the mathematical description of the VLEfluid components is based on one major assumption: the term dp/dt in the balance equations is treated as constant along the direction of flow for each pressure level of the system. Therefore, each model of the same pressure id uses the same derivative of the pressure with respect to time in its balance equations. This approach increases the time constants of the model and therefore improves simulation performance.
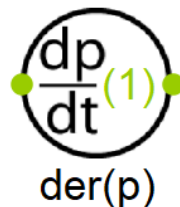

Figure 64 – Pressure state model icon

- **VLEFluid tube**

The VLEFluid tube model can simulate single pipes as well as a bundle of pipes. A discretization is realized using an alignment of VLEFluid cells in flow direction. The number of used cells will be defined by the integer nCells. The mass and energy balances are calculated by a transient balance equation for each cell individually. Corresponding to the

discretization of the medium flow, the wall of the tube is discretized by solid masses, represented by wall Cell models. The structure of the tube is shown in figure 65.
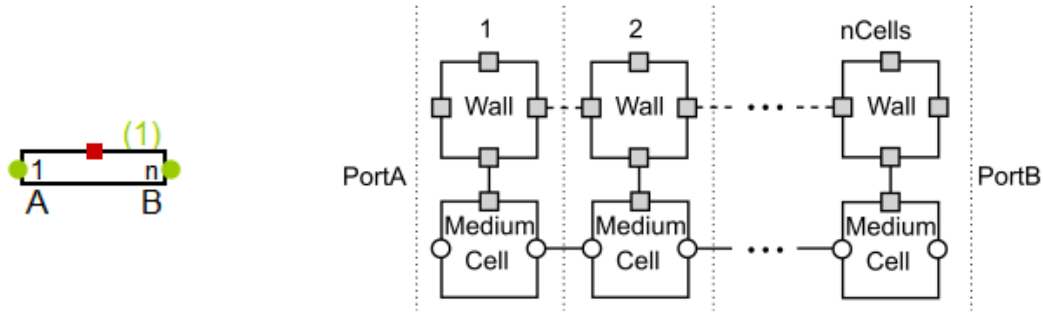

Figure 65 – VLEFluid tube icon and discretization

-   **ParallelFlowHX – Plate**

A variety of heat exchanger models for different geometries and medium combinations are available. Plate heat exchangers is selected, and the geometry can be customized directly via the graphical user interface. Only number, length and width of plates is modified, while other geometrical parameters are left to default values.
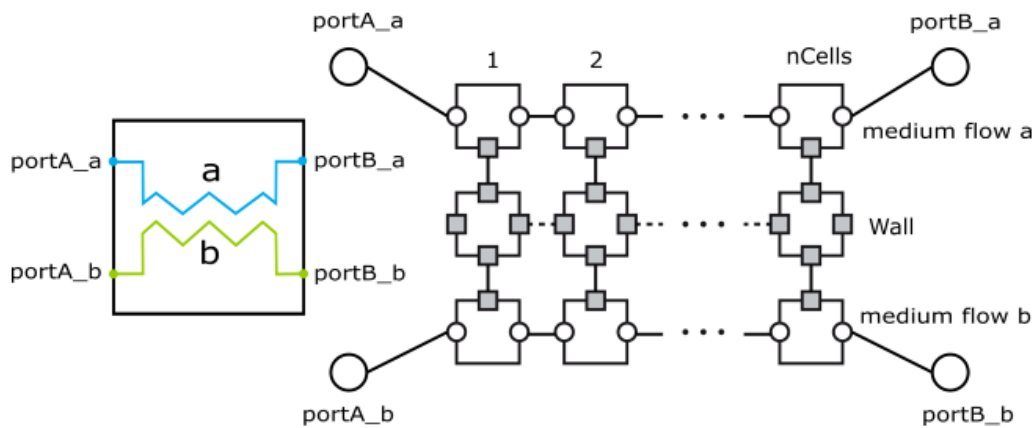

Figure 66– Parallel flow heat exchanger icon and discretization

-   **Efficiency based expander model**

The efficiency based expander model is defined by the rotational speed n, a fixed intake volume and three fixed efficiencies (fillFactor, η_{Is}, η_{EffIs}). This approach considers the physical effects, which lead to a deviation from an ideal expansion by impelling three efficiencies assumed to be constant and indipendent each other.
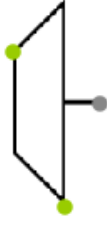
value	equation
fillingFactor	$m_{flow} = \text{fillFactor} \cdot \rho_{Suction} \cdot n \cdot \text{intakeVolume}$
isEff	$h_{Discharge} = h_{Suction} + \left(h\_Isentropic_{Suction} - h_{Suction} \right) \eta_{Is}$
effIsEff	$P_{shaft} = m_{flow} \cdot \left(h\_Isentropic_{Discharge} - h_{Suction} \right) \eta_{EffIs}$

Figure 67 – EffExpander model icon and constitutive equations

The filling factor is needed to calculate the total mass flow rate composed of a leakage mass flow rate and the effective mass flow rate. The isentropic efficiency is required to calculate the discharge enthalpy, whereas the effective isentropic efficiency is necessary to calculate the shaft power, namely it represents the mechanical efficiency. The difference between the shaft power and the change of the enthalpy flow rate is represented by the heat flow rate through the expander housing, which can be accessed in the simulation tab.

A mass flow rate is defined in this model, considering the value of the intake volume and the rotational speed, which can be set either as fixed value (nFixed) or set using a mechanical boundary condition.

- **VLEFluid junction**

The VLEFluid volume junction handles the connection of three medium flows using a dynamic mass and energy balance. The balance bases on the differential state of a fixed volume.

$$\frac{dH}{dt} = m_{flowA} \cdot \left(h_A - h \right) + m_{flowB} \cdot \left(h_B - h \right) + m_{flowC} \cdot \left(h_C - h \right) + \text{volume} \cdot \left(\frac{dp}{dt} \right)$$

$$\frac{d \cdot \xi}{dt} = \frac{m_{flowA} \cdot \left(\xi_A - \xi \right) + m_{flowB} \cdot \left(\xi_B - \xi \right) + m_{flowC} \cdot \left(\xi_C - \xi \right)}{m_{VLEFluid}}$$

Figure 68 – VLEFluid junction icon and constitutive equations

- **Orifice valce**

The orifice valve model calculates the mass flow rate in dependency of the pressure drop using the equation of Bernoulli.
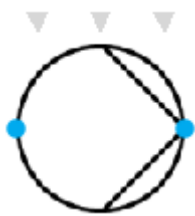

$$m_{flow} = A_{eff} \cdot \sqrt{\left(p_{Input} - p_{Output} \right) \cdot 2 \rho_{Input}}$$

Figure 69 – Orifice valve icon and constitutive equations

- **Simple pump**

The Simple Pump Model either defines a pressure increase or a mass / volume flow rate.

Power calculation		
P_hyd	hydraulic power transmitted to the medium	$P_{hyd} = dp \cdot V_{flow}$
P_loss	power losses during fluid acceleration. The power losses are assumed to be constant with the speed.	$P_{loss} = \eta_{drive} \cdot P_{drive} \cdot (1-\eta)$
P_drive	Required power input of the Pump	$P_{drive} = \left(\dfrac{1}{\eta}\right)\left(\dfrac{1}{\eta_{drive}}\right) P_{hyd}$

Figure 70 – Simple pump icon and constitutive equations

- **Sensors**

A sensor is used to monitor the thermo-physical properties and the hydraulic values of a medium flow at a certain point in a system. A state variable is monitored by connecting the sensor model with a port of the corresponding medium type in the system. A flow variable is monitored by passing the flow through the sensor, whilst connecting the inlet and outlet port of the sensor.

The fifth sensor of VLEFluid components represents a state point and allows a specific thermodynamic condition to be drawn on DaVE State Charts. It corresponds to a point in a thermodynamic cycle, for this reason it is denoted with an index.
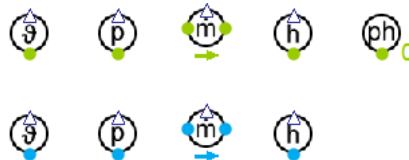

Figure 71 – Sensors

7.2 Steam pipeline

The model of the steam pipeline is shown in figure 72.
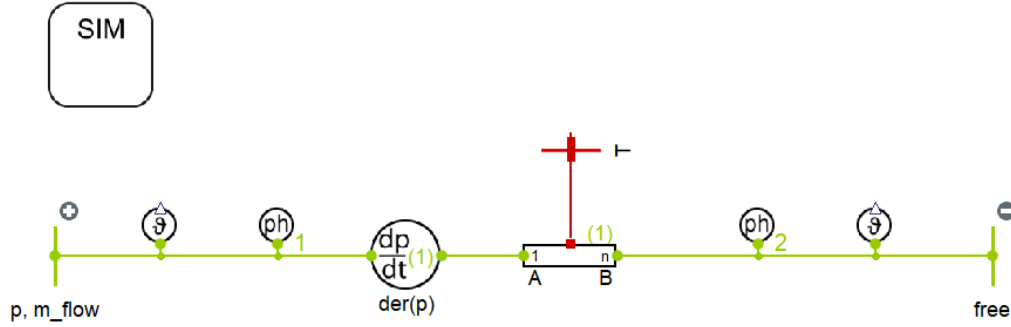

Figure 72 – Steam pipeline model

In this simple model, one boundary is connected to the inlet port of a component called tube and a second boundary to the outlet of the same component. Inside this tube component, transport phenomena are computed, namely pressure drop and heat losses are calculated.

Boundary representing the hot storage conditions is overdetermined: mass flow rate, pressure and temperature are given input properties, meaning the thermodynamic state is completely known. The boundary corresponding to the turbine inlet condition (tube outlet) is instead underdetermined and its properties are computed during the simulation and represent the simulation results.

Due to huge length, discretization is probably required. For each pipeline configuration, three different discretization are studied: $1/\,25/\,250$ cells, corresponding to single cell length of $2500\,/\,100\,/\,10\,m$.

Results with single cell pipeline, therefore with no discretization, should be more or less equivalent to the estimated value in the previous chapter.

Friction factor is computed with the Konakov correlation, (5.3). When a rough pipe wants to be studied, a correlation that considers surface roughness is adopted directly from the existing pressure drop models in TIL, namely the Swamee and Jain correlation [49]:

$$f = 0{,}25 \left(\log \left(\frac{\varepsilon}{3.7\, d_{in}} + \frac{5.74}{Re^{0.9}} \right) \right)^{-2}$$

Pressure drop is also carried out analogously, only with the addition of a correction for the discretization in the static pressure drop evaluation:

$$\Delta p_{st} = \rho\, H\, g\, (L_{cell}/L_{tube})$$

Heat losses can be simulated with different models. I already mentioned the intention of not considering flanges effect, therefore I will neglect both convective heat resistances to counterbalance this assumption.

The model ConstantAlphaA allows to estimate heat transfer between fluid and tube inner wall by setting a fixed value of the product between convective heat transfer coefficient and tube inner area, actually the inverse of the convective heat resistance. Convective coefficient can be easily estimated, and its value would lay around $\sim 2850 \, W/m^2 \, K$, but it is fixed to infinite, meaning ConstantAlphaA tends to infinite and convective thermal resistance to zero.

Heat transfer through the wall is simulated by fixing a value of the wall heat resistance. An eventual external convective heat resistance can be included in the wall heat resistance, but it is considered to be null. Every wall configuration heat resistance has already been computed in the last chapter and won´t change.

The external temperature is fixed at 5 ℃ with a heat boundary, which needs to have the same number of ports as the number of cells in the tube, such to have heat exchange all along the tube.

- **Mullite foam insulation**

	1 cell	25 cells	250 cells
Outlet pressure [bar]	226,13	226,99	227,02
Outlet enthalpy [kJ/kg]	3241,76	3241,83	3241,83
Outlet temperature [℃]	511,34	511,71	511,73
Heat losses [MW]	1,406	1,399	1,399

Effects of discretization are visible moving from single cell to 25. Cells of $100 \, m$ height each seem to be already sufficiently precise, in fact results are equivalent to the case of $10 \, m$ height cells. The main effect of discretization is the decrease of pressure losses, which lightly affects enthalpy drop and related thermal losses.

Anyway, differences aren´t pronounced and without discretization the computation is quite accurate. Main reason is that thermal resistance is given for the entire pipe and it isn´t influenced by discretization, while pressure losses computation is more effected by number of cells.
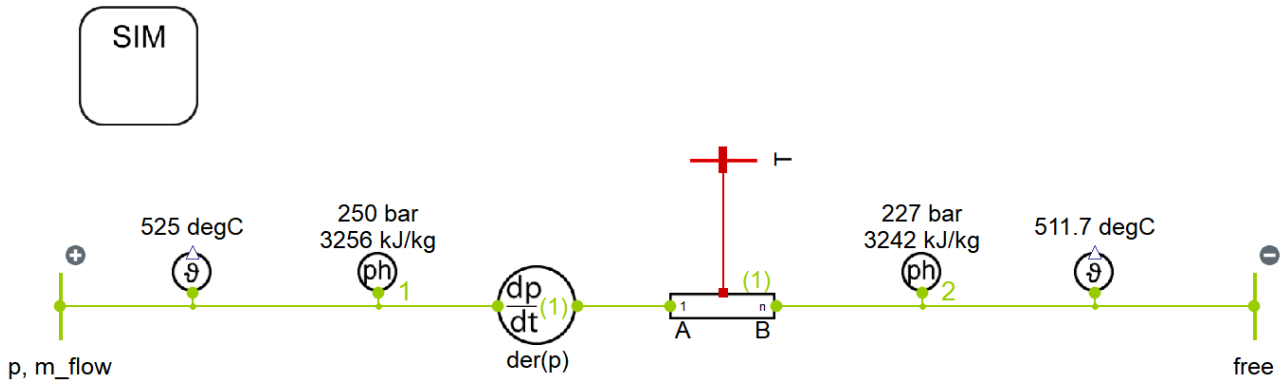
Figure 73 – Mullite foam insulated steam pipeline

With this steam pipe configuration, a lower hot storage temperature is required to reach the desired thermodynamic conditions at the turbine inlet. Hot storage temperature, or enthalpy, is adjusted until the outer conditions are obtained:
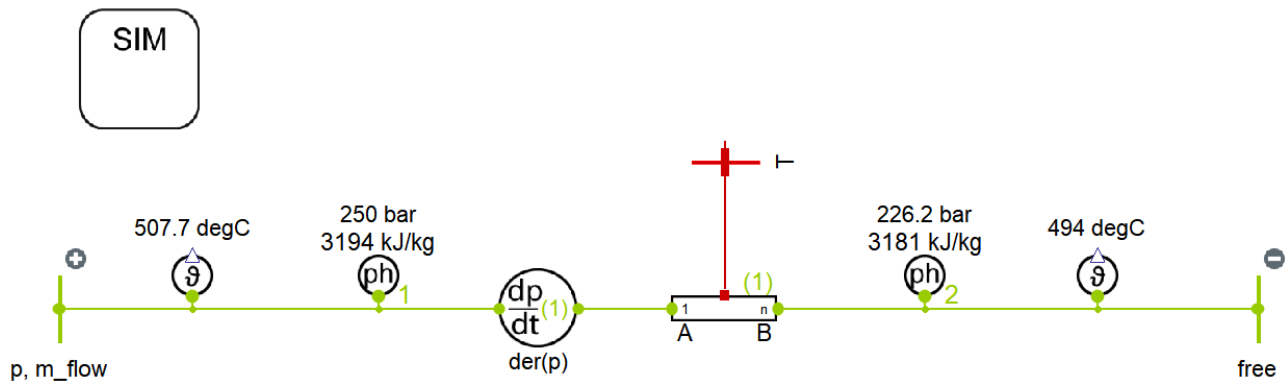

Figure 74 – Corrected mullite foam insulated steam pipeline

Hot storage conditions of $T_{hs} = 507,7\,°\text{C}$ and corresponding $h_{hs} = 3194,45\,kJ/kg$ has been found as solution, corresponding to outlet tube enthalpy of $3180,94\,kJ/kg$, pressure of $226,24\,bar$ and temperature $494\,°\text{C}$. This thermodynamic state slightly differs from the correct designed turbine inlet, but it is sufficient to consider pressure losses lightly higher in the tube to have the exact results for all properties.

Due to lower temperature in the tank, density increases and static pressure losses with it. Also, thermal losses are reduced because of lower supercritical steam temperatures, namely the temperature difference across the wall is reduced. Thermal losses result in $1,351\,MW$. Anyway, differences are small. Efficiency is calculated (see last chapter) to be $\eta = 98,4\,\%$. If the pipeline is considered to be rough with $\varepsilon = 0,05\,mm$, only couple of bars more are lost in comparison with smooth pipe wall.

This means it is sufficient to increase the storage pressure of around $2\,bar$ to enter the turbine at the desired condition with a rough pipe, namely pipeline inlet has to be $\sim 20\,m$ deeper. Temperature drop is slightly greater because of bigger depressurization, therefore hot storage temperature must be increased.
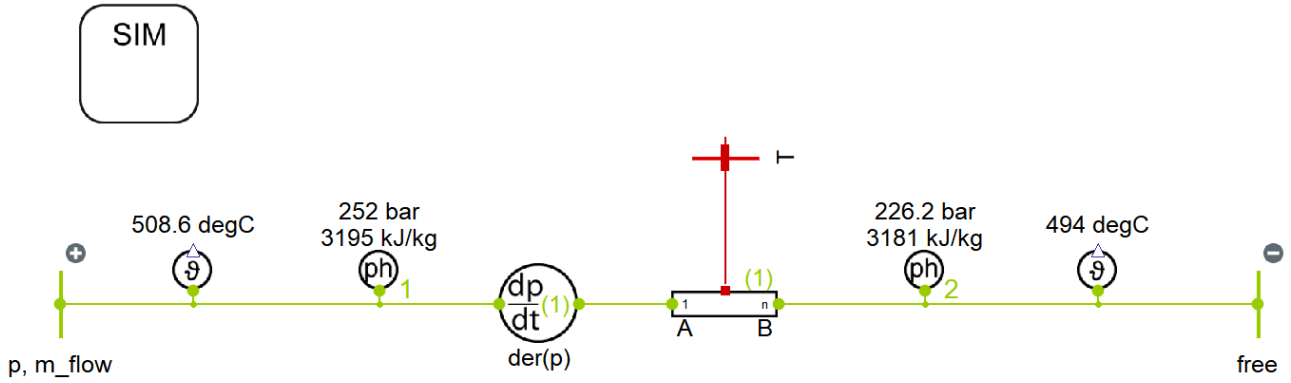
Figure 75 – Corrected mullite foam insulated rough steam pipeline

- **Glass particulate**

	1 cell	25 cells	250 cells
Outlet pressure $[bar]$	225,22	226,57	226,61
Outlet enthalpy $[kJ/kg]$	3178,78	3177,95	3177,92
Outlet temperature $[°C]$	492,93	493,29	493,3
Heat losses $[MW]$	7,704	7,786	7,790
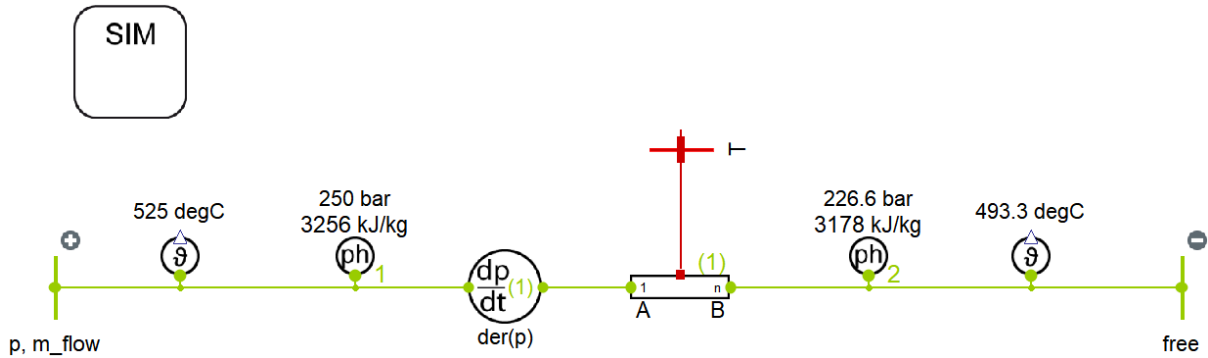
Figure 76 – Glass particulate insulated steam pipeline

The hot storage properties hypothesized in the beginning of the thesis are suitable for this specific pipeline configuration. To obtain the exact thermodynamic state at the outlet, inlet temperature should rise by less than one degree and an additional pressure drop of $0,61\ bar$ should take place. Efficiency of insulation is much lower as already discussed; it is found to be $\eta = 91,1\ \%$

The lower the thermal resistance of the pipe wall, the higher the hot storage temperature required to have the desired inlet power plant conditions. It also means the input energy of the storage system increases and the global efficiency decreases. In fact, if cold storage enthalpy is around $h_{cs}\sim 1210\ kJ/kg$ and charging mass flow rate equals the discharging one, input thermal energy would be $\dot{Q}_{in} = 204,6\ MW$ in case of glass particulate insulated pipe

and $\dot{Q}_{in} = 198,5\ MW$ with mullite foam insulation. An increase of 3 % in the input energy isn´t negligible and would affects the global performance of the battery.

7.3 Water pipeline

The model for the water pipeline is built in the exact same way. VLEFluid components and not liquid ones are used, because liquid domain does not consider compressibility effect and much more thermophysical properties are provided in VLEFluids. Properties evaluation is more precise.

Exact inlet properties aren´t known, they are fixed to $p = 70\ bar$ and $h = 1210\ kJ/kg$.

- **Glass particulate**

	1 cell	25 cells	250 cells
Outlet pressure smooth [bar]	252,76	253,9	253,95
Out pressure rough	247,93	249,03	249,07
Outlet enthalpy [kJ/kg]	1171,11	1170,51	1170,49
Outlet temperature [℃]	267,76	267,64	267,63
Heat losses [MW]	3,933	3,992	3,995
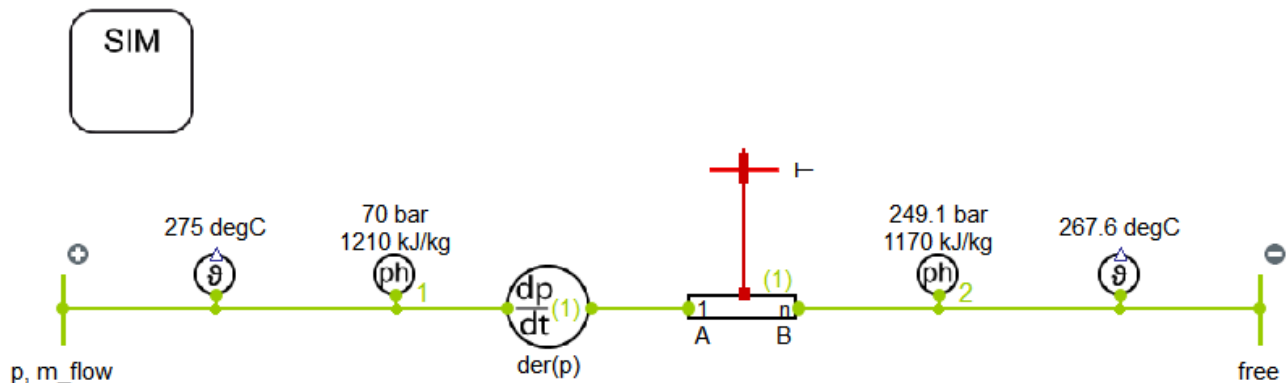
Figure 77 – Glass particulate insulated water pipeline

Inlet pressure should be increased by one bar to reach the storage pressure. Temperature difference across the wall is halved compared with steam pipe, therefore the same happens for heat losses. Efficiency is equivalent to the previously estimated one, namely $\eta = 98\ \%$, considering hot storage to be at 525 ℃ (steam pipeline with glass particulate).

- **Mullite foam**

	1 cell	25 cells	250 cells
Outlet pressure smooth [bar]	249,99	252,5	252,6
Out pressure rough	245,06	247,58	247,68
Outlet enthalpy [kJ/kg]	1202,89	1202,85	1202,85
Outlet temperature [℃]	274,35	274,35	274,35
Heat losses [MW]	0,755	0,759	0,759
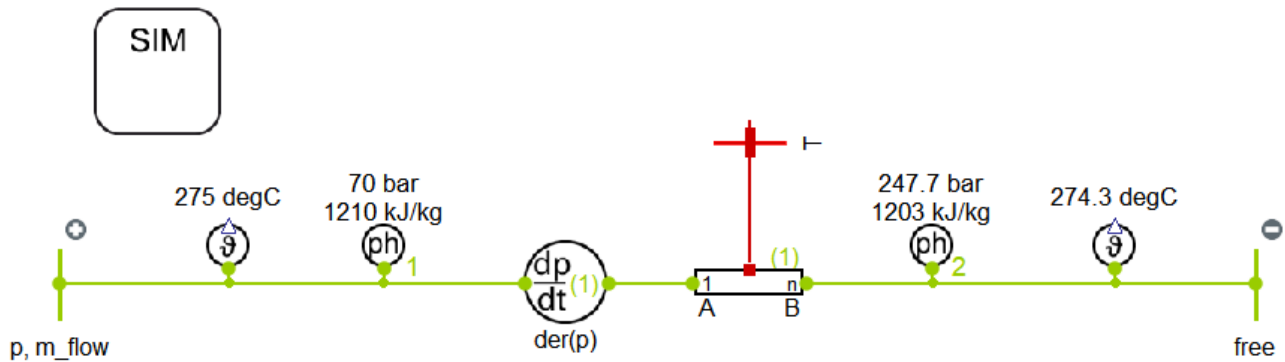
Figure 78 – Mullite foam insulated water pipeline

Temperature decrease due to heat exchange is counterbalanced by the increase of temperature caused by great gain in pressure. The overall temperature change is almost null and the specific enthalpy reduction is very much limited.

Inlet pressure is changed until the outer value is equal to 250 bar and it has been found to be $p_{in} = 72,25\ bar$:

Figure 79 – Mullite foam insulated water pipeline with pressure correction

With every component insulated with mullite foam, hot storage temperature would be around 507,7 ℃ and cold storage temperature around 274,3 ℃. Water pipeline efficiency results in $\eta = 99,6\ \%$ as before.

- **Vitreous carbon foam**

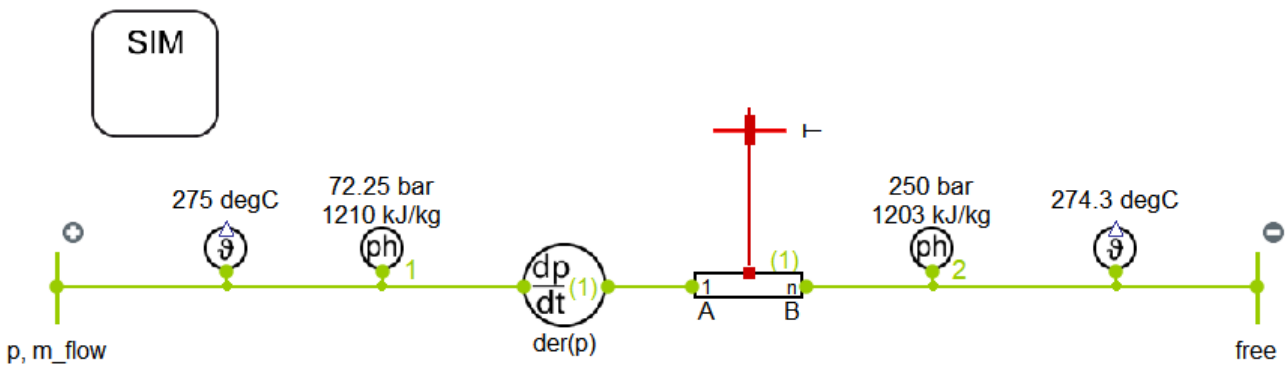|	1 cell	25 cells	250 cells
Outlet pressure smooth [bar]	249,7	252,37	252,47
Out pressure rough	244,76	247,44	247,54
Outlet enthalpy [kJ/kg]	1206,1	1206,09	1206,09
Outlet temperature [°C]	275	275	275
Heat losses [MW]	0,434	0,435	0,435
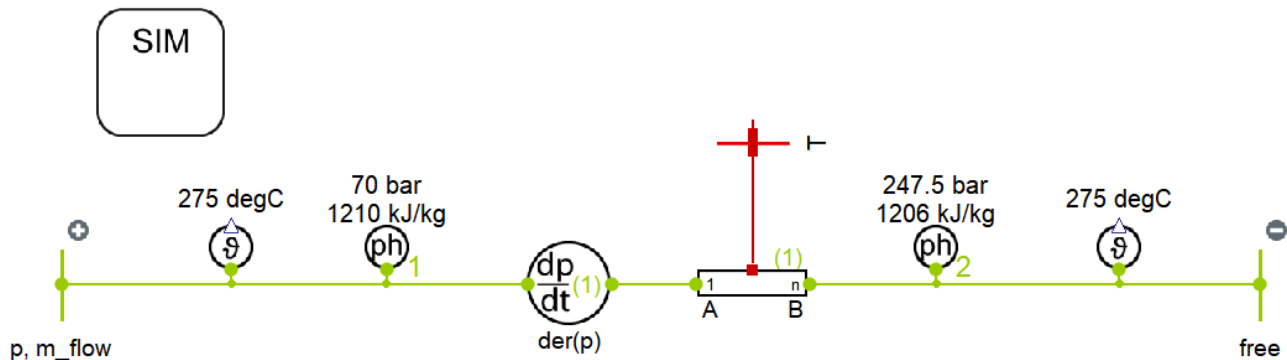
Figure 80 – RVC foam insulated water pipeline

Vitreous carbon foam insulated water pipeline allows the temperature to be unchanged between inlet and outlet. Efficiency is even higher, but material cost is also greater than mullite foam, which insulation effectiveness is in any case extremely good.

7.4 Power generation cycle

The reference Rankine cycle has been reproduced in smaller scale with TIL. One of the goals is also to determine the TIL capability of reproducing the cycle.

The BattMarines discharging mass flow rate has been fixed to $\dot{m} = 100\ Kg/s$. This means, the mass flowing in every component of the power generation cycle can be easily found as the percentage of the total mass flowing in the cycle. For example, mass flow rate entering the first turbine stage represents the 82,2% of the total mass flowing in the reference cycle, therefore in the simulated model this value will be equal to 82,2 Kg/s.

The reference cycle is characterized by three turbines aligned on the same shaft, a high-pressure turbine, an intermediate one and a low pressure one. The first turbine has two extractions of steam, while the second and the third have both three steam extractions.
None of the available expander models in TIL allows to have steam extractions in the component, that is, mass flow is unchanged between inner and outer port of the turbine model.

Therefore, the way to simulate steam extractions is to expand the steam with an expander model until the pressure at which an extraction occurs, then with a T-junction the mass flow is split. One of the two mass fluxes is the extraction and the other proceed to the next turbine stage.

On extraction lines there´s the need of controlling the extracted masses and it is done through a proportional integral controller (PI controller) and a valve. The mass flowing in the valve is proportional to the effective flow area of the valve itself: the controller controls and regulates this parameter to reach the desired mass flow rate.

Being connected to the same shaft, each turbine has to rotate at the same speed, and this can be imposed by a rotatory boundary connected to each turbine stage, in which constant rotation speed is fixed to $n = 50\ Hz$.

Due to model definition, only a stationary cycle operation is simulated. In fact, mass flux is determined in the expander model and if it is combined with other models, which also define the mass flow rate, the rotation speed must be set carefully to balance the pressure levels; but rotation speed is wanted to be constant at grid frequency. In addition, mass flow rate depends on inlet turbine thermodynamic condition, which therefore can´t change. Finally, water preheaters will be dimensioned to exchange a determined amount of heat corresponding to a specific mass flow rate, other reason for which mass fluxes are constant.

Each turbine stage intake volume is calculated by hand in order to have the desired mass flow rate in each stage. To increase by a factor of ten the mass flow rate and consequently the power output of the cycle, the volume of each turbine stage must be increased by a factor of ten. At the same time, heat exchange areas (plate areas) of all water preheaters and control set-point of steam extraction mass flux controllers have to be increased by the same factor.

Figure 82 shows th HP- turbine composed of two stages. Pressure and temperature are given as input in the boundary, mass flow rate is obtained fixing the first turbine model intake volume at $\sim 0,02\ m^3$ and the rotational speed at $n = 50\ Hz$ through a mechanical boundary. Every turbine model is characterized by same efficiencies, which are fixed at $\eta_{is} = 0,9$ and $\eta_{Effis} = \eta_{mec} = 0,98$ accordingly to the reference cycle [17]. Fill factor is considered to be unitary, meaning no leakages happen and all mass flowing in a turbine model is used to generate mechanical power.

Figure 81 – High pressure turbine stages in TIL (left) and process visualization in DaVe (right)

Steam extraction isn't visible in the left graph because sensors haven't been placed on steam extractions lines.

The need of using junction models forces to use a pressure state model next to each junction. Initial pressure in each pressure state model is set to the value at which steam extraction occurs in the reference cycle. The first extraction finds at $71,21\ bar$ and the second at $42,5\ bar$.

Steam extraction mass flow rates are also fixed as percentage of the total mass flow. The first extraction corresponds to 7,6 % of the total and it is obtained changing the effective flow area of the valve through a PI controller until the desired set point is reached.

After the second stage, the second extraction takes place, then the remaining steam undergoes reheating before entering the IP and LP-turbine stages. Reheater hot fluid is represented by the 17,8 % of the total mass at steam pipeline outer conditions and after the heat exchanger it gets mixed with the first turbine stage extraction in the first water preheater (the last one if counting from the condenser).

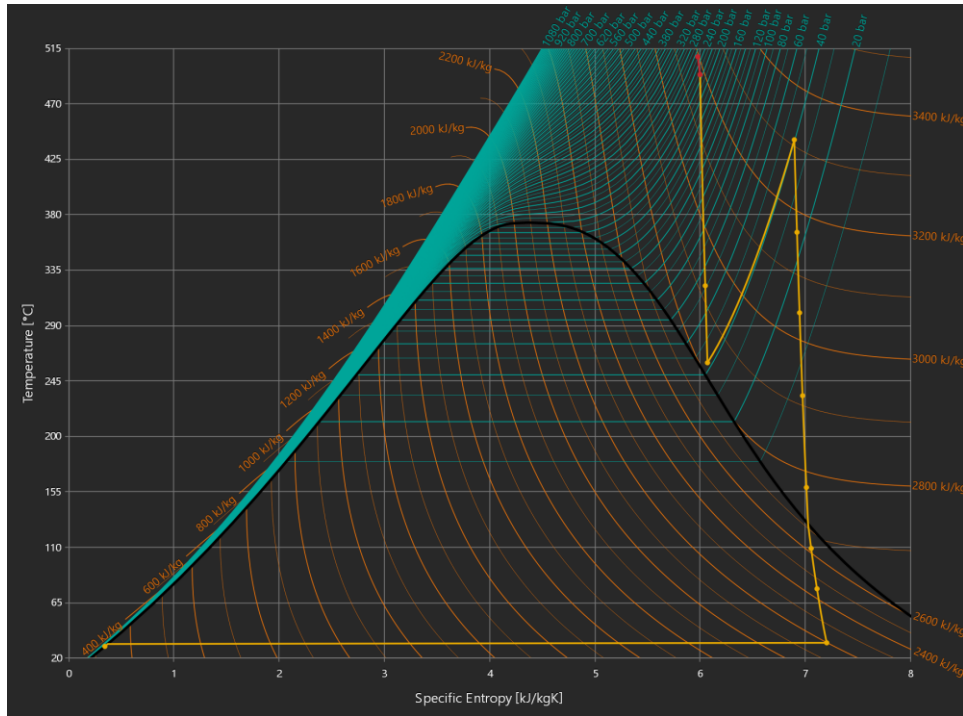Figure 82 – IP and LP turbine stages in TIL

Figure 83 – Main steam line complete expansion and condensation processes in DaVe together with transformation in the steam pipeline (red line)
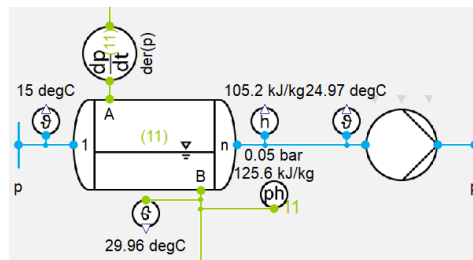

Figure 84 – Condenser in TIL

Water preheaters are modelled as parallel flow plate heat exchangers and their dimensions are modified until the wanted minimum temperature difference between two fluids is obtained. A real water preheater is typically a shell and tube heat exchangers with the feedwater flowing inside the tubes and steam condensing outside.

Each preheater receives turbine steam extraction, feedwater from condenser and drainage from the preceding preheater [50]. Three regions can be distinguished in the hot fluid side of a preheater: a first desuperheating region where only steam extraction is present and it is cooled down to saturation temperature; then drainage enters the component and get mixed with the steam extraction in the second region, at the end of which saturated liquid is present; finally, in the third region liquid phase is subcooled.

To simulate the real behaviour of such water preheater two heat exchanger with a junction in between should be needed, the first one with only steam extraction as hot fluid reaching the saturation temperature and the second one with the drainage addition for the remaining cooling of the total mass.

In order not to have too many heat exchangers in the system, I simulate it as single heat exchanger mixing the drainage and the extraction before it. What matters is the amount of transferred heat and that will be unchanged. Figure 86 shows that only two of the three beforementioned regions exist, due to pre-mixing of the flows. In every water preheater the mixing of drainage and extraction results in a saturated mixture because mass flow of drainage is much greater than the extraction one.

The bigger the cells number, the more the unknowns and equations describing the system, therefore the computational time increases, but also the results are more precise. Because the compressive number of heat exchangers is 9, including the condenser and the steam reheater, and because it isn´t wanted an excessive number of system equations, each heat exchanger is composed of 5 cells. Discretization won´t be perfect, but temperature evolution of fluids along the heat exchanger is visible.
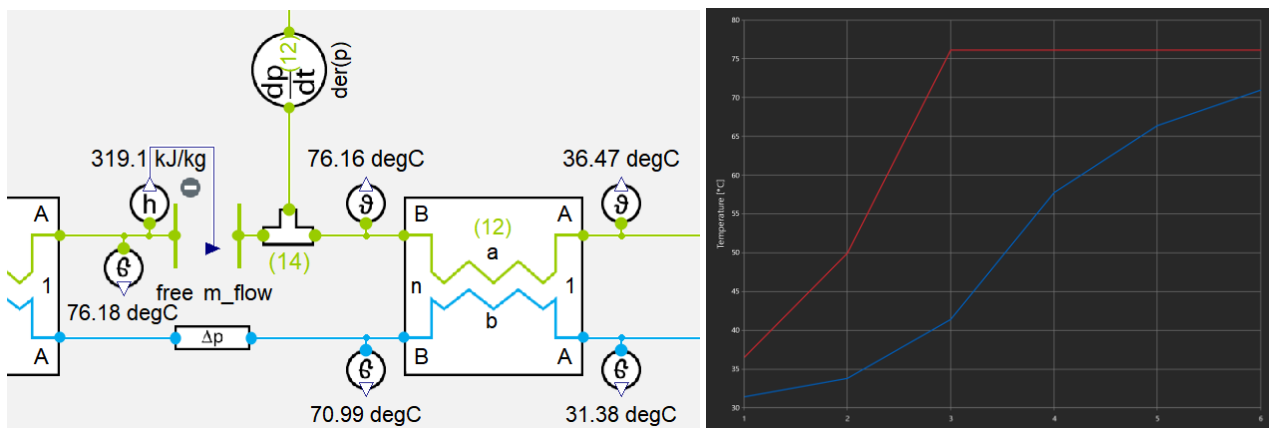

Figure 85 – First low pressure preheater in TIL and fluids temperature profiles in DaVe

The difference between the reference cycle and the BattMarines power cycle is the feeding water maximum pressure. In fact, in the reference cycle, $267\ bar$ is the pressure reached in the water after the feed water pump in order to exit the last preheater at $260\ bar$. In Battmarines, considering a mullite foam insulated rough water pipe with $0,2\ m$ inner diameter, the wanted pressure at the long pipe inlet was computed to be $72,25\ bar$. Fixing water pressure losses in high pressure preheater at $7\ bar$ would mean to pump the water up to $79,25\ bar$.

Powers exchanged by LP-preheaters are independent from the maximum pressure value, in fact, the condenser pump input power is constant and a pressure of $13,51\ bar$ is always reached after it. Instead, the pressure head given by the feed water pump must change accordingly to the descending water pipeline configuration, together with the design of HP-preheater.

Only in the third LP-preheater after the condenser the desuperheating is visible, in fact, steam extraction alone represents the hot fluid, without drainage addition. LP-preheaters fluid temperature profiles are the following:
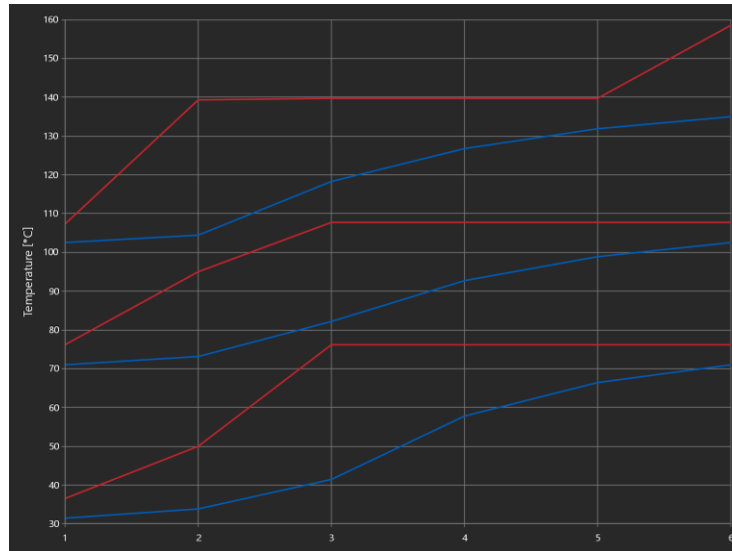
Figure 86 – LP-preheaters fluids temperature profiles

$\Delta T_{min} = 5,1$ °C ; $\Delta T_{min} = 5,2$ °C ; $\Delta T_{min} = 4,9$ °C (from bottom to top)

Heat exchangers have been dimensioned such to have a minimum temperature difference of ~ 5 °C as in the refeernce cycle. This constraint is quite well respected.

The design of HP-preheaters depends on the discharging water pipeline configuration and considering a rough mullite foam insulated water pipeline, a pressure of $72.25\ bar$ is wanted at the inlet. In figure 87 the HP-preheaters fluids temperature profiles are visible.

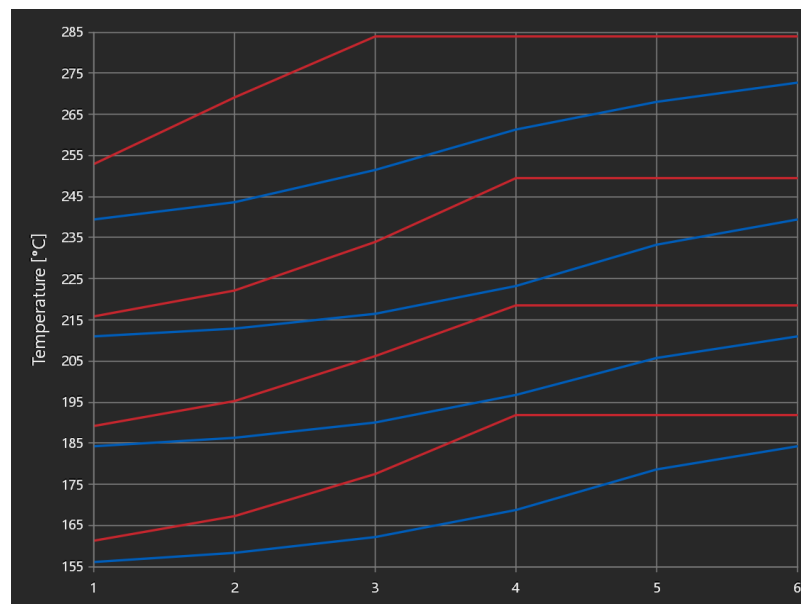Figure 87 – HP-preheaters fluids temperature profiles

$\Delta T_{min} = 5,2$ °C ; $\Delta T_{min} = 4,9$ °C ; $\Delta T_{min} = 4,9$ °C ; $\Delta T_{min} = 11,2$ °C

The constraint of minimum temperature difference is respected also in these heat exchangers, represented in figure 88:

Figure 88 – HP-preheater in TIL

Cycle efficiency is computed accordingly to the reference cycle efficiency calculation procedure. Powers extracted from the fluid, computed for each turbine model as mass flow rate times enthalpy difference, are reported in the column VLEFluid power. These values have to be multiplied by three efficiencies in order to find the electrical output: mechanical efficiency of turbine, mechanical efficiency of the generator and the electrical efficiency of the generator. They are all set at 98%.

	VLEFluid power [MW]	Electrical output [MW]
HP1	21,240	19,99
HP2	7,387	6,953
IP1	10,046	9,455
IP2	8,233	7,749
IP3	7,984	7,515
LP1	8,572	8,068
LP2	8,868	8,346
LP3	9,334	8,785
LP4	12,638	11,895
Total	94,303	88,757

$88,757 \; MW_{el}$ corresponds to the gross power output, to which the power consumption of pumps has to be subtracted to find the net electrical power output. Fluid power change across a pump is reported in the second column, as before it is the product of mass flow rate and enthalpy difference. Three efficiencies are the same (two mechanical and one electrical) but they have to divide the liquid power in order to find the required input electricity.

	Liquid power [MW]	Electrical input [MW]
Cooling water pump	0,207	0,22
Condenser pump	0,0973	0,103
Feed water pump	0,947	1,006
Total	1,252	1,33

$$\dot{W}_{net} = (88,757 - 1,33) \; MW_{el} = 87,427 \; MW_{el}$$

The feed water pump is the largest pump of the system. Compared with the reference cycle, its power is reduced by ~72 % and the whole power needed for pumps of is reduced by ~65 %.

It makes no sense to compute the cycle input power without considering the two vertical pipelines, in fact, pressure must be increased to ´boiler pressure´ before steam production. After estimating the input power, energy efficiency of the whole system can be computed.

8 ENERGETIC AND ECONOMIC ASSESSMENTS

8.1 Energy efficiency

Let´s consider an inlet pressure of $72\ bar$ and enthalpy unchanged from previous results. Properties evaluation slightly differs from VLEFluid and Liquid components, and the temperature corresponding to those pressure and enthalpy is $T_{in} \cong 274\ °\mathrm{C}$.
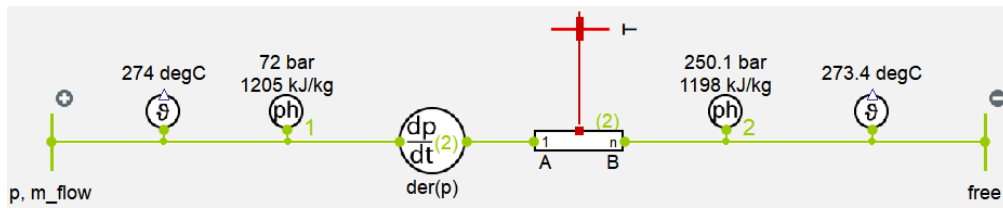

Figure 89 – Mullite foam insulated water pipeline for energy efficiency evaluation

Cold storage enthalpy results in $h_{out} = h_{cs} = 1197,71\ kJ/kg$. If the steam pipeline is insulated as well with mullite foam, the hot storage wanted enthalpy was calculated to be $h_{hs} \cong 3195\ kJ/kg$. If a cycle efficiency wants to be defined, the charging mass flow rate has to be the same of the discharging one. The input thermal power results in:

$$\dot{Q}_{input} = \dot{m}_{ch}\ (h_{hs} - h_{cs}) = 199,729\ MW_{th}$$

With the hypothesis of having low pressure losses in the charging pipeline and in the electric heater, for example $\Delta p \cong 4\ bar$, the corresponding underwater pump power is computed considering the three efficiencies as before:

$$\dot{W}_{pump} = \frac{\dot{V}\ \Delta p}{\prod_i \eta_i} = \frac{\dot{m}_{ch}\ \Delta p}{\rho_{cs}\ \prod_i \eta_i} = 0,05\ MW_{el}$$

Discharging process efficiency is equivalent to the product of the Rankine cycle efficiency and pipelines efficiencies. It can be computed in terms of power or energy. It makes sense to define it in terms of power, but in combination with the maximum storing time allowed.

During charging, electrical power is converted into heat with an efficiency of $\eta_{charging} = 100\ \%$. Electric resistance heating has unitary efficiency in the sense that all incoming electrical energy is transformed into heat. Of course, the renewable generation of electricity has its own efficiency that isn´t considered here. An interesting alternative is to charge the

battery operating the cycle in inverse direction, namely as a heat pump, in order to obtain roundtrip efficiency close to the unity.

The roundtrip efficiency of the battery corresponds to the discharging process efficiency, in case of mullite foam insulated pipelines:

$$\eta = \frac{\dot{W}_{net}}{\dot{Q}_{input} + \dot{W}_{pump}} = 43,76 \ \%$$

For a glass particulate insulated system, it is expected to be lower. In fact, old storage and hot storage enthalpies would be the following:

$$h_{cs} \cong 1165 \ kJ/kg$$

$$h_{hs} \cong 3258 \ kJ/kg$$

Therefore, higher power input is required and it is the reason for the lower efficiency, due to constant net power output of the Rankine cycle.

$$\dot{Q}_{input} = \dot{m}_{ch} \ (h_{hs} \ - \ h_{cs}) \cong 209,3 \ MW_{th}$$

$$\eta = \frac{\dot{W}_{net}}{\dot{Q}_{input} + \dot{W}_{pump}} = 41,76 \ \%$$

Thermal losses during storing period must be considered in order to fix the maximum storing period, but they do not influence the roundtrip efficiency in terms of power. Efficiency of glass particulate insulated system is acceptable, reduction in comparison with the other configuration is only ~2 %.

Nevertheless, the biggest difference between a mullite foam and a glass particulate insulated system is in the maximum allowable storing time. Considering an insulation thickness of $4 \ m$, in the first case, for high filling levels, steam can be stored for around one week without losing more than 1% of the stored energy. In the second case not much more than one day is required.

One last important factor must be considered: $\dot{Q}_{standby}$. It represents the thermal power required to heat up materials (heat capacity of walls) and the power that has to be extracted from the steam hot storgae tank during storing period to keep all turbines in hot stand-by. In fact, normal steam turbine operation is continuous and it isn't use for load-following operation, but rather for base load power generation. The reason is the long time needed for the turbine to reach its stationary condition from a cold start.

It is therefore necessary to keep power plants components at operating temperatures for the whole storing period and an adequate thermal insulation is wanted to use as little energy as possible. Common insulation materials can be adopted on the platform, and they should be pretty effective.

To conclude, a very approximate results for the efficiency in terms of energy for a mullite foam insulated system can be 40 % for a storing period of one week, with 1 % of the stored energy lost to the ambient and around $2 - 3$ % of the energy used to maintain the power plant ready for the discharging process to start.

	Max Power Rating (MW)	Discharge time	*Max cycles* or lifetime	Energy density (watt-hour per liter)	Efficiency
Pumped hydro	3,000	4h – 16h	30 – 60 years	0.2 – 2	70 – 85%
Compressed air	1,000	2h – 30h	20 – 40 years	2 – 6	40 – 70%
Molten salt (thermal)	150	hours	30 years	70 – 210	80 – 90%
Li-ion battery	100	1 min – 8h	*1,000 – 10,000*	200 – 400	85 – 95%
Lead-acid battery	100	1 min – 8h	6 – 40 years	50 – 80	80 – 90%
Flow battery	100	hours	*12,000 – 14,000*	20 – 70	60 – 85%
Hydrogen	100	mins – week	5 – 30 years	600 (at 200bar)	25 – 45%
Flywheel	20	secs - mins	*20,000 – 100,000*	20 – 80	70 – 95%

Characteristics of selected energy storage systems (source: The World Energy Council)

Figure 90 – Characteristics of some storage technologies [51]

Pumped hydro and CAES are the two biggest grid-scale EES system existing. Pumped hydro has much higher efficiency than BattMarines, which problem is the efficiency of the thermodymìnamic cycle used in the discharging process.

CAES efficiency is comparable to BattMarines because the discharging process is a thermodynamic cycle.

8.2 Energy density

Discharging process power output was calculated to be $\dot{W}_{net} = 87,427 \, MW_{el}$ with a mass flow rate of $\dot{m}_{dis} = 100 \, kg/s$. Energy density of the battery in terms of mass and volume:

$$\frac{\dot{W}_{net}}{\dot{m}_{dis}} \cong 243 \ \frac{Wh}{kg}$$

$$\frac{\dot{W}_{net}}{\dot{m}_{dis}} \rho_{hs} \cong 21{,}3 \frac{Wh}{l}$$

Where density is considered in case of mullite foam insulated system.

Let´s consider mullite foam as insulation material with filling level set to 99 %, corresponding to a stored mass of $m_v \cong 68e+6 \ kg$, power density can be computed as

$$\frac{\dot{W}_{net}}{m_v} \cong 1{,}3 \ \frac{W}{kg}$$

If the power output is wanted one order of magnitude greater, the discharging mass flow rate can be increased by adding other 10 steam pipelines to obtain $\dot{m}_{dis} = 1100 \ kg/s$ and $\dot{W}_{net} = 962 \ MW_{el}$. Energy density would be unchanged, but power density would increase by a factor of 11, namely:

$$\frac{\dot{W}_{net}}{m_v} \cong 14 \ \frac{W}{kg}$$

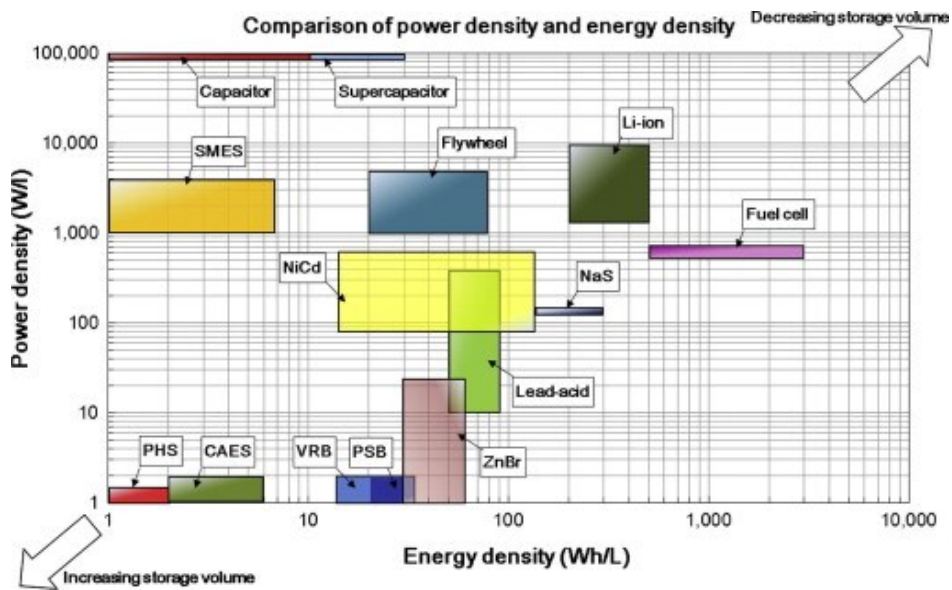$$\frac{\dot{W}_{net}}{m_v} \rho_{hs} \cong 1{,}2 \frac{W}{l}$$

Figure 91 – Comparison of power and energy density for different storage technologies

Compared to pumped hydro (PHS is figure 91), power density has the same order of magnitude, while energy density is one order of magnitude higher.

A way to increase the energy density is to store steam at higher temperatures. Consequently, the power plant should be different. What if the supercritical steam wants to be stored to feed a USC steam power plant? The comparison cycle is decided to be the thermoelectric power plant of Torrevaldaliga Nord [50] in Italy, characterized by a maximum pressure of $247 \; bar$ and temperature of $610 \; °C$.

Submerged vessels have to be installed deeper due to higher pressure, but static pressure losses in the steam pipeline are reduced because of lower steam density. The thermodynamic cycle efficiency is consistently higher and can reach $46 - 47 \; \%$ and it results in a bigger value of the ratio between net power output and total mass flow rate, which is around $0,35 \; kWh/kg$.
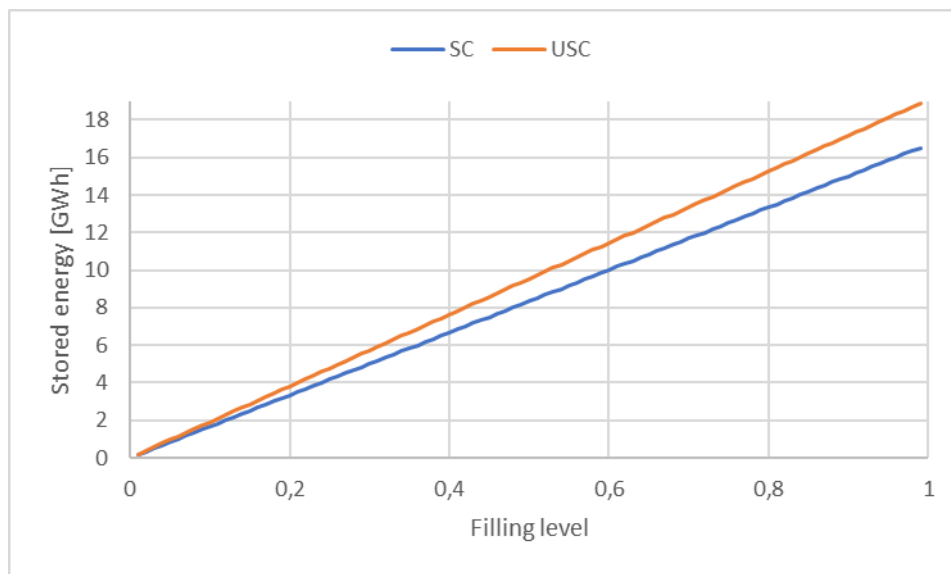
Figure 92 – Stored energy in SC

In figure 92, the blu line represents the studied BattMarines, while the orange line has been drawn considering a hot storage temperature of $T_{hs} = 625 \; °C$ and $p_{hs} = 260 \; bar$, reasonable values for a potetial BattMarines connected to the Torrevaldaliga Nord power plant.

Despite containing less mass, more energy is stored at higher temperature with a more efficient connected power plant, meaning a higher energy density can be achieved. Due to temperature increase, thermal losses increase and, at half filling level with a $4 \; m$ mullite foam thick wall, storing time is reduced by a factor of $\sim 7 \; \%$. The biggest disadvantage is, anyway, the more important increase in price of steel to operate at such high temperatures, reason why it isn´t considered a possible energetic improvement of the system.

A third comparison is done with EES systems about the dimensions. It has been said the goal was to prove the energetic feasibility of a grid-scale EES system, therefore power output and amount of energy stored have to be comparable with PHES.

Figure 93 compares a lot of EES systems, BattMarines has been added by hand very approximately. It is comprable with PHES for sure; in order to store more energy, it is

sufficient to build more tanks on the seafloor. To increase the power output more power plants are needed.
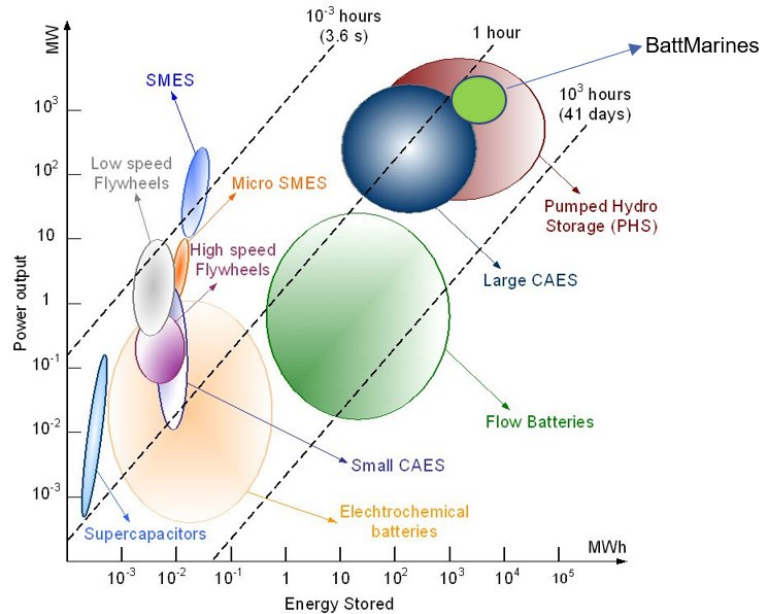
Figure 93 – Comparison of power output and energy stored for different storage technologies [52]

Greatest disadvantage of BattMarines is the storing time. PHES has storing times much bigger, in fact energy could be stored for months without problems, while BattMarines has a defined maximum storing time that depends on materials and also on the filling level of the battery. If discharging process do not occur, the whole stored energy gets lost.

The ratio between net electric power output and total mass flow rate is slightly higher in the studied mullite foam insulated system than the reference rankine cycle. Moreover, tank losses have been estimated with a storing temperature of $T_{hs} = 525\,°C$ in figure 51, which isn´t correct in case of mullite foam insulated tank. New losses are computed at $T_{hs} \sim 508\,°C$:

Figure 94 - Time to dissipate 1% of stored energy as function of filling level for different mullite foam thicknesses

Instead of $6\ days$ and $13\ h$, the supercritical steam can be stored for more than one week, namely $7\ days$ and $7\ h$ ($174{,}75\ h$).

These times are computed for the simplified vessel design, in which supercritical steam is facing the containment structure. If a right design of figure 44 is cons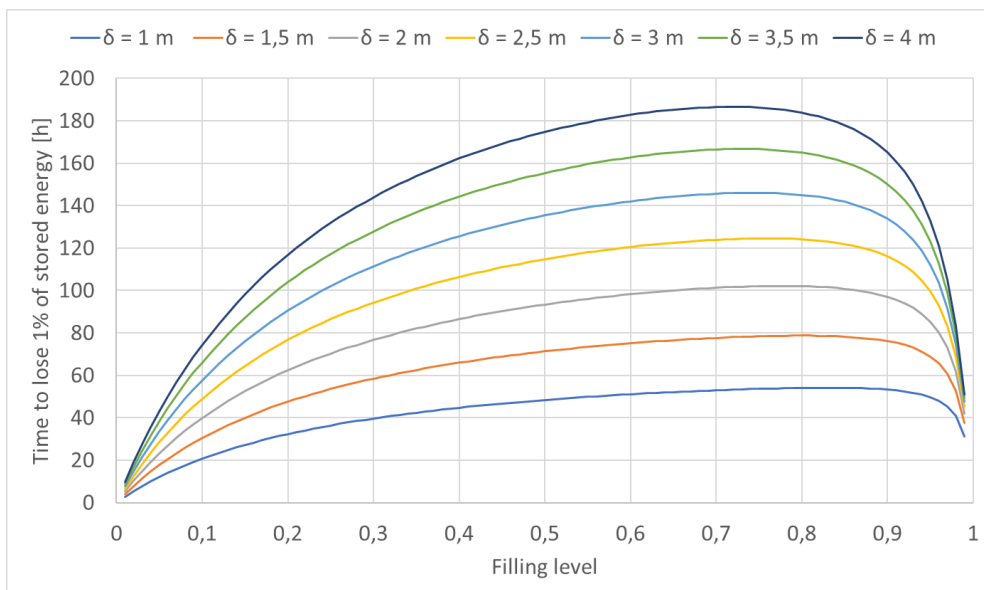idered, the temperature difference across the huge external cylinder is much lower. A still conservative approach could be to consider an increase of storing time of 50 %, resulting in more than $11\ days$ for high filling levels at $4\ m$ wall thickness.
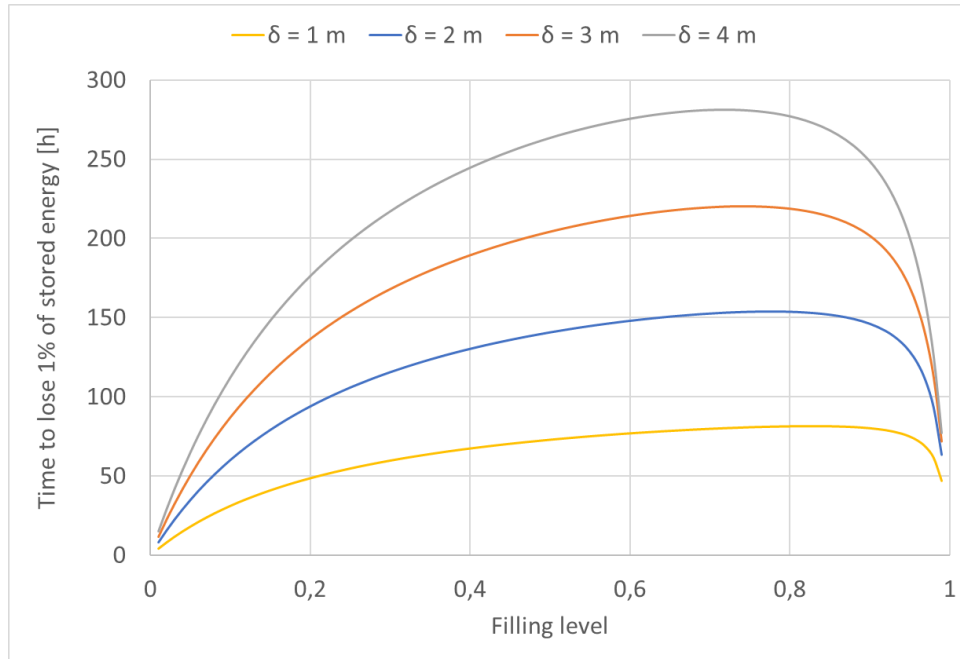
Figure 96 – Time to dissipate 1% of stored energy as function of filling level for different mullite foam thicknesses of containment structure in a realistic inner vessel design

For the particulate glass insulated tank the considered temperature was correct and only the stored energy per kg increases a bit. It translates in a very little increase of storing time, for example at half filling level the time to lose one percentage of the stored energy passes from 30 to $31\ h$.

To conclude the comparison between the two system configurations; stored mass, stored energy and discharging time are reduced by 4,5 % passing from mullite foam to glass particulate insulated hot tank.

8.3 Levelized cost of storage

A very approximate economic analysis can be done estimating the order of magnitude of the battery LCOS, namely the levelized cost of storage. It is the equivalent of LCOE for

conventional generation technologies but *uses charging cost as fuel cost and takes the discharged electricity instead of generated electricity.*

LCOS expresses the cost of kWh or MWh electricity discharged from a storage device when accounting for all cost incurred and energy produced throughout the lifetime of the device [53]. Only results and brief description of the procedure is done.

$$LCOS = \frac{Investment + \sum_n (O\&M + c_{el}W_{in})(1+i)^{-n}}{\sum_n W_{out}(1+i)^{-n}}$$

Investment cost of power plant is found considering a specific price for MW of installed power in usual supercritical steam turbine plants [50] and subtracting the $50\,\%$ of it that would be required for the boiler and the fuel treatment components.

Investment cost of submerged components is carried out computing the cost for the total material required and hypothesising it corresponds to one third of the total installation costs. Great difference in amount of material needed in case of single containment $100\,m$ diameter vessel and multiple smaller scale vessel enclosed by the huge containment. Investment cost is found to be doubled.
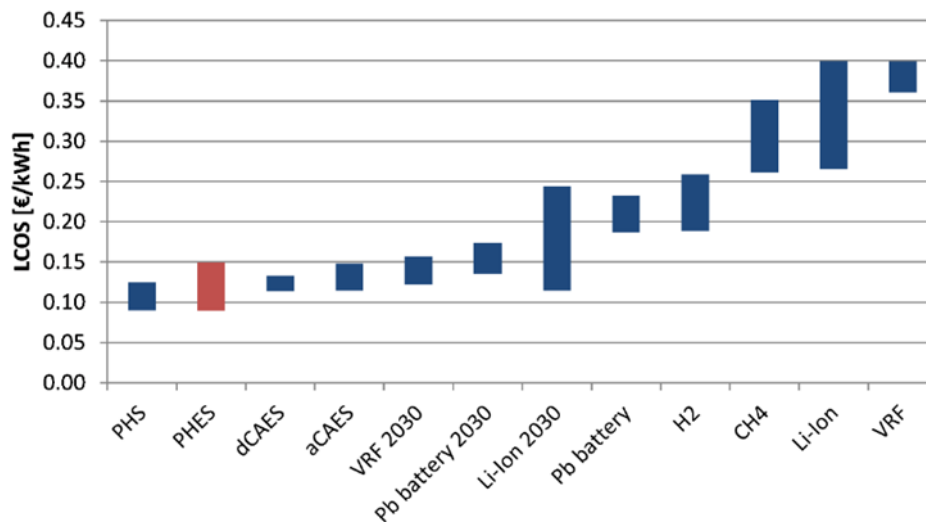
Figure 97 – Comparison of LCOS for different technologies

Investment cost estimation results in $3 - 4\,B€$ in the complex design. Different scenarios are considered, with system lifetime varying from 15 to 30 years and daily charge-discharge from $3\,h$ to $12\,h$ daily.

Interest rate is fixed to 5 %, price of purchased eletricity is fixed at $20\,€/MWh$ and $O\&M$ costs are considered to be 5 % of the investment cost.

Figure 97 compares LCOS for different technologies. PHS represents the pumped-hydro and the cost of the kWh produced is the lowest that can be found, together with the red bar that represents small scale Carnot batteries.

BattMarines LCOS estimation results in a very wide range due to different studied scenarios:

$$0{,}15 \ \text{€}/\text{kWh} < \text{LCOS}_{\text{BattMarines}} < 0{,}55 \ \text{€}/\text{kWh}$$

LCOS in the range desired for a grid-scale storing technology is obtained only considering a daily 12 h charge-discharge cycle with a lifetime of the system of 30 years. Such operation isn't realistic at all, because it is like if storage does not occur (null storuing time). The upper layer for the LCOS is found for a daily charge-discharge of 3 h and half lifetime, that is a more realistic behaviour.

LCOS of a specific BattMarines probably lays is such interval, and from this simple estimation it seems the technology isn't cost effective at all compared to pumped-hydro.

Economic analysis couldn't have a lot of meaning, because BattMarines is a storing technology suitable for the future energy market in which renewable generated energy on the grid should be always the required amount or in excess, therefore the battery should be charged for free. In addition, it isn't yet known how expensive the electricity in the future will be, in particular in those periods of lack of rewenable generated energy.

In other words, it could be that LCOS of $0{,}4 - 0{,}5 \ \text{€}/\text{kWh}$ will be common for furture EES systems, since they will be discharged only in periods of consistently high electricity price. If there is a real need of large EES systems

9 CONCLUSIONS

A successful energy transition requires grid-scale electric energy storage and Carnot batteries represent a potential solution. BattMarines is a Carnot battery concept relying on storing large quantities of high-pressure steam ready to be expanded in a conventional steam power plant. The key idea is to take advantage of high pressure ambient at large sea depths, so that a thin shell vessel can be utilized to store high quality steam at low cost. Power plant is built on a platform/ship with steam pipeline connection to the vessel on the seafloor.

The thesis has considered the general concept including a rough description of plant configuration. Due to Carnot Battery operation, the better configuration has both the cold and the hot storage tanks built on the seafloor connected by the charging pipeline.

Hot vessel has inner diameter and height of $\sim 100\ m$, cold vessel of $\sim 50\ m$. Single steam pipeline of $d_{in} = 0,36\ m$ carries $100\ kg/s$ to have small enoungh pressure losses. The same mass flow rate characterizes the water pipeline of $d_{in} = 0,2\ m$.

To increase the mass flow rate and the power output, the number of pipelines must be increased together with the turbine dimensions.

Stresses induced in the containment wall are great, therefore a possible more realistic configuration has been described, named inner vessel design, where the same volume is replaced with smaller tanks. These tanks are characterized by enough low stresses, so that normal marine steel can be used.

Potential insulation materials have been searched and two main solutions have been analyzed: granular glass insulation and Mullite foam insulation. Roundtrip efficiency is weakly influenced by the choice because thermodynamic cycle efficiency really limits the efficiency. It lays between $41 - 44\ \%$.

In a Mullite foam insulated system, the energy saved in the pumping system of the power plant is comparable to the energy lost in the discharging pipelines, in fact the efficiency of the discharging process (that is also the roundtrip efficiency) is actually slightly higher than the efficiency of the reference power cycle.

Differently from the roundtrip efficiency, the storing time strongly depends on the material selection, in fact thermal resistance of the tank wall changes significantly. The better the steam pipeline is insulated, the lower the temperature needed in the hot storage and the lower the proportional thermal losses.

The time to lose 1 % of the stored energy was defined as the maximum storing time: it results in $\sim 31\ h$ for the glass particulate insulated tank and $\sim 11\ days$ for the Mullite foam insulated tank, considering the same containment wall thickness.

REFERENCES

[1]   T.M. Christensen, A.S. Hurn, K.A. Lindsay, «Forecasting spikes in electricity prices», *International Journal of Forecasting,* 2011.

[2]   L. Mauler, J. Leker, F. Duffner, «Economies of scale in battery cell manufacturing: The impact of material and process innovations», *Applied Energy*, 2021.

[3]   M.C. McManus, «Environmental consequences of the use of batteries in low carbon systems: The impact of battery production», *Applied Energy*, 2012.

[4]   IEA (2021), Energy Storage, IEA, Paris. Available: https://www.iea.org/reports/energy-storage.

[5]   R.A. Verzijlbergha, L.J. De Vriesa, G.P.J. Dijkemab, P.M. Herdera, «Institutional challenges caused by the integration of renewable energy sources in the European electricity sector », *Renewable and Sustainable Energy Reviews,* 2016.

[6]   IEA, «Innovation in batteries and electricity storage», September 2020.

[7]   A. Fyke, «The Fall and Rise of Gravity Storage Technologies», *Joule,* 2019.

[8]   H. Lund, G. Salgi, «The role of compressed air energy storage (CAES) in future sustainable energy systems», *Energy Conversion and Management,* 2009.

[9]   O. Dumont, G.F. Frate, A. Pillai, S. Lecompte, «Carnot battery technology: A state-of-the-art review», *The Journal of Energy Storage*, September 2020.

[10]   S.K. Lee, Y.C. Song, S.H. Han, «Biaxial behavior of plain concrete of nuclear containment building», *Nuclear Engineering and Design*, September 2003.

[11]   Fraunhofer Institute for Solar Energy Systems ISE, «Energy-Charts». Available: https://energy-charts.info/.

[12]   W.D. Steinmann, H. Jockenhöfer, D. Bauer, «Thermodynamic Analysis of High-Temperature Carnot Battery Concepts», *Energy Technology*, 2020.

[13]   Wikipedia,   2007.   Available: https://en.wikipedia.org/wiki/Rankine_cycle#/media/File:Rankine_cycle_layout.png.

[14]   J. Zone, «Rankine Cycle», *Chemical & Process Engineering*, February 2021. Available: https://www.arhse.com/rankine-cycle/.

[15]   G. Cornetti, «Macchine Termiche», Ed. Il Capitello Torino

[16]   T. Zhang, «Methods of Improving the Efficiency of Thermal Power Plants», *Journal of Physics*, 2020.

[17]   M.M. Schlagenhaufer, «Simulation des Dampf-Wasserkreislaufs und der Sicherheitssysteme eines High Performance Light Water Reactors», Karlsruhe Institute of Technology, KIT SCIENTIFIC REPORTS 7582, 2010.

[18]   S.K. Neenu, «Normal Concrete vs. High-Strength Concrete Properties and Difference», *The Constructor*. Available: https://theconstructor.org/concrete/normal-high-strength-concrete-properties/17771/.

[19]   OpenSeaMap. Available: http://map.openseamap.org/.

[20]   Nickel Institute, «High-Temperature Characteristics of Stainless Steel», DESIGNERS' HANDBOOK SERIES NO 9004, 2020.

[21]   V. Kodur, «Properties of Concrete at Elevated Temperatures», *ISRN Civil Engineering*, 2014.

[22]   Ansys, «Ansys Granta EduPack».

[23]   The Vermiculite Association, «Properties». Available: https://www.vermiculite.org/resources/properties.

[24]   Wikipedia. Available: https://en.wikipedia.org/wiki/Basalt_fiber.

[25]   A. Zeb, M. Abid, M.A. Zeb, M.O. Qureshi, U. Younas, I. Batool, «Measurement and Prediction of Thermal Conductivity of Volcanic Basalt Rocks from Warsak Area», *Advances in Materials Science and Engineering,* August 2020.

[26]   MatWeb.   Available: http://www.matweb.com/search/datasheet.aspx?matguid=2442d7acc494421fb46d1b986c356eae&c+kck =1&ckck=1.

[27]   Foamglass. Available: https://www.foamglas.com/en-gb.

[28]   Imerys. Available: https://www.imerys.com/minerals/mullite.

[29]   Superior Technical Ceramics. Available: https://www.ceramics.net/ceramic-materials-solutions/silicates/mullite.

[30]   B. Wischnewski, Peace Software. Available: https://www.peacesoftware.de/einigewerte/luft_e.html.

[31]   S.M. Bekkouche, C.M. Kamal, T. Benouaz, «Thermal resistances of air in cavity walls and their effect upon the thermal insulation performance», *International Journal of Energy end Environment*, 2013.

[32]   E. Chiavazzo, «Pressure loss according Idelchik in sphere beds», PoliTo, Energy storage course 2020.

[33]   Henan Lite Refractory Material Co.Ltd.. Available: https://www.henanlite.com/insulating-bricks/mullite-insulation-brick/2019/0716/308.html.

[34]   M.I. Osendi, R. Barea, P. Miranzo, J.M.F. Ferreira, «Thermal conductivity of highly porous mullite material», *Acta Materialia,* 2005.

[35]   CUNSE - csrefractory.com. Available: https://www.csrefractory.com/product/insulation-brick/Mullite-Insulation-Brick.html.

[36]   Ultramet – Advanced Matrials Solutions. Available: https://ultramet.com/refractory-open-cell-foams/properties-of-foam-materials/.

[37]   P. Konakov, «Report of the Academic Society for Science of the UDSSR», 51 (7), pp. 503-50, 1946.

[38]   R. Sesana, «Structural mechanics», PoliTo, Thermal Machines and Structural Mechanics course 2018-19.

[39]   A. Ibrahim, Y. Ryu, M. Saidpour, «Stress Analysis of Thin-Walled Pressure Vessels», *Scientific Research Publishing*, 2015.

[40]   P.Poworoznek, «Elastic-Plastic Behavior of an Cylinder Subject to Mechanical and Thermal Loads», Rensselaer Polytechnic Institute Hartford, CT December, 2008.

[41]   R. Khan, «Pipe Thickness Calculation for Internal Pressure», Make Piping Easy. Available: https://makepipingeasy.com/pipe-thickness-calculation-for-internal-pressure/.

[42]   P. Webb, «Introduction to Oceanography».

[43]   Forbes Marshall, «www.forbesmarshall.com». Available: https://www.forbesmarshall.com/Knowledge/SteamPedia/Steam-Distribution/Steam-Pipe-Sizing.

[44]   Octalsteel, «Large Diameter Steel Pipe». Available: https://www.octalsteel.com/large-diameter-steel-pipe.

[45]   Material-properties.org, «Material Properties». Available: https://material-properties.org/sand-density-heat- capacity-thermal-conductivity/.

[46]   TLK-Thermo GmbH – Engineering Services and Software for Thermal Systems. Available: https://www.tlk-thermo.com/index.php/de/.

[47]   TIL Suite, TLK-Thermo GmbH. Available https://www.tlk-thermo.com/index.php/de/software/til-suite.

[48]   The Modelica Association. Available: https://modelica.org/.

[49]   Swamee, P.K. Jain, A.K. (1976). "Explicit equations for pipe-flow problems". *Journal of the Hydraulics Division.*

[50]   N. Pedroni, PoliTo, Uso Ottimale e Sicurezza degli Impianti Energetici course, 2018/2019.

[51]   A. Zablocki, «Fact Sheet | Energy Storage», EESI – Environmental and Energy Study Institute. Available: https://www.eesi.org/papers/view/energy-storage-2019.

[52]   H. Ibrahim, A. Ilinca, «Techno-Economic Analysis of Different Energy Storage Technologies», *Energy Storage - Technologies and Applications,* 2013.

[53]   A. Smallbone, V. Jülch, R. Wardle, A.P. Roskilly, «Levelized Cost of Storage for Pumped Heat Energy Storage in comparison with other energy storage technologies», *Energy Conversion and Management,* 2017
a

APPENDIX 1